

Department of Medical Radiation Sciences

**Scanning protocol optimisation for dual-
energy computed tomography
angiography in peripheral artery stenting**

Abdulrahman Marzouq Almutairi

This thesis is presented for the degree of
Doctor of Philosophy
of
Curtin University

May 2016

Declaration

To the best of my knowledge and belief this thesis contains no material previously published by any other person except where due acknowledgment has been made.

This thesis contains no material which has been accepted for the award of any other degree or diploma in any university.

The research presented and reported in this thesis was conducted in accordance with the National Health and Medical Research Council National Statement on Ethical Conduct in Human Research (2007), updated March 2014. The proposed research study received human research ethics approval from the Curtin University Human Research Ethics Committee (EC00262), Approval Number # HR 167/2013, and King Fahad Specialist Hospital, Dammam, Saudi Arabia # IRB-RAD029-FB.

Signature. .....

Date: May 2016

Abstract

Peripheral artery disease (PAD) is commonly treated by peripheral artery stents during angiography procedure. This procedure is invasive and expensive, with associated complications and without the ability to give additional information about the stented vessels. To eliminate some of these deficits, a recent approach named dual-energy computed tomography angiography (DECTA) in peripheral arterial imaging has been developed, but whose diagnostic accuracy needs to be confirmed and a reduction of the associated radiation dose deserves to be investigated. Only a few studies have investigated the use of DECT applications in peripheral arterial stent evaluation, with results indicating that the image quality of DECTA is greater than that obtained with conventional computed tomography angiography CTA; but more evidence is needed to determine the optimal scanning protocols of DECTA in peripheral arterial stenting. The purpose of this study is to establish the optimise scanning protocols for DECTA of peripheral arterial stents, to enable reduction of the radiation dose and improvement of the image quality.

This project was carried out in four stages. In Stage I, dose-saving scanning protocols were devised based on a systematic review of the literature, and in Stage II experiments on a phantom study were conducted with different DECTA protocols to determine an optimal scanning protocol. In Stage III, the devised optimal protocol obtained from Stage II was used in a clinical study to evaluate and compare two different volumes of contrast medium in peripheral artery imaging. In Stage IV, the optimal protocol obtained from Stage II and verified in stage III was also used in a group of prospectively recruited patients treated with peripheral arterial stents, aiming to achieve the main objectives of the project.

A systematic review was conducted to determine the diagnostic performance of DECT in PAD based on an analysis of the current literature. Nine of the works studied, covering 286 patients who underwent lower extremity DECTA, were analysed. The mean estimates of sensitivity and specificity of DECTA were 95.8% and 79.8%. Reduction of the contrast medium volume up to 50% was found to achieve an adequate image quality at the optimal kiloelectron volt (keV) setting. The mean effective dose of DECTA was similar to or lower than that of conventional CTA.

In the phantom experiments, a custom-made peripheral arterial phantom, consisting of a main peripheral arterial tree and arterial branches, was developed with use of a computer-aided design program to represent realistic anatomic dimensions. The aim of this study was to identify the optimal DECT scanning protocol for peripheral arterial stents while achieving

a low radiation dose while maintaining diagnostic image quality, as determined by an in vitro phantom study. A total of 15 stents of different sizes, materials and designs were deployed in the phantom. Thirty-six scans from pre-set gemstone spectral imaging (GSI) protocols (GSI-36, -48 and -51), with 180 reconstructions at different virtual monochromatic spectral (VMS) images and adaptive statistical iterative reconstruction (ASIR) values, were evaluated in this study. Image quality indices such as CT attenuation, SNR, CNR and image noise were evaluated. A significant reduction of image noise with a higher SNR between the VMS images was achieved in all investigated GSI protocols. Radiation doses were evaluated and compared between different scans; the lowest dose was achieved with the GSI-48 protocol. An outcome of this study is the recommendation of the use of GSI-48 with pitch value 0.984, combined with 50% of ASIR at a low keV value.

A prospective study consisting of quantitative and qualitative analysis was conducted, firstly to design an optimal CT imaging protocol by determining the feasibility of using a reduced contrast medium volume in peripheral arterial DECTA, and secondly to compare the results with those obtained using routine contrast medium volumes. A total of 34 patients who underwent DECT angiography for diagnosis of PAD were randomly assigned to two groups: a routine contrast volume group (n = 17), with 1.5 mL/kg and an injection rate of 4–5 ml/s; and a low contrast volume group (n = 17), with 0.75 mL/kg and an injection rate of 4–5ml/s. Six datasets of VMS images were reconstructed with ASIR at 50%. Qualitative and quantitative image quality was evaluated. The lowest image noise was found in the low contrast volume group between 65 and 70 keV, while the highest SNR and CNR were found at 65 keV. This suggests that the use of low contrast medium yields a respectable diagnostic image quality compared to the routine contrast volume; therefore, a reduction of 50% of contrast medium using VMS is recommended for peripheral arterial DECTA.

Finally, Stage IV is a prospective study comparing two groups of patients, conducted to determine the optimal scanning protocols of DECTA in terms of radiation dose and image quality at different keV levels, compared with conventional CTA in patients treated with peripheral artery stents. This study involved recruitment of 29 patients with prior stent placement in peripheral arteries. A total of 56 uniquely identified stents with different types and diameters, which were located in common iliac arteries, external iliac arteries and superficial femoral arteries, were evaluated. Images were reconstructed with VMS imaging at 65, 68, 70 and 72 keV and ASIR at 50%, compared with conventional CTA. Qualitative and quantitative image quality were assessed. Image quality assessments from DECTA were found to be better than those from conventional CTA, with the lowest image noise achieved at 72 keV. Radiation dose was highly significant between DECTA and conventional CTA

scans (6.98 vs 19.78 mSv, $p < 0.0001$). An optimal scanning protocol consisting of 72 keV and 50% ASIR is recommended as it leads to better image quality for DECTA in peripheral arterial stenting compared to conventional CTA.

Results from this research show that with appropriate selection of DECT protocols, peripheral arterial stent may be evaluated by DECTA and provide a higher image quality at similar or even lower radiation doses than in conventional CTA. In addition, contrast medium volume may be reduced by up to 50% without showing deterioration in the image quality. With increasing use of DECT in the diagnosis of cardiovascular disease including peripheral arterial disease, implementation of optimal DECTA scanning protocols is of paramount importance for reduction of both radiation dose and contrast medium while preserving diagnostic quality.

Acknowledgements

In the Name of Allah, the Most Merciful, the Most Compassionate all praise be to Allah, the Lord of the Worlds; and prayers and peace be upon Mohamed His servant and messenger.

First and foremost, I must acknowledge my limitless thanks to Allah, the Ever Magnificent; the Ever Thankful, for His help and blessing. I am totally sure that this work would have never become truth without His guidance.

It has been three years and ten months since I started as a PhD student in the Department of Medical Radiation Sciences at Curtin University. Throughout this journey many have participated and helped make this thesis happened.

I would first like to thank my research supervisor, Professor Zhonghua Sun, for his support over the years. I am grateful for his guidance and the opportunities he has afforded me. In addition, I would like to extend my thanks to Mr Gil Stevenson for helping me to overcome the issues related to data analysis. I would also like to thank King Fahad Specialist Hospital in Dammam, Saudi Arabia, for financial support of my PhD study. Furthermore, I would like to express my appreciation to the Saudi Cultural Mission in Canberra. I would like to take this opportunity to give warm thanks to the staff in the Department of Medical Radiation Sciences for their assistance throughout my study. In particular, the administration staff in the front desk were very helpful dealing with issues related to my study.

This study would not have been a success without the love, inspiration, support, and encouragement of my family. I am grateful to my precious parents for their endless support throughout my whole life; to my beloved wife Hanan Almousa for her great patience and motivation; and to my lovely children (Mashaal, Abdullah, Osama, Almaha and Omar) who are added sweetness to my life and keep me busy.

Last but not least, deepest thanks go to all people who took part in making this thesis real.

This thesis has been professionally edited by Dr Margaret Johnson of The Book Doctor, in accordance with the guidelines established by the Institute of Professional Editors and the Deans and Directors of Graduate Studies.

Table of Contents

Abstract	ii	
Publications	xv	
Conference presentations	xv	
List of abbreviations	xvi	
Chapter 1	General introduction	1
1.1	Background	1
1.2	Study aims and objectives	3
1.3	Thesis structure	3
1.4	References	5
Chapter 2	Literature review	7
2.1	Introduction	7
2.2	Peripheral artery disease	7
2.3	Imaging modalities in the diagnosis of PAD	8
2.3.1	Digital subtraction angiography	9
2.3.2	Doppler ultrasound	9
2.3.3	Magnetic resonance angiography	11
2.3.4	Computed tomography angiography	12
2.4	Radiation dose in CT	27
2.4.1	Radiation dose effects	27
2.4.2	Radiation dose quantity and measurements	28
2.5	Peripheral arterial stents	30
2.6	Peripheral arterial stents evaluation by DECT	31
2.7	Contrast medium optimisation	32
2.8	Evaluation of image quality	33
2.8.1	Objective evaluation of image quality	34
2.9	Factors influencing radiation dose and image quality	37

2.10	Scanning parameters.....	37
2.10.2	Reconstruction parameters.....	42
2.10.3	Image processing techniques.....	44
2.11	Summary.....	45
2.12	References.....	46
Chapter 3	Dual energy computed tomography angiography in the peripheral arterial imaging: A systematic review of image quality, radiation dose and diagnostic value.....	59
3.1	Introduction.....	59
3.2	Materials and methods.....	60
3.2.1	Literature searching and data selection criteria.....	60
3.2.2	Study selection.....	61
3.2.3	Data extraction.....	61
3.2.4	Data analysis.....	61
3.3	Results.....	61
3.3.1	Study selection.....	61
3.3.2	Image quality assessment.....	65
3.3.3	Radiation dose.....	65
3.3.4	Diagnostic value of DECTA.....	65
3.3.5	Contrast medium assessment.....	66
3.4	Discussion.....	68
3.5	Conclusion.....	70
3.6	References.....	71
Chapter 4	Optimal scanning protocols for dual-energy CT angiography in peripheral arterial stenting: An in vitro phantom study.....	75
4.1	Introduction.....	75
4.2	Experimental Section.....	76
4.2.1	Peripheral artery phantom design and stent placement.....	76
4.2.2	DECT scanning protocols and image reconstruction.....	78

4.2.3	Quantitative image assessment	79
4.2.4	Qualitative assessment of image quality	80
4.2.5	CT dose	80
4.2.6	Statistical Analysis	81
4.3	Results and Discussion	81
4.3.1	Image quality assessment	85
4.3.2	Effect of keV on image quality	86
4.3.3	Effect of GSI and pitch on image quality	87
4.3.4	Effect of stents on image quality	87
4.3.5	Subjective image quality assessment	87
4.3.6	Discussion	92
4.4	Conclusions	93
4.5	References	94
Chapter 5	Dual energy CT angiography of peripheral arterial disease: feasibility of using lower contrast medium volume	97
5.1	Introduction	97
5.2	Materials and methods	98
5.2.1	Patient population	98
5.2.2	CT scanning protocol	99
5.2.3	Qualitative assessment of image quality	100
5.2.4	Quantitative assessment of image quality	100
5.2.5	Radiation dose estimation	101
5.2.6	Statistical analysis	101
5.3	Results	101
5.3.1	Scan time	102
5.3.2	Image quality assessment	106
5.3.3	Radiation dose	108
5.4	Discussion	108

5.4.1	Limitations of the study	116
5.5	Conclusion	117
5.6	References.....	118
Chapter 6	Dual energy CT angiography in imaging peripheral arterial stents: An investigation of optimal scanning protocols with regard to image quality and radiation dose	121
6.1	Introduction.....	121
6.2	Material and methods	122
6.2.1	Patient population and stent characteristics.....	122
6.2.2	DECT scanning protocol	123
6.2.3	Conventional CTA scanning protocol	124
6.2.4	Image reconstruction and image quality assessment.....	124
6.2.5	Radiation dose estimation.....	125
6.2.6	Statistical analysis.....	126
6.3	Results.....	127
6.3.1	Image quality assessment	128
6.3.2	Radiation dose	139
6.4	Discussion.....	139
6.5	Conclusion	141
6.7	References.....	142
Chapter 7	Conclusion and future directions	145
7.1	Conclusion	145
7.2	Future directions	146

List of Figures

2.1.	Mean prevalence of peripheral arterial disease	10
2.2.	Dual-x-ray-source geometry: Independent x-ray tubes, detectors and generators allow simultaneous collection of dual-energy data. Each tube can be operated by using optimal tube current settings and with optimum spectral filtration.	22
2.3.	Fast kilovoltage (kVp) switching: The x-ray tube potential is switched between successive views in either axial or spiral mode. Dual-energy processing can be performed by using projection or image data, with the temporal resolution remaining essentially unchanged.....	22
2.4.	CT numbers of three known materials in low- and high-energy images, plotted on the y- and x-axis, respectively. Unknown materials are then mapped onto this plot to determine the percent composition of each of the three basis materials.....	26
2.5.	The region of interest placed in the inner vessel lumen for measurement of SNR.	35
3.1	Flow chart showing search strategy for identifying eligible studies	62
4.1	Photograph of the phantom with stent insertions	77
4.2	The region of interest was placed in the inner stent lumen for measurement of image noise	80
4.3	Figures A-E show the comparison of noise level at different kiloelectron voltage (keV) with the three preset GSI protocols and three pitch values. Figures F and G represent the mean of CT value in unstented area and all stents with these scanning	83
4.4	A total of 13 stents (No. 7 and 14 were not included due to difficulty placing the region of interest in the area) with axial and coronal reformatted images demonstrated with three GSI protocols and three pitch values at a keV of 65.	85

4.5	A and B are graphic representations showing the noise level when ASIR is used within the both unstented and stented areas, while C and D represent the means of SNR when ASIR is used.....	86
4.6	A-E: A comparison of relationship between noise levels measured with different GSI protocols and pitch values at 65 keV with different diameters of stents. F represents the mean of CT values measured in all stents with the use of three GSI and pitch protocols	90
4.7	Box plots demonstrate the radiologist’s evaluation of the image quality using a 3-point scale	90
5.1	Comparison of CT attenuation and image noise measured at two contrast groups at different body parts with variable keV sets. A: Comparison of the measured CT values in the monochromatic images for the two contrast groups. B: comparison of the measured CT values of three body parts at different keV sets. C: image noise values in the monochromatic images for the two contrast groups. D: comparison of image noise of different body parts at different keV sets.	111
5.2	Comparison of SNR and CNR measured at two contrast groups at different body parts with variable keV sets. Comparison of calculated and measured SNR in monochromatic images with A showing the differences between the two contrast groups at different keV sets, B representing the SNR values of keV sets with three body parts, C showing the comparison of calculated and measured CNR in monochromatic images for the two contrast groups, and D demonstrating the CNR values of three body parts at different keV sets. In the range of 55–65 keV, both of the two curves increase sharply with the gradual rise in keV. Between 65 and 75 keV, both curves of the contrast values decrease sharply with 65 keV, resulting in the highest value.....	114
5.3	DECTA images acquired with different keV values using routine contrast medium. Examples of image quality of DECTA maximum-intensity projection (MIP) are shown in a 53-year-old female with a body weight of 54 kg, using 80 ml of contrast medium. Comparison among DECTA acquisitions in the different virtual monochromatic energies (50, 55, 60, 65, 70 and 75 keV) shows higher image noise at 50 and 55 keV which affects visualisation of the vascular lumen details.	

	VMS images acquired at 65 keV were shown to have better image quality (higher SNR and CNR) than other keVs.	114
5.4	DECTA images acquired with different keV values using low contrast medium. A series of MIP images of DECTA were obtained in a 43-year-old male with body weight of 56 kg using 50 ml of contrast medium in the diagnostic assessment of peripheral arteries. Comparison among DECTA acquisitions in the different virtual monochromatic energies (50, 55, 60, 65, 70 and 75 keV) shows higher image noise at 50 and 55 keV which affects visualisation of the vascular lumen details. VMS images acquired at 65 keV were shown to have better image quality (higher SNR and CNR) compared to the other keVs.	115
6.1	Box-and-whisker plots of image quality. A-D: Comparison between the 4 VMS and conventional CTA of CT attenuation value (HU) and image noise in measured in CIA and SFA stents. Box-and-whisker plots (O, outliers) show difference of image quality in different stent locations.....	136
6.2	A line graph of comparison between the 4 VMS and conventional CTA for stents at CIA and SFA. A and D: CT attenuation (HU) shows the highest CT value at the lower keV; B and E: image noise demonstrates that the lowest image noise was found at 72 keV protocol and the highest image noise at the conventional CTA, followed by 65 keV protocol, and C and F contrast-to-noise ratio (CNR) of CIA shows that CNR decreased with increase in VMS; all the VMS were found to be better than conventional CTA.....	137
6.3	Example of mage quality of multiplanar reformatted images at different VMS of CIA stents at (a) 65 keV (b) 68 keV (c) 70 keV and (d) 72keV. The protocol of 72 keV shows the optimal image quality.....	138

List of Tables

2.1	Comparison of performance parameters of the currently available most advanced dual energy CT scanners.....	20
2.2	A 5 year patency rates observed after different types of endovascular (stent) intervention, and patency rates observed according to the level of revascularisation procedure: iliac, femoro-popliteal and below the knee [3].....	30
3.1	Study characteristics of dual energy CT angiography in peripheral arterial disease.	63
3.2	Contrast protocols used in dual-energy CT angiography in peripheral arterial disease.	67
4.1	Details of the examined stents.	77
4.2	Details of scan parameters by protocols.	79
4.3	Summary of CTDIvol values, dose-length products, and effective doses across the protocols.....	81
4.4	Results of factorial ANOVA.	91
5.1	Patient characteristics and contrast protocols.....	103
5.2	Results of factorial ANOVA	104
5.3	Objective and subjective Image Quality.....	106
5.4	CT value, Image noise, SNR and CNR	108
6.1	Patient characteristics of the study groups.....	129
6.2	Quantitative assessment of image quality based on stents location	131
6.3	Results of ANOVA.....	132
6.4	Quantitative assessment of image quality based on the stents type.....	134

Publications

The thesis is composed of a collection of research papers and posters that were either published, or have been submitted to journals and are currently under review.

1. Almutairi A, Sun Z. Dual energy computed tomography angiography in peripheral arterial imaging: A systematic review of image quality, radiation dose and diagnostic value. *Curr Med Imaging Rev* (accepted 14 April, 2016).
2. Almutairi A, Sun Z, Al Safran Z, Poovathumkadavi A, Albader S, Ifdailat H. Optimal scanning protocols for dual-energy CT angiography in peripheral arterial stents: an in vitro phantom study. *Int J Mol Sci* 2015;16(5):11531–49.
3. Almutairi A, Sun Z, Poovathumkadavi A, Assar T. Dual energy CT angiography of peripheral arterial disease: feasibility of using lower contrast medium volume. *PLoS ONE* 2015;10(9): e0139275.
4. Almutairi A, Sun Z, Al Safran Z, AlZaabi S. Dual energy CT angiography in imaging peripheral arterial stents: an investigation of optimal scanning protocols with regard to image quality and radiation dose. *EJR* (submitted).

Conference presentations

International conferences

1. Almutairi A, Sun Z. Optimal scanning protocols for dual-energy CT angiography in peripheral arterial stents: an in vitro phantom study. The 9th Congress of the Asian Society of Cardiovascular Imaging, 11–13 June 2015, Kuala Lumpur, Malaysia. Moderated poster presentation.

National conferences

1. Almutairi A, Sun Z. Dual energy CT angiography of peripheral arterial disease: can we reduce the contrast medium volume? WA branch meeting and student papers night, Perth, Australia, 10 November 2015. Oral presentation.
2. Almutairi A, Sun Z. Dual energy CT angiography of peripheral arterial disease: investigation of image quality and radiation dose using lower contrast medium volume. Annual Scientific Meeting of Medical Imaging and Radiation Therapist Conference (ASMMIRT), 22–24 April 2016, Brisbane, Queensland. Oral presentation.

List of abbreviations

ABI	Ankle brachial index
ADMIRE	Advanced modelled iterative reconstruction
AIDR-3D	Adaptive iterative dose reduction 3D
ANOVA	Analysis of variance
ANCOVA	Analysis of covariance
ASIR	Adaptive statistical iterative reconstruction
BMI	Body mass index
CE-MRA	Contrast-enhanced magnetic resonance imaging
CIA	Common iliac artery
CIN	Contrast-induced nephropathy
CNR	Contrast to noise ratio
CT	Computed tomography
CTA	Computerised tomography angiography
CTDI	CT dose index
CTDI _{vol}	Volume CTDI
CTDI _w	Weighted CT dose index
DECT	Dual energy computed tomography
DECTA	Dual energy computed tomography angiography
DLP	Dose-length product
DM	Diabetes mellitus
DSA	Digital subtraction angiography

DSCT	Dual source computed tomography
DS-DECT	Dual-source dual energy computed tomography
DU	Duplex ultrasound
E	Effective dose
EIA	External iliac artery
FBP	Filtered back projection
FOV	Field of view
GSI	Gemstone spectral imaging
IR	Iterative reconstruction
IRIS	Iterative reconstruction in image space
HU	Hounsfield units
keV	kiloelectron volt
kVp	Peak kilovoltage
mA	Milliamperere
mAs	Milliamperere second
MBIR	Model based iterative reconstruction
MDCT	Multidetector computed tomography
MDCTA	Multidetector computed tomography angiography
MEIs	Monochromatic energy images
mGy	Milligray (absorbed radiation dose)
MIP	Maximum intensity projection
MPR	Multi-planar reconstruction
MRA	Magnetic resonance angiography

MRI	Magnetic resonance imaging
MSAD	Multiple scan average dose
PAD	Peripheral arterial disease
PEI	Polyenergetic images
ROI	Region of interest
SAFIRE	Sinogram affirmed iterative reconstruction
SD	Standard deviation
SFA	Superficial femoral artery
SNR	Signal-to-noise ratio
SS-DECT	single-source dual energy computed tomography
VMS	virtual monochromatic spectral
VR	Volume rendering

Chapter 1 General introduction

1.1 Background

Peripheral artery disease (PAD) is a common sign of atherosclerosis. PAD is one of the main diseases that affects large and middle-sized arteries in the human body. The location of atherosclerosis lesions in lower extremities is concentrated in the intima, and the pathologic feature of atherosclerosis is foam-cell formation. PAD prevalence is linked with age advancement [1,2]. When PAD becomes lifestyle-restricting, a revascularisation procedure is considered after a diagnostic imaging work-up. Common revascularisation methods are angioplasty and stent implementation for artery stenosis and occlusions in peripheral arteries [3,4]. However, as restenosis is usually found after the first year of stent implementation, follow-up examinations are essential to detect any restenosis and plan appropriate treatment before the stents are fully occluded [5]. Conventional digital subtraction angiography (DSA) is the standard follow-up procedure [6], but this is invasive and expensive, often causes complications, and does not provide information about the tissue surrounding the vessels.

A range of less invasive and more affordable techniques have been developed during the last decade, including doppler ultrasound (DU), magnetic resonance angiography (MRA) and computed tomography angiography (CTA) [7]. DU is time-consuming, does not provide an overview of the affected area, and its effectiveness is dependent on the operator's experience [8]. MRA as a follow-up procedure may be limited if there is a signal decrease or loss caused by metallic stents; other contraindications include such things as a pacemaker, implanted metal, or a claustrophobic patient [9]. CTA has become accepted as a robust alternative to invasive DSA for the diagnostic and evaluation of PAD. It plays an important role in vascular imaging because of its high temporal, spatial and contrast resolution as well as its wide availability. In addition, the optimal image quality of computed tomography (CT) imaging results in superior spatial and contrast resolution. However, in vascular imaging, CTA is limited by its high radiation dose and its inability to reliably differentiate between attenuation caused by a high intravascular iodine concentration and that caused by calcium [10, 11].

The main limitation on reducing radiation dose in CT is the resulting degradation of image quality caused by increased noise and reduced spatial resolution. If these limiting factors can be reduced or eliminated, CTA will become a viable replacement for conventional

angiography in the regular assessment of stent patency [12], as improvement of CT technology in both hardware and software will lead to lower radiation dose and better image quality.

In recent years, various technological advances have been introduced to address the problems noted above. Dual energy computed tomography (DECTA) is one of the latest forms of CTA: based on the application of two different X-ray energies during the scan, iodine can be differentiated from calcification and other materials [13]. Further advantages of DECTA are (a) optional bone removal from images, (b) reduction of metal artefacts in images and (c) tissue re-composition quantification for better diagnostic accuracy [6].

Although DECTA qualifies as a valuable diagnostic tool for a stenting intervention follow-up, the radiation dose delivery to patients is high at present and may lead to cancer in the future; lowering the radiation dose is therefore paramount.

A range of dose optimisation techniques has been developed to address the problem of radiation risk from DECTA such as uses of low X-ray tube potential (kVp) and special scan and image reconstruction modes [14]; but their uses may have negative effects on image quality leading to inaccurate diagnosis because radiation is the source of the signal for structure visualisation and dose reduction weakens this signal for imaging, which may affect the diagnosis. The most common tube potential used in DECTA is 80 and 140 kVp, although other kVp can be selected from 70 to 100 kVp for low energy and 140 or 150 kVp for higher energy. As CT radiation exposure is approximately proportional to the square of the tube potential, a dose reduction can be obtained when lowering kVp and increasing the pitch values but image noise increases accordingly [15]. A range of iterative image reconstruction algorithms are usually available in the latest DECT scanners for use in conjunction with different dose reduction techniques, which offset their negative effect on image quality [5,6]. Recently, peripheral stents which have a lower atomic number, made by less dense materials and with thinner struts such as stainless steel (316 L) and Nitinol, reduce the chance of having metal artefacts [5]. In addition, extrapolating from the coronary literature, if peripheral CTA is performed at sub-millimetre resolution at least for larger stents, it should perform well in terms of blooming artefact reduction [14]. This may compensate for any degradation in image quality when used with dose reduction techniques and even achieve a better image quality, improving diagnostic accuracy.

Previous studies have explored the effect of individual dose optimisation techniques in peripheral arterial stenting imaging [15,16]. However, intertwining effects between different factors such as lowering tube potential with special scan mode and the newer image reconstruction algorithm for dose optimisation are not well demonstrated. This indicates that

a comprehensive study to determine the feasibility of use of a range of techniques for radiation dose optimisation in DECTA for peripheral stenting imaging is necessary.

1.2 Study aims and objectives

This study aims to optimise the scanning protocol for DECTA in peripheral artery stenting to improve image quality and to reduce the radiation dose level. The specific objectives of this study are to address the following:

1. Identify factors (machine related) that affect the image quality (including visualisation of stent lumen) and the radiation dose.
2. Improve the scanning protocol according to the identified factors.
3. Test the quality of images that are produced using the new imaging protocol.
4. Apply the new scanning protocol in experimental and clinical settings.

This study intends to lead to a reduction in the radiation dose delivered to patients and will therefore allow for safer use of DECTA as a follow-up examination for peripheral artery stenting. This will reduce the number of patients suffering from procedural complications associated with conventional angiography and furthermore help to minimise the risk of radiation-induced cancer. An improved DECTA procedure will likely reduce costs associated with the management of peripheral artery disease. This study will also pave the way for future studies in various body parts beyond the scope of this study.

1.3 Thesis structure

This thesis is subdivided into seven chapters. The manuscript consists of a series of research publications. The relationships between these chapters and the research papers are presented in the introductory and concluding chapters, where they are placed in a wider context. Because all chapters are stand-alone manuscripts, their formats may differ based on the requirements and formatting guidelines of each individual journal. In addition there is a small amount of unavoidable repetition, specifically in the methodology sections.

Chapter One (this chapter) starts with an overview highlighting the importance of controlling peripheral arterial disease, and its prevalence among elderly population. It is followed by general information about the peripheral arterial disease management and imaging modalities used to diagnose and evaluate PAD. Finally, the goals of this study and thesis structure are outlined.

Chapter Two is a literature review including an overview of the background to this study and different imaging modalities, with focus on the use of computed tomography technology, its application to lower extremities imaging and its limitations. The principles of DECT and vascular application are also covered in this chapter. Peripheral arterial stents and the role of DECT on stents evaluation is also discussed, as are a wider range of factors affecting radiation dose and image quality on DECT angiography.

Chapter Three offers a systematic review of identification of factors influencing image quality and radiation dose of DECTA in peripheral stenting, used as an indicator for devising potential dose saving scanning protocols. The outcomes from Chapters 2 and 3 are used to devise the suitable dose saving scanning protocols.

Chapter Four is a phantom experiment on peripheral arterial stents evaluation using DECTA. A peripheral arterial phantom is manufactured to simulate normal lower extremities anatomy with different types and diameter stents and verified on DECT, to devise optimum DECTA scanning protocols for peripheral arterial stents.

Chapter Five is a prospective study investigating image quality between two groups of patients with routine and low contrast volume for lower extremities DECTA using the proposed protocol based on Chapters 2 and 3 and presented in Chapter 4.

Chapter Six is a prospective study derived from the optimal scanning protocol that was devised from the phantom study in Chapter 4. Four different virtual monochromatic spectral images are compared with conventional CTA to find the optimal DECTA protocol for peripheral arterial stents.

Chapter Seven summarises the key findings and significances of this study. It provides links between the individual chapters originally presented as manuscripts. Finally, it outlines the implications of this study and recommendations for future studies.

1.4 References

1. Rosamond W, Flegal K, Furie K, Go A, Greenlund K, Haase N et al. Heart disease and stroke statistics—2008 update: a report from the American Heart Association Statistics Committee and Stroke Statistics Subcommittee. *Circulation* 2008; 117(4):25–146. Available from: <http://search.proquest.com/docview/70235515?accountid=10382>.
2. Norgren LH, Hiatt WR, Dormandy JA, Nehler MR, Harris KA, Fowkes FGR, Rutherford RB. Inter-society consensus for the management of peripheral arterial disease. *Int Angiol* 2007; 26(2):81–157.
3. Rooke TW, Hirsch AT, Misra S, Sidawy AN, Beckman JA, Findeiss LK et al. 2011 ACCF/AHA focused update of the guideline for the management of patients with peripheral artery disease (updating the 2005 guideline). *Vasc Med* 2011; 16(6):452–76. Available from: <http://search.proquest.com/docview/907240719?accountid=10382>.
4. Tapping C, Ahmed M, Scott P, Lakshminarayan R, Robinson G, Ettles D et al. Primary infrarenal aortic stenting with or without iliac stenting for isolated and aortoiliac stenoses: single-centre experience with long-term follow-up. *Cardiovasc Intervent Radiol* 2013:1–7. doi:10.1007/s00270-012-0372-6.
5. Köhler M, Burg MC, Bunck AC, Heindel W, Seifarth H, Maintz D. Dual-Source CT angiography of peripheral arterial stents: in vitro evaluation of 22 different stent types. *Radiol Res Pract* 2011; doi:10.1155/2011/103873.
6. Brockmann C, Jochum S, Sadick M, Huck K, Ziegler P, Fink C et al. Dual-energy CT angiography in peripheral arterial occlusive disease. *Cardiovasc Intervent Radiol* 2009; 32(4):630–7. Available from: <http://search.proquest.com/docview/227373922?accountid=10382>.
7. Napoli A, Anzidei M, Zaccagna F, Cavallo Marincola B, Zini C, Brachetti G et al. Peripheral arterial occlusive disease: diagnostic performance and effect on therapeutic management of 64-section CT angiography. *Radiology* 2011; 261(3):976–986. doi:10.1148/radiol.11103564.
8. Josephs SC, Rowley HA, Rubin GD, 3 fWG. Atherosclerotic peripheral vascular disease symposium ii: vascular magnetic resonance and computed tomographic imaging. *Circulation* 2008; 118(25):2837–2844. doi:10.1161/circulationaha.108.191173.
9. Li X-m, Li Y-h, Tian J-m, Xiao Y, Lu J-p, Jing Z-p et al. Evaluation of peripheral artery stent with 64-slice multi-detector row CT angiography: prospective comparison with digital subtraction angiography. *Eur J Radiol* 2010; 75(1):98–103. doi:http://dx.doi.org/10.1016/j.ejrad.2009.03.032.
10. Langenberger H, Schillinger M, Plank C, Sabeti S, Dick P, Cejna M et al. Agreement of duplex ultrasonography vs. computed tomography angiography for evaluation of native and in-stent SFA re-stenosis—findings from a randomized controlled trial. *Eur J Radiol* 2012; 81(9):2265–2269. Available from: <http://search.proquest.com/docview/1033155774?accountid=10382>.

11. Kiernan TJ, Hynes BG, Ruggiero NJ, Yan BP, Jaff MR. Comprehensive evaluation and medical management of infrainguinal peripheral artery disease: ‘when to treat, when not to treat’. *Tech Vasc Interv Radiol* 2010; 13(1):2–10. Available from: <http://search.proquest.com/docview/733886641?accountid=10382>. 15.
12. Langenberger H, Schillinger M, Plank C, Sabeti S, Dick P, Cejna M et al. Agreement of duplex ultrasonography vs. computed tomography angiography for evaluation of native and in-stent SFA re-stenosis—findings from a randomized controlled trial. *Eur J Radiol* 2012; 81(9):2265–2269. Available from: <http://search.proquest.com/docview/1033155774?accountid=10382>.
13. Coursey CA, Nelson RC, Boll DT, Paulson EK, Ho LM, Neville AM et al. Dual-energy multidetector CT: how does it work, what can it tell us, and when can we use it in abdominopelvic imaging? *Radiographics* 2010; 30(4):1037–1055. doi:10.1148/rg.304095175.
14. Uhrig M, Simons D, Kachelriess M, Pisana F, Kuchenbecker S, Schlemmer HP. Advanced abdominal imaging with dual energy CT is feasible without increasing radiation dose. *Cancer Imaging*. 2016; 16(1):15. DOI:10.1186/s40644-016-0073-5.
15. Zhang LJ, Wu SY, Niu JB, Zhang ZL, Wang HZ, Zhao YE, et al. Dual-energy CT angiography in the evaluation of intracranial aneurysms: image quality, radiation dose, and comparison with 3D rotational digital subtraction angiography. *AJR Am J Roentgenol*. 2010; 194(1):23-30. DOI:10.2214/ajr.08.2290.
16. Duddalwar VA. Multislice CT angiography: a practical guide to CT angiography in vascular imaging and intervention. *Br J Radiol* 2004; 77(suppl 1):S27–S38. doi:10.1259/bjr/25652856.

Every reasonable effort has been made to acknowledge the owners of copyright material. I would be pleased to hear from any copyright owner who has been omitted or incorrectly acknowledged.

Chapter 2 Literature review

This chapter reviews the literature and previous research on peripheral arterial disease, aiming to cover the first and second objectives of this study, and comprises eight sections pertaining to the following topics:

1. An introduction to the aetiology, risk factors, diagnosis, treatment and worldwide prevalence of PAD.
2. A review of previously published research on different imaging modalities used for diagnosing and evaluating PAD, compared to the gold standard technique. The topics of discussion include the development of CT technology as a diagnostic tool for the evaluation of PAD and the outcomes of multidetector and dual energy CT for assessing PAD of the lower extremities.
3. An introduction to the quantitative aspects of CT like radiation dose effects, quantities and measurements.
4. The application of the stent in peripheral arteries, common locations and primary patency. This section reviews research literature related to the efficacy of DECT in the evaluation of peripheral arterial stents.
5. The use of contrast medium in lower extremities and its optimisation with DECT.
6. Details about image quality.
7. Factors influencing radiation dose and image quality in DECT.
8. Summary of the review of literature.

2.1 Introduction

2.2 Peripheral artery disease

Aetiology – prevalence – risk factors – diagnosis – treatment

Peripheral artery disease is one of the manifestations of atherosclerosis in the cardiovascular system, and usually occurs due to the formation and development of plaques, the result of accumulation of lipids and fibrous elements in the vessel walls [1]. PAD is the third most common vascular disease in the world and a common healthcare problem in developed countries, affecting more than 200 million individual globally, including ten to 16% of patients belonging to the age group 70 years and above [2]. Figure 2.1 shows that the incidence of PAD increases with age [3]. By year 2020, it is estimated, PAD will become the primary cause of death [4]. Furthermore, it is linked independently with cardiovascular

disease morbidity and mortality [5]. Between 2000 and 2010, the prevalence of PAD has increased about 25% worldwide, which qualifies it to be classified as a high risk disease [2].

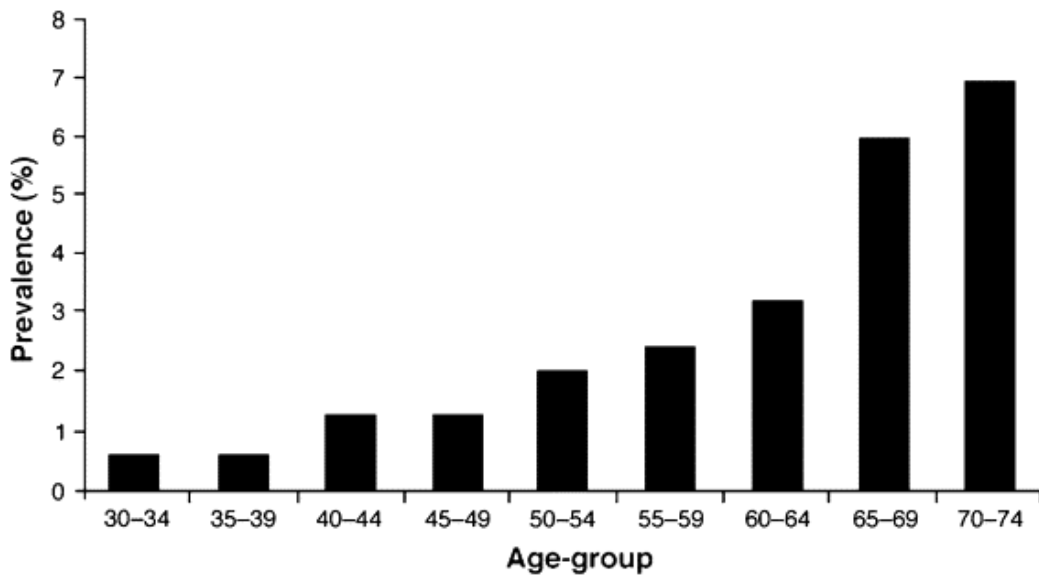


Figure 2.1. Mean prevalence of peripheral arterial disease

Reprinted with permission from Norgren L et al. [3]

The risk factors for PAD are similar to those for atherosclerosis: gender, age and smoking history of patients, and a history of diabetes, hypertension and hyperlipidaemia [6].

Diagnosis of PAD is usually initiated with a physical examination, and an accurate record of the patient's history. When PAD is suspected, the ankle brachial index (ABI) base line test confirms the diagnosis and predicts the severity of the disease [7]. Because of the limitations of ABI, diagnostic imaging is preferentially performed in patients who are at risk of atherosclerosis and require further evaluation, particularly patients with heavily calcified vessels [8]. Peripheral stenosis greater than 50% usually requires intervention revascularisation. Stent implementation or balloon angioplasty is the common corrective procedure to treat stenosis of the occluded PAD, making diagnosis of PAD possible through different imaging modalities and greatly reducing the need for investigative surgery, which was formerly essential for evaluation of this disease. These new modalities have replaced most of the old procedures.

2.3 Imaging modalities in the diagnosis of PAD

Planning of revascularisation procedures requires accurate mapping of the affected vessels. According to Rofsky et al. [9], it is essential to characterise both inflow and outflow from a lesion when planning lower extremity intervention. Recent developments in peripheral

arteries imaging technology present a wide range of diagnostic imaging modalities that facilitate proper management of the affected vessels, a feature that is vital for planning and evaluating intervention procedures in patients with PAD. The imaging modalities available for PAD diagnosis include conventional DSA, DU, magnetic resonance imaging (MRI), and CTA. In the following pages, each imaging technique is reviewed from the perspective of its diagnostic value and limitations.

2.3.1 Digital subtraction angiography

Digital subtraction angiography is an invasive procedure that requires catheterisation of the arterial system to introduce the contrast medium into the blood vessels, by either intravenous or intra-arterial administration [10]. Intra-arterial administration is preferred because intravenous administration results in dilution of the contrast medium. DSA is now performed only as part of an endovascular intervention. The technique offers high-resolution and high-contrast 2D images with very high diagnostic accuracy, and is widely accepted as the reference standard for vascular imaging [11].

DSA has some disadvantages, which include invasiveness, risk of complications, potential contrast nephrotoxicity of iodinated contrast agents, mainly in patients with pre-existing renal impairment, allergic reactions to the contrast agent, and high radiation exposure of patients as well as staff. It is also expensive and time-consuming. To overcome these difficulties, DSA is being increasingly replaced by less invasive imaging modalities such as Doppler ultrasound, magnetic resonance angiography and multidetector CT angiography.

2.3.2 Doppler ultrasound

Duplex ultrasound refers to the examination of Doppler flow patterns in a specifically defined part within the vessel lumen, to identify the localisation of arterial stenosis. In the presence of stenosis, the DU flow pattern is graded by the ratio between (a) the peak systolic velocity of the abnormal vessel and (b) adjacent or contra-lateral normal vessels [12]. Although DU does not provide a direct overview of the suspect vessels, the ultrasound operator can draw up an illustration and succeed in distinguishing those patients requiring angioplasty from those requiring surgical reconstruction [13, 14].

DU is used as a non-invasive imaging technique that provides both anatomical and functional information about PAD. It is also useful for following up angioplasty procedures in PAD patients [8]. The addition of colour flow imaging greatly improves the diagnostic performance of DU for evaluating aortoiliac and femoropopliteal arteries [15]: a lack of visibility of the colour Doppler signal in the vessel is suggestive of arterial occlusion. The assessment of lower limb vessels by DU, however, is time consuming and sometimes technically challenging, leading to an incomplete evaluation of a patient's peripheral arterial system.

2.3.2.1 Diagnostic accuracy

In PAD patients with more than 50% of stenosis or occlusion in the lower extremities, DU has a high sensitivity, ranging from 81% to 95%, and moderate specificity ranging from 88% to 84% [16]. In contrast, a recent study evaluating superficial femoral artery (SFA) for in-stent re-stenosis reported sensitivity and specificity values of 88% and 84% respectively [16]. Baril et al. [17] compared SFA with DSA, for the identification of stenosis >80%, and reported high sensitivity (94%) with moderate specificity (74%). In their study, Krnic et al. [18] demonstrated the wide range of sensitivity displayed by DU when detecting significant arterial stenosis (46% to 88%). Low sensitivity (72%) was observed for significant obstruction detection in the pelvic region [18]. The accuracy of DU can be markedly improved, depending on the operator's experience; it follows, therefore, that the diagnostic accuracy of DU in PAD is highly operator-dependent, necessitating caution during interpretation modality.

2.3.2.2 Limitations

Despite its safety and efficacy, DU suffers from several major drawbacks: its diagnostic accuracy may be restricted in some vascular territories, e.g., iliac arteries affected by twisted arterial anatomy or the existence of bowel gases. Moreover, the method is extremely operator dependent [19]. The presence of acoustic shadow limits its efficacy in identifying calcified vessels [20]; visualisation with DU is also restricted by stented calcified vessels. Furthermore, the procedure is time-consuming, does not provide a complete overview of the affected area, is dependent on the operator's experience and patient's body habitus for its reproducible documentation [19, 21, 22], and does not offer an accurate roadmap or detailed description of the length, severity, or type of the diseased portion of the vessel for the planning of possible re-interventions [23].

2.3.3 Magnetic resonance angiography

Over the past 20 years, the non-invasive technique of MRA has been increasingly used for confirming the diagnosis of suspected PAD. This technique uses strong magnetic fields to create cross-sectional images of different body regions. The use of MRI scanners for angiographic procedures does not expose the patient or operator to radiation. The dynamic imaging associated with MRA facilitates the evaluation of blood flow [24], and the direction and velocity of arterial blood flow can be visualised by phase-contrast MRA [25]. Peripheral MRA examination is applicable not only for the evaluation of vessels but also for the assessment of the anatomy and functioning of the surrounding areas [26].

Both contrast-enhanced magnetic resonance imaging (CE-MRA) and non-contrast-enhanced MRA can be employed to generate angiographic images. Although non-contrast MRA is a safe option, it has some technical snags, and CE-MRA is more accurate for stent evaluation. CE-MRA was first introduced into clinical practice in the early 1990s [27] but, owing to hardware limitations of MRI scanners at that time, the technique was not used for the lower extremities until the late 1990s [24]. The characteristics of the CE-MRA technique have come to be the backbone of clinical MRA, but if a patient shows contraindications for its use, an alternative imaging modality should be sought for the patient's benefit.

2.3.3.1 Diagnostic accuracy

Performing peripheral MRA prior to intervention procedures achieves a sensitivity of 98% (range 92–100%), and a specificity of 96% (range 91–99%), for the detection of $\geq 50\%$ arterial stenosis [25, 26, 28, 29]. A recent study of stent evaluation with CE-MRA using gadofosveset as the contrast medium concluded that both sensitivity and specificity were $>95\%$ for superficial femoral artery in-stent re-stenosis [30]. Notwithstanding these excellent results, MRI is not suitable for patients with contraindications for this procedure. In addition, stents cause susceptibility artefacts on the T1 weighted and CE-MRA, and the severity of artefacts depends on the stent material, geometry and size [31]. Accordingly, in most cases, in-stent re-instenosis cannot be accurately measured using MR angiography.

2.3.3.2 Limitations

The major drawback of MRA as a follow-up procedure for peripheral stents is that a decrease or loss in signal may well be caused by metallic stents, leading to inaccurate evaluation of vessel or stent patency [31, 32]. Nor can MRA visualise arterial calcifications, so if a surgical bypass is the appropriate decision, it could become a limitation for the selection of the anastomotic site [33]. Another issue is the length of time required to

complete the procedure. Moreover, the smaller field of vision required to perform an MRA scan in three phases, to cover the lower limbs, may lead to venous contamination [15, 34].

There are several contraindications for MRI, including pacemakers, claustrophobia, metal implants, neuro stimulating devices, otological implants, and the unsuitability of gadolinium contrast in patients with renal insufficiency [35, 36]. Since obesity is considered to affect optimal accuracy with MRA, the smaller diameter-size of the magnet bore represents another limitation [33].

2.3.4 Computed tomography angiography

2.3.4.1 Technological developments of CT angiography

Since the introduction of computerised tomography in 1972, it has become the imaging modality of choice for the evaluation of a number of diseases [37]. Many generations of CT scanners have been developed over the years, ranging from single-slice to multi-slice CT (4-slice to 320- and 640-slice), and single detector to multidetector CT, revolutionising the field of clinical imaging the world over. Slip ring technology plays a critical role in this revolution by enabling the continuous rotation of CT gantry for one second. As a result of its higher spatial and temporal resolution, scanning of the lower extremities is achieved in a very short time. The past few decades have witnessed rapid developments in CTA procedures with respect to many body regions. Several attempts have been made to validate CTA as a less invasive modality than, and more appropriate alternative to, conventional DSA for the mapping and evaluation of the vascular tree [19, 38, 39].

Modern CTA scanners are accurate, robust, cost effective and less invasive imaging instruments to be used in patients with coronary or arterial diseases. The inadequacies of earlier modalities succeeded in sparking the development of multi-detector computerised tomography angiography (MDCTA) as an alternative method for evaluating peripheral arterial disease [23, 32]. In comparison with DU and DSA modalities, CTA provides 3D datasets which open up more options while processing diagnostic images with high accuracy. Compared to MRA, the spatial resolution of CTA is much higher with a voxel size of 0.35 x 0.35 x 0.35 mm³ available with contemporary scanners. Additionally, the cost effectiveness, protocol reproducibility, availability of MRA scanners, and experienced staff gives the CTA an edge over others to become the modality of choice for lower extremities imaging.

2.3.4.1.1 MDCT

CT reached its peak in the early part of this century, and is today considered a routine diagnostic modality. The introduction of spiral CT has given a new impetus to manufacturers to invest in this technology. The 4-slice multi-detector computed tomography (MDCT) was introduced in 1998, followed by the 16-slice and 64-slice systems in 2001 and 2004 [40]. It overcame the limitation of longitudinal coverage, enabling CTA of the lower extremities [41, 42]. To fulfil the objective of reducing scanning time, manufacturers became creative: improvements in this modality were reflected in a high spatial and temporal resolution in CT, resulting in significant isotropic resolution levels and fast scanning equitation. Research literature reports the high diagnostic accuracy of CTA in many of the cardiovascular diseases, including PAD.

2.3.4.1.2 Peripheral CT angiography by MDCT

MDCT, or Multislice CT as it is also known, performs peripheral CTA efficiently, acquiring high resolution quality images within a short time. This technique involves the simultaneous injection of contrast medium via proper veins to achieve opacification of the arterial system. Scanning protocol relies on specific scanning parameters such as tube potential, amperage, gantry rotation time and table increment, coupled with contrast injection parameters like injection rate and injection duration.

Scanning protocols vary from one CT scanner manufacturer to another. Reconstruction parameters for peripheral CTA include field of view (FOV), reconstruction kernels, slice thickness, and interval. The interval chosen in CTA scanning is usually smaller than the slice thickness; this produces an overlap of up to 50%, and generates reformat images inclusive of volume rendering, 3D and multiplanar reconstruction images. A disadvantage of MDCT is that image quality is slightly reduced, with an increase in the number of parallel slices because of scattered radiation and cone beam artefacts [43].

2.3.4.1.3 4- and 8-slice CT

The design of detector arrays is the main feature differentiating the single-slice CT from the MDCT. The clinical applications of CT took a significant leap with the advent of four-slice CT scanners in 1998. These were designed with a parallel row of detectors in the z-direction, connected as a single detector to provide flexibility in slice thickness of the four obtained slices [44]. Initially there were two types of 4-slice MDCT detector: the fixed-array detector with equivalent size in the longitudinal direction consisting of detector elements, and the adaptive-array detector with different-sized detector rows in the longitudinal direction.

These technologies allowed for a thinner slice thickness, with beam collimation of 4×2.5 mm, pitch of 1.5 and gantry rotation time of 0.5s, affording a coverage speed of 30 mm/s. The shorter time and thinner slice thickness facilitated scanning of the lower extremities, and improved the visualisation of 3D images and MPR [45]. Overlapping image reconstruction resulted in an adequate visualisation of the main peripheral arteries, and promoted the assessment of medium artery branches in the presence of minimum calcification [46]. The technical limitation for the 4-slice MDCT was the decreased z-axis resolution, which lengthened the scan time and caused discomfort to patients with mild or no inflow due to severe PAD [45, 47]. In 2000 the 8-slice MDCT was introduced to overcome the limitations of the 4-slice version, but despite the shorter scan time, the longitudinal resolution remained challenging.

2.3.4.1.4 16-slice CT

The encouraging results of clinical CTA spurred CT vendors to develop faster gantry revolution times to increase volume coverage and overcome this limitation of the earlier models: the 16-slice-CT emerged in 2002. Its improved features like the provision of near isotropic resolution data and marked reduction of time acquisition allowed for high quality procedures in lower extremities CTA [46]. These scanner systems used only adaptive array detectors [40] and improved volume coverage up to 27.5 mm/s using gantry rotation time, and 16×0.625 mm or 16×0.75 mm collimation, depending on individual manufacturer. The 16-slice achieved better longitudinal resolution for peripheral CTA than the 4- and 8-slice CTs [42]; visualisation of small arterial branches in the lower limb was vastly improved. However, image noise and high radiation dose were observed with this scanner, especially in the abdominal and pelvic regions.

2.3.4.1.5 64-slice CT and beyond

The 64-slice CT was introduced in 2004, with a single X-ray tube mounted opposite the detector array in the gantry [40]. Temporal resolution had been improved with a gantry rotation time of 0.33 seconds; scanning time was consequently reduced, permitting better utilisation of the contrast medium. The 64-slice CT scanner brought isotropic image voxels closer to reality: a minimum voxel dimension of 0.4 to 0.6 mm in the z-axis was attainable with a collimation of 64×0.625 and a volume coverage speed of 32 mm/s, resulting in a total coverage of 4 cm. Improved image quality with high sensitivity and specificity was evident in most cardiovascular procedures. A lower degree of invasiveness, higher accuracy and shorter procedural time makes this the preferred method for evaluation of PAD in the lower extremities [48]. However, radiation exposure is a serious concern with the 64-slice

scanner and needs to be addressed. In particular, the radiation dose must be preserved in the context of the average annual background radiation, which is approximately 2–5 mSv [49].

2.3.4.1.6 CTA accuracy in PAD

CTA is commonly used as an alternative to DSA in most arterial studies, due to its less invasive nature, cost effectiveness and high diagnostic value. As a result of its high accuracy, CTA has been confirmed as the method of choice for aortic artery evaluation [50]. Likewise, a considerable amount of literature has been published on the accuracy of CTA to evaluate PAD [45, 51-55]. In a study that set out to determine the accuracy of 64-slice CTA in peripheral arteries, Shareghi et al. [51] found its accuracy to be about 98%, compared to DSA. In another study, Ota et al. [54] reported a 99% accuracy using 4-slice CT for peripheral arterial CTA. Loswed et al. [55] used a 16-slice CT scanner for detecting more than 50% of stenosis in peripheral arterial disease, and reported a sensitivity and specificity of 100%.

A meta-analysis by Sun [45] of relevant published articles between 2003 and 2005 found that, at all arterial levels, the use of 4-slice and 16-slice CTs for peripheral arterial evaluation displayed an accuracy of 91%. More recently, Met et al. [42] summarised the literature published from 1980 to 2008 in a systematic review and meta-analysis of MDCT scanners with 2 to 64 detector rows, and concluded that the overall sensitivity and specificity of peripheral CTA for detecting either stenosis greater than 50%, or occlusion, were 95% and 96%, respectively.

A recent single-centre study compared the diagnostic performance of the 64-slice CTA with DSA, for the detection of stenosis >70% on a per segment basis. CTA achieved a sensitivity of 99%, a specificity of 97% and an accuracy of 98% [56]. In a more recent systematic review and meta-analysis, Jens et al. [28] evaluated the diagnostic accuracy of CTA for identifying significant stenosis and occlusions, and reported values in the range of 92–97% and 93–98%, respectively, with summary estimates of 96% and 95% for sensitivity and specificity, in that order [28].

More specifically, early studies of the accuracy of CTA for the evaluation of peripheral stents revealed that the 4-slice CT yielded suboptimal results [42, 57]. Although the 16-slice CT produced more favourable results, its application was limited by its insufficient spatial and temporal resolution [51]. These shortcomings were overcome with the introduction of the 64-slice CT. In a study evaluating peripheral arterial stents, Li et al. [32] reported sensitivity values of 95.4% and 96.4%, and specificity values of 100% and 98.2%, with a 64-slice CT scanner. Despite the proven accuracy of CTA in peripheral arteries, its use was

restricted because of beam hardening phenomena from vessel wall calcification, stent struts and adjacent bones. The quest to overcome these obstacles has led to the exploration and emergence of dual-source CT/dual energy CT, capable of using dual sources of energy.

2.3.4.2 Dual source CT

Recent developments in the field of CT scanners have rekindled interest in CTA applications. In this respect, one of the most important achievements of this century is the introduction of dual-source computed tomography (DSCT) in an attempt to overcome the limitations of the temporal resolution of conventional CT; it is now one of the most promising radiological diagnostic techniques [58]. Low-dose CTA has grown into an efficient, less invasive tool for the diagnosis of vascular disease with DSCT. The emergence of this technology paves the way for more anatomic and functional details with CT applications. A DSCT system offers image acquisition techniques that go beyond conventional CT, such as scanning that obeys patients. It deserves mention that improvements in CT technology did not stop at this point: DSCT-first generation entered the picture in 2006, complete with multiple-energy image acquisition for clinical applications [59].

DSCT was developed by Siemens Healthcare (Forchheim, Germany), based on two x-ray tubes (Fig. 2.2) to produce high and low energies of 140/80 for Somatom Definition (1st generation), 140/100 for Somatom Definition Flash (2nd generation), and subsequently Somatom Force (3rd generation) [60]. All DSCT scanners consist of two X-ray tubes and two parallel detectors with an angular offset of 90–95° [59, 61]. Each detector comprises an adaptive array of 40 rows. Both tubes can function independently with regard to kVp and mA settings as a single scanner. For the non-DECT procedure the second-generation kVp offers five options starting with 70 kVp, while in the third generation selection can be made from nine options of kVp ranging from 70 to 150 kVp (in 10-kVp increments). The third generation of DSCT launched in 2013 (Somatom Force), showed significant improvement in the temporal resolution to reach 66 ms. This model boasted of the following improvements: increase in slice thickness to 192 slices with rotation time up to 0.25 sec; increase in FOV to 35.5 cm for detector B, and a new X-ray filter ‘Sn filter’ in both tubes in turbo flash mode [62]. The X-ray tube power was stepped up to 120 kW for both tubes, enabling tube current up to 1300 mA at low kVp values [62], and there was a resultant improvement in temporal resolution for cardiovascular imaging with DSCT systems. In addition, DSCT introduced the use of dual energy applications with the use of low and high energies to achieve a large range of energy spectra [63].

2.3.4.3 Dual energy CT

The birth of DECT added impetus to the development of MDCT in the last decade, making it one of the most exciting and promising breakthroughs in medical imaging technology.

DECT added functional evaluation to the standard examination based on X-ray attenuation that is usually obtained in CT examination. It was originally initiated by Godfrey Hounsfield in 1973 when two images of the same slice were taken with different kVp to enhance the area with high atomic number [64]. Several technical snags meant it could not be used for clinical application, but the recent revolution in CT technology has revived interest in DECT [65-67], one of the latest forms of DSCT. The basic principles of DECT are not new: as early as 1973 Hounsfield described the use of two different kVp in the same location, and reported that the atomic numbers on images taken at low energy had higher values [64].

In current clinical practice there are two types of dual-energy computed tomography (DECT): dual-source (DS-DECT) and single-source (SS-DECT) (Table 2.1). The underlying principle of these systems is to differentiate materials based on the physical X-ray interactions with these materials. Both modalities, DS-DECT and SS-DECT, have advantages as well as limitations, and there are a number of important differences between them. The two systems can be used in both conventional and dual energy CT. The main concept of both types is the use of high and low energies, such as 80 or 100 and 140 kVp [65, 68, 69]. Details of dual energy specifications and application are given in the following sections.

Table 2.1 Comparison of performance parameters of the currently available most advanced dual energy CT scanners

Specifications	64-slice dual source (Definition)	128-slice dual source (Definition Flash)	192-slice dual source (Somatom Force)	64-DECT (Discovery 750HD)	Philips IQon CT
Detector configuration	2 x 32 x 0.625	2 x 64 x 0.625	2 x 96 x 0.6	64 x 0.625	2 x 64 x 0.625
Slice thickness	0.625/1 mm	0.625/1 mm	0.5/1mm	0.625/1.25 mm	0.625/1mm
FOV	26 cm	33 cm	35 cm	50 cm	50 cm
Time between images	83 ms	75 ms	NA	0.3 - 0.5ms	NA
Technique used for dual-energy	2 tubes	2 tubes	2 tubes	Fast kVp switching	Multi-layered detector
Gantry rotation time for dual-energy mode	330 ms	300 ms	250ms	350 ms	270 ms
Temporal resolution for dual-energy mode	165 ms	150 ms	125 ms	175 ms	135 ms
Strengths	<p>For each tube potential, tube current and tube filtration can be selected independently</p> <p>Relatively low degree of spectral overlap, which improves contrast-to-noise ratios in material-specific images</p> <p>Beam-hardening corrections are applied prior to image reconstruction</p> <p>Material-specific images to be created in the image domain</p>			<p>Almost simultaneous acquisition of the 80- and 140-kVp data set</p> <p>Allows dual-energy material-decomposition algorithms in either projection data or reconstructed images</p> <p>Decreases beam-hardening artefacts in virtual mono-energetic images</p>	<p>Ideal alignment of low- and high-energy datasets, rendering images less likely to motion artefacts.</p> <p>Perfect beam-hardening correction. Affords conventional and dual-energy datasets with a single scan without changes of the clinical workflow.</p>

<p>Weaknesses</p>	<p>Requires specialised hardware.</p> <p>A 90°-95° phase shift between low- and high-energy data.</p> <p>The use of both x-ray sources permits cross-scattered radiation which requires specialised scatter correction.</p>	<p>Requires specific hardware</p> <p>Moderately high overlap of the energy spectra.</p> <p>Spectral separation is not feasible to be improved by applying filtration.</p>	<p>The accuracy of the different energy separation is lower than the other systems using different X-ray tube voltages. Spectral separation cannot be improved by applying filtration. Relatively high overlap of the energy spectra.</p>
--------------------------	---	---	---

As discussed in the previous section, DECT involves the acquisition of two different data sets of images with different X-ray energies, within the same study [65]. The difference between high and low energies enables the differentiation of bodily elements/substances [70]. In the first generation of DS-DECT, the dual energy mode is limited by the FOV: one detector covers 50 cm FOV, while the other covers only 26 cm FOV [71]. The advantage of this scanner type is that the two types of dual energy tube can be operated at different kVp and mA settings [59]. The main disadvantage is that the FOV is limited to about 27 cm in diameter [70], and therefore is unable to cover a patient's entire body [66].

The second generation of DECT, with a markedly improved temporal resolution, was introduced in 2009 to overcome this particular limitation [62, 72]. This model uses a 128-slice CT with a wider FOV of 33 cm for detector B; on the downside, dual energy evaluation with DSCT is restricted by the relatively small FOV. Since the high- and low-energy projections are not concurrently attained at the same z-position, the image and raw data-based dual energy algorithms are difficult to realise [40]. In the slightly more advanced third-generation model, the FOV increased to 35.5 cm, but this increment was still insufficient to cover the patient's entire body. Another challenge was presented by cross scatter radiation, formed because of the simultaneous activation of dual energy.

The SS-DECT, developed by GE health care, is based on the use of a single X-ray tube with rapid kVp switching technology (Fig. 2.3), which uses a generator electronically that alternates the tube energy between 80 kVp and 140 kVp in less than 0.5 ms. The temporal resolution for dual energy acquisition in the fast switching is 175 ms. In this type of scanner, the key contributor to fast kVp switching acquisition is a detector called Gemstone spectral imaging (GSI), which is associated with higher optical properties (shorter afterglow) than other ordinary detectors [73]. Another advantage of SS-DECT is the utilisation of full FOV '50cm' and the absence of cross scatter radiation. The disadvantages of this modality include a lack of current tube modulation; a likelihood of motion during the switching between energies, and resultant temporal misregistration; an inability to produce direct conventional images; and the impossibility of adding beam filtration for both kVp since it is a single source system [73].

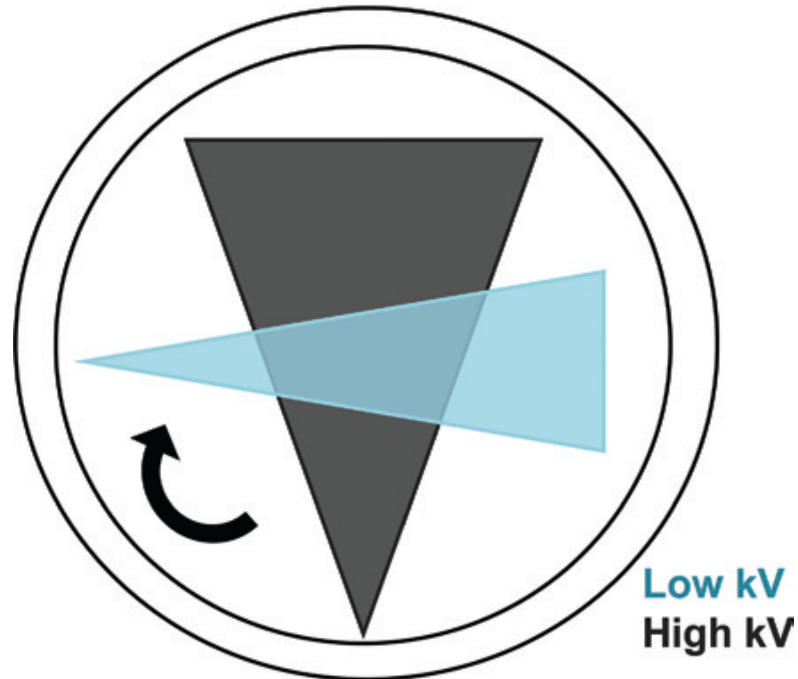


Figure 2.2. Dual-x-ray-source geometry: Independent x-ray tubes, detectors and generators allow simultaneous collection of dual-energy data. Each tube can be operated by using optimal tube current settings and with optimum spectral filtration.

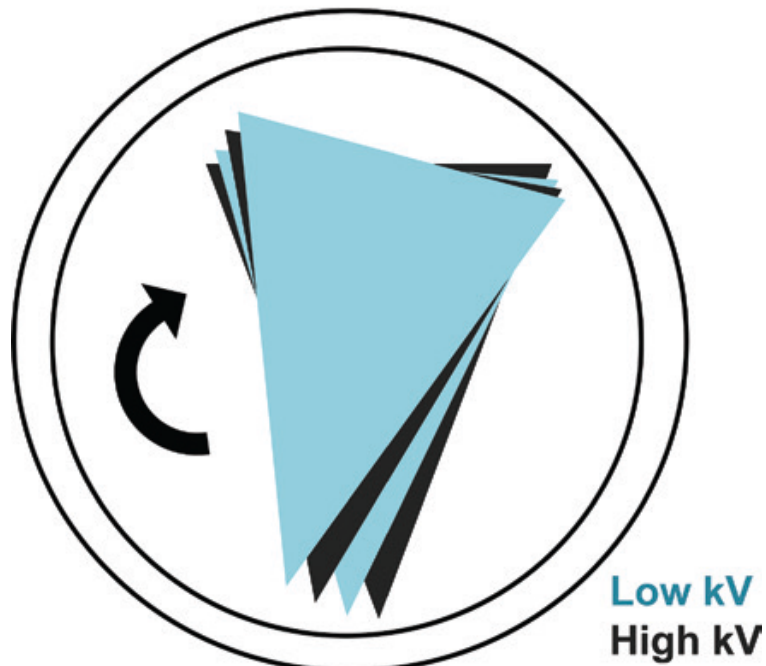


Figure 2.3. Fast kilovoltage (kVp) switching: The x-ray tube potential is switched between successive views in either axial or spiral mode. Dual-energy processing can be performed by using projection or image data, with the temporal resolution remaining essentially unchanged.

Reprinted with permission from McCollough et al.[74].

DECT imaging, therefore, is dependent on the properties of variances in both X-ray attenuation and tissue attenuation; it is also sensitive to the object's chemical composition. More specifically, DECT image quality is determined by the actual separation of the energy spectra. In a CT image, the CT value of each voxel is computed by averaging the contribution of different materials to the attenuation coefficient; however, as body regions consist of different tissue types, it is difficult for conventional CT to distinguish and classify them [74] because of the accumulative attenuation over the entire energy range for all tissues within the measured voxel. The addition of attenuation measurement at the second energy level in DECT, however, results in differences between the two energy spectra that are captured by the detectors to discriminate the chemical composition of different materials. DECT becomes clinically useful at this juncture, as the energy depends on the attenuation of the converted elements' atomic numbers.

Some materials exhibit different attenuation values – either higher or lower – upon exposure to an X-ray beam at different kVp values: this is the fundamental principle of DECT imaging. Substances with a high atomic number (Z) like iodine (I), xenon (Xe), and calcium (Ca), for which Z values are 53, 54 and 20 respectively, are attenuated to a greater quantity of low kVp than are high kVp photons [67]. The photoelectric effect takes place because the k-edge of these substances (I = 33 keV, Xe = 34.6 keV, Ca = 4.03 keV) corresponds more closely with the mean energy of the low-kVp source [75]. Consequently, a switch of X-ray energy produces variations in the K-shell absorption edges for different materials. The outcome is that the nearer the X-ray energy level is to the K-shell of a component, the more superior the attenuation [66]. DECT has the ability to differentiate materials with large Z values: e.g., iodine ($Z = 53$) can be separated from calcification ($Z = 20$) and from other materials as well [76] – a characteristic that is not available in traditional CTA. Additionally, at the desired energy level, DECT can produce virtual monochromatic images (MEIs) which have the benefits of reducing beam hardening artefacts and facilitating the precise measurement of the attenuated X-ray beam in DECT [69].

Since the capability of DECT for material differentiation enhances the improvement of iodine detection at low energies, vascular structure and related diseases can be visualised with better image quality and without an increase in radiation doses to patients, both of which are not usually possible with conventional CT imaging. Further advantages of DECTA are (a) bone removal algorithms and plaque display [66], (b) metal artefact reduction [77], and (c) tissue re-composition quantification for better diagnostic accuracy [78]. Although DECTA is at present a valuable diagnostic tool for the follow-up of stenting intervention, it requires the delivery of a high radiation dose to patients, which may pre-

dispose the patient to cancer in the future; lowering the radiation dose is therefore of paramount importance. Rapid advances in CT technology have led to the reduction of both radiation dose and image noise; nevertheless, in order to address the radiation risk associated with DECTA, as in conventional CTA, a range of dose optimisation techniques has been developed, including the use of a low kVp and implementation of special scan and image reconstruction modes [79]. Again, these techniques may negatively affect the image quality: a reduction in the radiation dose weakens the imaging signal, and may adversely affect diagnoses.

2.3.4.3.1 DECT clinical applications

Although clinical applications of DECT have been increasingly accepted, only a few studies have investigated the use of bone algorithm peripheral arterial disease with DECT [80-82]. It has been found that the use of automated bone subtraction algorithms improves image quality. Brockmann et al. [78] evaluated the accuracy of DECTA by comparing the bone removal algorithm of DECT with the conventional bone removal algorithm of MDCT and the gold standard DSA in PAD, and reported that DECTA was superior to the conventional bone removal technique. In another study, Huang et al. [83] reported that DECTA improved image quality beyond MDCT and DSA. These studies did not take into account the issue of dose reduction as they were focused only on the accuracy of bone removal applications. Research has not yet been directed at addressing the radiation dose issue and image quality of DECT in PAD, although DECT has been widely reported as a useful application for the imaging of renal stones and gout [68]. A comparison between the efficacies of conventional MDCT and DECT in chest applications reveals that DECT is more valuable – even without an increment in radiation dose – than conventional MDCT. Zordo et al. [84] and Broucker et al. [85] reported a dose reduction of about 28% when using DECT for assessing pulmonary embolism when compared with single-source MDCT at 120 kVp with improved image quality.

2.3.4.3.2 Spectral imaging with DECT

Previously, all X-ray beams produced by MDCT were polychromatic. Since the arrival of DECT, to facilitate post-processing of spectral images the kVp, which was the conventional as a measure of energy, has been replaced with kiloelectron volts (keV), which is a simplified way to express X-ray energy. There are three elements in spectral CT imaging, all of which can be acquired by DECT: (i) X-ray sources producing different energies; (ii) a detector that can differentiate quanta of different energies, and (iii) material differentiation [37]. The second-generation DS-DECT makes possible the optimisation of the spectral

separation of photons by introducing Sn pre-filtration, the ‘tin filter’, which is a pre-filtration onto the 140 kVp used to filter the high energy spectrum and increase image contrast [61]. In the third generation of DS-DECT, the adding of Sn pre-filtration to the new Vectron x-ray tube strengthens the x-ray spectrum by removing low energy photons that are usually fully absorbed by the patient’s body.

Spectral imaging can be obtained using conventional polyenergetic images (PEIs) to generate MEIs at different keV levels [69]. PEI is an image generated by conventional CT due to the full spectrum of photon energies with the kilovolt peak chosen by the CT technologist, e.g. 80, 100, 120 or 140 kVp [63]. MEI can be obtained from a pair of material density images and mass attenuation coefficients [86]. As the standard low and high tube potential of DECT are 80 kVp and 140 kVp, the mean effective energies are 53 keV and 72 keV respectively [70] (effective energies range between 40 keV and 190 keV).

Delesalle et al. [87] assessed the spectral optimisation of thoracic arteries and found that virtual monochromatic energy at 60 keV and 100 keV provided similar or better image quality than standard chest CTA. Maturen et al. [88] investigated endovascular aneurysms of the aorta and demonstrated high sensitivity in the detection of endoleaks using 55 keV MEI, compared with standard PEI. Sudarski et al. [89] stated that compared to dual-energy PEI, using a 70 keV MEI achieved a high contrast to noise ratio (CNR) in the abdominal arteries. They observed that the best images were obtained for the lower extremities with 60 keV, in comparison to PEI. Pehno et al. [90] compared the subjective and objective image quality of virtual MEI DECTA and PEI in aortoiliac arteries, and demonstrated optimal contrast enhancement and improved image quality using 70 keV MEI in preference to single-energy CTA. Yu et al. [63] studied various sizes of phantoms to evaluate MEI at multiple keV levels for the optimisation of image quality in the chest region. The best image quality was seen with energies of 66 keV for the small, 68 keV for the medium, 70 keV for the large and 72 keV for the extra-large phantoms [63]. In addition, this study concluded that the optimal MEI was used for each phantom, and that the noise levels were similar to, and the CNR better than, that observed in single-energy CT at 120 kVp with the same radiation dose [63]. Using a combination of low and high X-ray energies distinguishes DECT scanners from conventional MDCTs.

2.3.4.4 Multi- energy CT

The x-ray tube in CT scan produces a spectrum of energies in a polychromatic form. A set of images representing the x-ray attenuation characteristic for specific organ exposed to the x-ray is the result of CT measurement and data reconstruction. In practice the detection

technology calculates the x-ray energy as mono-energetic CT measurements by conventional CT detectors, which are unable to deal with the spectrum of x-ray beam. Recently, energy-selective X-ray detectors are developed to take advantage of the spectral energy in the x-ray beam resulting in multi-energy CT utilization. Therefore, the image reconstruction in CT scanner are based on two methods: image-based or projection-based reconstruction [65]. This process occurs at the detector level as the x-ray detection technology is the key to accomplish multi-energy CT. Consequently, the x-ray detectors can be categorized into two groups: energy-integrating and energy-discriminating [74]. Yet, all the available CT scanners use the energy-integrating detectors where the interactions between the x-ray beam and materials are accumulated over the total energy spectrum. While the energy-discriminating detectors deal with each photon, based on a specific threshold, the energy is counted and categorized into different energy bins [91].

The human body is a composite of vastly different tissues, and imaging techniques aimed at differentiating these tissues require many levels of energy to be accurate. DECT is limited in that it can distinguish only between two or three materials, and therefore is limited in scope. X-ray attenuation is subjected to the energy from photons. In CT scanners, the combination of robust X-ray generation and innovative detection technology allow for multi-energy CT applications. Theoretically, multi-energy CT is a more specific material disintegration technique, which can differentiate between more than three types of material in a single data set (Fig. 2.4). Multi-energy CT is also called spectral energy-selective spectroscopy, or energy sensitive CT [91].

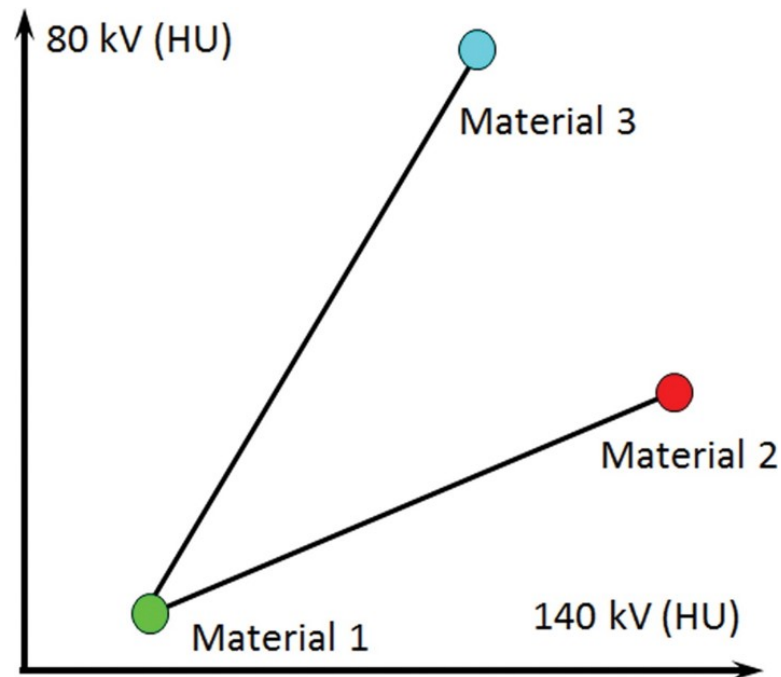


Figure 2.4. CT numbers of three known materials in low- and high-energy images, plotted on the y- and x-axis, respectively. Unknown materials are then mapped onto this plot to determine the percent composition of each of the three basis materials. Reprinted with permission from McCollough et al. [74].

In this technique a wide spectrum of photon energies is produced by a single X-ray tube, and detected by a special energy-sensitive detector, known as a photon-counting detector, which separates the beam into different energy bands [92]. This method classifies detected X-ray photons into energy bins [74, 93], and this ability for photon discrimination (leading to the distinguishment of the attenuation spectrum of all materials within the voxel) makes the detector's response a key role in multi-energy generation. Photon-counting detectors are based on energy thresholds and provide a method to count any photon that reaches the detector, regardless of its energy. At this point, the multi-energy applications of clinical CTA show great promise because they rely on the k-edge of multiple contrast agents [93]. This modality is suitable for distinguishing high energy when heavier elements are used with contrast agents such as iodine, gadolinium, barium, platinum and gold [93]. It may be stated here that CT will graduate to multi-energy applications that generate images beyond the grayscales. This promising technique is presently under investigation, is restricted to research purposes only, and is not yet clinically applicable.

2.4 Radiation dose in CT

2.4.1 Radiation dose effects

The main drawback of CT imaging is the use of ionising radiation, which brings with it risks of tissue impairment and cancer induction. The radiation dose in CT depends on peak tube

voltage, tube current and scan time [94]. The effects of the radiation dose may be represented in either a deterministic or a scholastic form. When the radiation dose touches the threshold dose level (which differs from one subject to another), deterministic effects are manifested, with the damage significantly correlated to the radiation dose. Studies have reported cataract, hair fall, and skin injuries as deterministic effects in patients who were irradiated beyond the threshold dose. In clinical practice, Bogaert et al. observed that deterministic skin effect occurs when the radiation dose exceeded the threshold dose at 2 Gy [95]. Scholastic effects of radiation, on the other hand, may manifest at any time, irrespective of the radiation dose and without any correlation to the threshold dose. The best examples of scholastic effects are genetic changes and radiation-induced cancer. The classic case of the atomic bomb explosion in Japan in the last century allowed for the estimation of cancer risk in survivors who had been exposed to high radiation [49, 96, 97]. Several studies have validated the link between cancer risk and radiation exposure: evidence for this is strong, good and reasonable at radiation exposures of greater than or equal to 100 mSv; between 50 and 100 mSv, and between 10 and 50 mSv [98, 99].

2.4.2 Radiation dose quantity and measurements

Since CT is one of the major sources of radiation in medical imaging, and involves higher quantities of radiation than other radiological examinations, it is essential to ascertain the optimum method of dose measurement for this method. The available radiation parameters for CT dose monitoring include the following: (i) CT dose index (CTDI), comprising $CTDI_{100}$, weighted CTDI ($CTDI_w$), multiple scan average dose (MSAD), and volume CTDI ($CTDI_{vol}$); (ii) dose length product (DLP), and (iii) effective dose (E).

2.4.2.1 CT dose index (i)

The computed tomography CTDI, which is the fundamental radiation dose parameter in CT, is an estimate of the average radiation dose in an irradiated volume. It reflects the amount of radiation absorbed in the production of one tomographic image during a single CT scan. Its measurement is very labour-intensive. CTDI is not expressed in terms of tissue but in terms of air, which considers the CTDI to be a step away from tissue dosimetry [100]. Since the CTDI represents an averaged dose to a standardised cylindrical phantom (16 cm and 32 cm diameter), the measurements are estimations and not a precise calculation of dose. The measurement of $CTDI_{100}$ is a more convenient procedure, indicating the radiation exposure of a single axial scan over a length of 100 mm. This parameter can be used to derive $CTDI_w$, which is the weighted average of $CTDI_{100}$. A multiple parallel scan mode is a better option,

and is possible for CTA, or $CTDI_{vol}$, but MSAD has the limitation of being time-consuming [94].

Measurements for $CTDI_{vol}$ and DLP (derived from $CTDI_{vol}$ to indicate the total absorbed dose during the examination) are usually available on recently developed CT consoles. However, these do not give the exact dose for a specific patient, but are based on the CT phantom used to determine body CTDI [94]. Since a body less than 32 cm actually absorbs a higher dose, and conversely a body greater than 32 cm absorbs a lower dose, this measure can only be regarded as providing an approximate estimation of the dose absorbed by a specific body part that has been exposed to the radiation dose.

2.4.2.2 Dose length product (ii)

Dose-length product is an indicator of the integrated radiation dose of a given scan protocol, and can be computed by integrating the $CTDI_{vol}$ value over the scan length. DLP represents the overall absorbed energy calculated from a particular scan protocol [101], obtained by multiplying $CTDI_{vol}$ with the given scan length in centimetres. DLP is available on the operator's console as is $CTDI_{vol}$. The system international unit (SI unit) for DLP is $mGy \cdot cm$. Since it does not take into account the radiosensitivity of organs within the irradiated body area, DLP cannot be routinely used as an indicator of risk. To overcome these difficulties, the concept of E has been born.

2.4.2.3 Effective dose (iii)

Effective dose (E) is the most important parameter in CT imaging, of great value for weighing and comparing the potential biological risks of a given examination.

Radiosensitivity of body tissues is taken into consideration by this measure [102, 103]; it also takes into account direct and scattered radiation for all exposed regions. Effective dose is used to estimate the radiation risk of the procedure, based on the Monte Carlo simulation for average patients [104]. Its value is given by multiplying each equivalent dose of a relative organ with the tissue-weighting factor (k) that is representative of the radiation sensitivity or risk of that particular organ, and aggregated over all exposed organs.

In 2007 ICRP report 103 incorporated major changes into the tissue weighting factor values recommended and published in ICRP publication 60 [105]. Another recent research report proposed a new weighting factor for DECTA application for peripheral arteries, as DECT uses two different energy sources [106]. Without doubt, for the purpose of radiation safety and image quality, the basic protection concept when dealing with patient doses from MDCT

is the ‘as low as reasonably achievable’ (ALARA) principle, which makes sure that patients receive radiation doses as low as practically possible.

2.5 Peripheral arterial stents

Revascularisation is the preferred method for patients with PAD, both to improve the quality of life and to reduce the risk of amputation [2, 107]. Angioplasty and stent implantation are commonly used for artery stenosis and occlusions in peripheral arteries [7, 108]. This method is commonly employed with beneficial results in PAD patients [109, 110]. It must be emphasised that the use of stents requires careful evaluation – depending on the location and size of stents – to ensure patency; most stents are located in the aortic bifurcation, common iliac arteries, external iliac arteries, superficial femoral arteries and popliteal arteries. The size of the stent depends on its location and the extent of stenosis; it extends from ≤ 4 mm in the popliteal arteries, to ≥ 10 mm in the aortic bifurcation.

Endovascular interventions result in positive outcomes in treated patients, giving a success rate as high as 95% [111]; however, the restenosis rate is also high, at 60% in the first 12 months [111, 112]. Most stents show a significant reclusion and restenosis rate, depending on the location and material used [107]. Stents in the superficial femoral artery display a restenosis rate of from 40% to 60% in the first year [113]. In comparison to angioplasty, however, the rate of restenosis in the SFA after one to two years is approximately 20–30% lower following primary stenting [33]. Table 2 displays the primary patency rate in peripheral vessels, for angioplasty with or without stents [3].

Some stents are associated with metal artefacts that restrict the diagnostic accuracy of the imaging modalities. In such instances, appropriate evaluation of stent patency can help in decreasing the rate of limb amputation and subsequent mortality. Evaluation of lower extremity arterial disease usually involves a series of non-invasive tests designed to indicate its level and severity. Consequently, vessel imaging has become an essential requirement of medical imaging. To fulfil this need, many methods have been designed and established to show a detailed picture of relevant blood vessels, along with their condition, and provide essential data needed for planning of therapeutic treatment and decision-making.

Table 2.2. A 5 year patency rates observed after different types of endovascular (stent) intervention, and patency rates observed according to the level of revascularisation procedure: iliac, femoro-popliteal and below the knee [3]

Endovascular Stents	Primary Patency rates (%)
Iliac stenting	80%
Femoro-popliteal stenting	60–70%
Femoro-popliteal stenting with DES	70–80%
Below the knee angioplasty +/- stenting	30–60%

2.6 Peripheral arterial stents evaluation by DECT

Imaging of implanted stents by CTA is usually associated with blooming artefacts [32] that occur mainly due to the metal artefacts created by the stents. These blooming artefacts make stent struts appear thicker because they cause an underestimation of the stent lumen [22]. The metal artefacts, in turn, are the result of photon starvation and beam hardening [22]. Photon starvation induces a relationship between blooming artefacts and beam hardening artefacts because the quantity of photons that passes through high-density body regions is less than that which passes through normal body regions; this is considered to be the main factor preventing accurate evaluation of in-stent restenosis [114], adversely affecting image quality. The type and size of peripheral stents exert an obvious influence on the scanning protocol in MDCT, which determines the image quality. Much effort has been expended to minimise these artefacts, including a reduction in the amount of metal used in stents (a major remedial measure) [115] and the use of high kVp to reduce the photon starvation phenomenon [22]. This approach, however, is problematic, leading to a higher radiation dose to patients.

Earlier studies reported that an association between beam hardening artefacts and stents is one of the major limitations in MDCT scanners [32, 51]; using DECT scanners could be an effective alternative to overcome these shortcomings. Huang et al. [83] observed that beam hardening correction with the help of pixel by pixel data during post-processing leads to contrast improvement in DECT. Similarly, Pinho et al. [90] and Matsumoto et al. [76] demonstrated a reasonable reduction in beam hardening and blooming artefacts with DECT. In DECT, virtual monochromatic images at high energy levels are able to reduce the artefacts caused by metal [63, 69, 76]. In the same way, the new reconstruction technique of iterative reconstruction (IR) with DECT may improve image quality and reduce radiation doses to patients [116]. Although extensive research has been carried out on radiation dose

reduction and image quality, no single study exists which adequately covers the topic of peripheral arterial stents.

Earlier studies have explored the effectiveness of individual dose optimisation techniques for imaging peripheral artery stents [114, 117], but there still remains a gap in information about the adjustment of a combination of factors such as tube potential, special scan mode, an improved algorithm for image reconstruction, and balancing attenuation, contrast and noise to optimise image quality. Reduction of radiation dose is not the only challenge in peripheral arterial CTA; the identification of in-stent restenosis still needs investigation, because the stent material can lead to an overestimation of the severity of a lesion. Blooming and beam hardening artefacts in conventional CTA limit the accurate assessment of restenosis. In a recent study, Zou et al. achieved a reduction in blooming artefacts by using DECT [118]. In a phantom study, 80% stent lumen visibility was reported with metal stents, and 100% with bio re-absorbable stents [119]. However, most available studies do not evaluate the diagnostic value of this modality in stent imaging.

2.7 Contrast medium optimisation

All CTA examinations involve the intravenous administration of a contrast medium to the subject. Contrast media expose the patient to the risk of developing contrast-induced nephropathy (CIN), which may lead to acute renal failure; it has been reported as the third leading cause of hospitalisation [120]. Decreasing the volume of contrast medium is clinically as important as reducing radiation dose, especially for patients who show risk factors for CIN or have renal insufficiency. Striking a balance between contrast medium, radiation dose and image quality is imperative when planning lower extremities CTA.

Iodine and water exhibit a difference in the energy dependence of their linear attenuation coefficients, which gives rise to different CT numbers for iodine at different tube potentials. Bolus opacification more or less parallels the scanner speed in 4-, 8-, and even 16-slice CT systems [121], but CT scanners using 64 slices and beyond may simply out-run the opacification of the bolus through the arterial system [20]. Contrast delivery is also affected by patient-related factors such as cardiac output, body weight and peripheral arterial obstructive disease [122]. It follows that the contrast protocol must be considered one of the core aspects of CTA protocol optimisation in DECTA, because of the fast scanning time and ability to use the low kVp option.

With respect to the use of low energy for evaluation of contrast medium enhancement in conventional CT, Utsunomiya et al. [123] observed that an energy value of 80 kVp produced

better contrast enhancement than 120 kVp, and required less volume of contrast medium. Nakayama et al. [124] evaluated the aorta using a 16-slice CT with 90 kVp and reported that a reduced volume of contrast material yielded vascular enhancement equivalent to that of standard tube voltage CTA. Manousaki et al. [117] employed 100 kVp with 16-slice CT and demonstrated that the evaluation and assessment of renal stents is feasible with a significant dose reduction. Similarly, when evaluating peripheral arterial CTA with a 64-slice CT scanner, Iezzi et al. [125] noted an appreciable reduction in radiation dose with the use of 80 kVp, without compromising image quality. These studies also reported a higher attenuation of contrast on the investigated arteries with low kVp CTA than with standard kVp. However, low kVp results in decreased photon penetration and increased noise, because most of the photons are absorbed by the patient's body. This occurs especially with large patients, and leads to degradation of image quality [126]. Large patients do not benefit from low-potential techniques because they require high beam penetration. A higher tube potential of more than 140 kVp, on the other hand, will result in a reduction of soft tissue contrast, which affects the differentiation of soft tissues [65]. In contrast, the use of DECT for vascular angiography improves iodine enhancement with lower amounts of contrast medium [66, 90].

Lower tube voltage has been found to be closer to the k-edge of iodine, and may lead to a reduction in contrast volume [65, 78]. Previous studies of peripheral arteries DECTA have not dealt with contrast material volume reduction, with the exception of a report by Megibow and Sahani [126], who demonstrated a reduction in contrast volume of up to 30% in abdominal aortic aneurysms, when using DECT. Numerous investigators have shown that, for chest imaging, low contrast medium volume or concentration is accurately used in DECT [87, 89, 127, 128]. Yuan et al. [127] showed a 50% reduction in contrast medium volume in pulmonary embolism when image reconstruction was performed at 50 keV, while maintaining image quality with the same effective radiation dose. Finally, to the best of our knowledge, there is no study published on peripheral CTA or peripheral stent procedures, with respect to evaluating contrast material reduction using DECT. The overview from the literature points to the feasibility of a reduction in contrast material volume in the peripheral arterial stent protocol. In the present thesis, one of the objectives is to optimise contrast volume by using different keV sets. The utility of this optimisation in dual energy CT methods will be discussed in Chapter 4.

2.8 Evaluation of image quality

Image quality is a generic and subjective measure of the readability of an image; image quality optimisation is a very sensitive subject that must be evaluated by a qualified

observer. A reliable evaluation method is essential to ensure an acceptable, diagnostic quality of CT image optimisation [129, 130]. There are a number of parameters that directly measure image quality, but nothing can replace the dedicated participation of a trained and experienced reader. Assessment of image quality comprises both an objective and a subjective evaluation.

2.8.1 Objective evaluation of image quality

CT images can be assessed quantitatively by means of the following parameters: CT attenuation value or CT value (HU), image noise, SNR, CNR and spatial resolution.

2.8.1.1 CT value

CT value or CT number (mean attenuation expressed as Hounsfield Units or HU) is preferably measured in a homogeneous area or in a phantom organ, to avoid interference from structural information [94]. A difference in reconstruction algorithms significantly affects CT value. In peripheral CTA, CT value is assessed with the help of a circular tool which measures attenuation in the region of interest (ROI). It is recommended to draw the ROI as large as possible, in order to include maximum portion of the contrast-filled vessel in the image, and to exclude the calcified vessel walls.

2.8.1.2 Image noise

Image noise in CT is usually expressed as the standard deviation (SD) of the CT value in an ROI – assuming a normal distribution – and is measured in a homogeneous phantom, typically water [94]. The major source of noise in a CT image is the contribution made at different energy levels, by X-ray photons to the detectors. The first source is the quantum noise, which is dependent on tube potential, tube current, and the patient's size, which has an obvious effect on low contrast resolution [131]. The second source of image noise depends on the system's performance and its physical limitations, if any. The third source includes the reconstruction parameters; a strong determinant of image noise is the type of reconstruction filter used in the scanner [94]. Image noise is also inversely proportional to the square root of the radiation dose, and to the slice thickness. It is clinically desirable for patients of all sizes, and it has been proposed that some scanners should maintain a constant level of noise, which requires a large range of mA values, as different patient sizes affect X-ray absorption [132]. Consequently, increased image noise in CTA procedures with lower tube potential may be acceptable due to the vascular enhancement that is associated with higher attenuation. Application of low kVp without considering the effects of other parameters can increase image contrast, but may also introduce streak artefacts. The

combination of low and high kVp in DECTA allows for a proper balance between the high contrast generated from the low kVp and, conversely, the low image noise from the high kVp [37]. Adjustment of weighting factors can help in attaining the required effect on image fusion. A combination of 50% weighting factors from both 80 and 140 kVp is reported to offer the highest SNR with optimal image enhancement [133]. Image noise characteristics are improved in second-generation DS-DECTA scanners, by means of a non-linear blending and a combination of Sn 140/100 kVp or Sn 140/80 kVp [134]. In the recent advanced DS-DECT third-generation scanner, non-linear blending is achieved with both sources. There are no reports on the effect of non-linear mixing algorithms of DE on lower extremities DECTA.

2.8.1.3 Spatial resolution

Spatial resolution represents the ability of the system to distinguish small intricately spaced structures in an image. It is usually determined in a phantom by using test objects with large differences in CT values, to exclude overlapping from image noise. Factors affecting spatial resolution consist of focal spot size, detector size, displayed pixel size and motion [130]. Spatial resolution can be evaluated subjectively by visualisation of line pairs of increasing density [94]. Low contrast resolution is significantly affected by radiation dose and corresponding image noise. High spatial resolution is necessary in peripheral artery CTA, to enable an accurate detection of small arteries. Isotropic source data is essential for multiplanar image reconstruction, which means an optimal spatial resolution.

2.8.1.4 Signal-to-noise ratio

Signal-to-noise ratio (SNR) can be expressed as the CT value in HU divided by noise SD in the same homogenous ROI as shown in the equation below:

$$\text{SNR} = \text{CT value of specific ROI} / \text{Image noise (SD)} \quad (1)$$

Increasing spatial resolution by decreasing pixel size at the same effective dose brings about a drop in the SNR per pixel. Therefore a high SNR is indicative that accurate information (signal) has overcome noise. SNR in CT imaging may be affected by many different confounding factors such as pitch and dose, which are detrimental to image quality. On the other hand, SNR is improved by new iterative reconstruction techniques that reduce image noise [135]. DECT depends on dual energy, so a higher contrast attenuation is normally associated with 80 kVp images with an inherently lower SNR. Conversely, lower contrast attenuation is normally achieved with 140 kVp images, which have better SNR [136]. A combination of these energies leads to a higher SNR. Furthermore, non-linear and linear blending images have been found to improve the SNR in vascular studies [136, 137].

The common regions of interest that are used for measuring the SNR in peripheral arterial CTA are the aorto-iliac area, the femoro-popliteal region, and the lower leg segment, as shown in Fig. 2.5.



Figure 2.5.The region of interest placed in the inner vessel lumen for measurement of SNR

2.8.1.5 Contrast-to-noise ratio

Contrast to-noise ratio (CNR) is estimated by dividing the difference between the attenuation values of contrast enhancement at two different areas, by the image noise equation 2 (below):

$$\text{CNR} = (\text{HU}_{\text{iodine}} - \text{HU}_{\text{soft tissue}}) / \text{Noise}_{\text{soft tissue}} \quad (2)$$

CNR is an objective method to assess contrast resolution, and represents the ability of CT systems to reproduce two adjacent objects with similar CT values as separate structures [130]. When evaluating CT image quality through CNR, the results are typically a comparison of CNR variances between two methods, rather than direct CNR values. It follows that image noise and iodine CNR are essential parameters of image quality for the correct assessment of peripheral CTA procedures, and are usually employed to throw light on the interactive effect of iodine contrast enhancement and image noise. As was shown earlier with SNR, non-linear blending images and linear blending images also improve CNR

values [136, 137]. Optimal CNR can also be achieved at different keV, and may be affected by patient size. Yu et al. [63] noted that maximum CNR can be achieved in monochromatic images when the optimal energy is kept lower than that required for minimising image noise. This will occur when higher weighting factors are selected from lower energy levels.

2.9 Factors influencing radiation dose and image quality

DECT is considered a less invasive follow-up modality for peripheral arterial stents with high spatial resolution. Scanners vary in their image quality and radiation exposure; additionally, scanning and reconstruction parameters exert a significant effect on radiation dose and image quality. Scanning parameters include kVp, tube current (mA), rotation time, collimation and pitch. Reconstruction parameters comprise slice thickness, reconstruction kernel, FOV and IR, all of which have a marked effect on image quality but a lesser influence on radiation dose [138].

2.10 Scanning parameters

2.10.1.1 Tube potential selection

Object penetration depends on both the quality of the beam that is generated by the X-ray tube, where electrons are accelerated from cathode to anode, and the quantity of photons. In fact, low tube voltage causes an increase in CT tissue attenuation. Reduction in tube voltage benefits small patients by reducing their exposure to radiation. By and large, CT provides tube potential options ranging between 80 and 140 kVp, but DECT is based on dual sources of energy, requiring a wide range of X-ray spectra to obtain sufficient differences of tissue attenuation [65]. The standard low and high tube potential of DECT, i.e., 80 kVp and 140 kVp, are used in most DECT scanners, but 100 kVp and 140 kVp can also be used in second-generation DECT scanners [70].

As previously stated, decreasing the low kVp will increase the attenuation of the contrast medium in CTA, but this is accompanied by greater image noise stemming from decreased tissue penetration by photons [89]. The use of higher kVp leads to less noise, but also to less contrast between materials, because contrast is generated by X-rays and absorbed by the body. In this situation a reduction of tube potential from 120 to 100 kVp for aortoiliac arteries results in a 37% dose reduction [139]. Feuchtner et al. [39] reported a 50% dose reduction when tube potential ranged from 120 to 100 kVp. Iezzi et al. [140], who investigated the possibility of reducing radiation dose in abdominal aortic aneurysms,

decreased the kVp from 120 to 80 and achieved a 74% overall reduction. Apfaltrer et al. [141] demonstrated a fall in radiation dose of around 45–50% when performing aorta angiography using second-generation DSCT scanners with a high pitch and no compromise on image quality. Controlling tube potential in DECTs still faces restrictions, but the availability of several options leads to better evaluation of spectral energies. Thus, in DECT, the noisy 80-kVp data is balanced by the decreased noise of 140 kVp; the resulting combination of dual energies helps to maintain image quality. Changing tube voltage within a single protocol (according to the patient's body habitus) presents difficulties [89], and this challenge has led to the exploration of tube potential modulation as a solution.

2.10.1.2 Tube potential modulation

The obvious strategy of using low tube potential for radiation dose reduction in CTA entails an increase of intravascular contrast, even at low photon energy, because of the higher attenuation of iodine. However, lower tube potential also leads to high image noise, and the objective of maintaining diagnostic image quality may remain unfulfilled, especially with obese patients. Low tube potential needs to be accompanied by higher tube current to overcome the deficiency of image noise. X-ray tubes in the most widely used CT systems are limited in their ability to produce maximum tube current, which, especially at low kVp DSCT, not only enables the use of different kVp but also allows the use of high mA with low kVp, to overcome the high noise that accompanies low kVp. The latest developments in scanners with automatic tube voltage selection suggest the potential to surmount these problems.

Primarily, automated tube potential selection was introduced in Siemens scanners (CARE kVp), which are based on second-generation DSCT [89]. The optimal tube voltage is selected according to patient size and specific CT protocol [62]. In these scanning systems, tube current faced the limitation of being insufficient to produce high mA. This problem was overcome in the next generation systems by increasing the X-ray tube power to 120 kW, thereby producing tube current up to 1300 mA [62]. The efficacy of this option has been reported in single energy studies which achieved a 16-42% reduction in radiation dose compared with 120 kVp studies [142, 143]. Theoretically this option is difficult to use with DECT, because this modality needs a wide range of spectral energy. A few studies have, however, validated the use of this approach with DSCT. A phantom study conducted by Schindera et al. [144] confirmed a significant fall in radiation dose with the automatic tube potential selection system, compared to a standard 120 kVp protocol. In clinical practice Eller et al. [145] achieved a dose reduction of 12% in chest and abdominal CTA, and in a recent study on chest CTA by the present author, a dose reduction of 27% was achieved with

satisfactory diagnostic image quality [146]. Krazinski et al. [147] demonstrated an overall dose reduction of 20% in cardiovascular CTA, while Hough et al. [148] reported a 25% reduction in abdominopelvic CT, with the exception of one patient in whom a slightly higher radiation dose was noticed. The use of automated tube potential can, therefore, improve cardiovascular CTA protocol, with acceptable diagnostic image quality at a reduced radiation dose.

2.10.1.3 Weighted average images

DS-DECT uses two sources of energy coupled with the generation of different image sets such as 80 kVp, 140 kVp and weighted average images from a single acquisition, as a part of the post-processing procedure in the CT acquisition workstation [149]. Weighted average images are generated from the combined HU data attained by two X-ray sources of the DSCT, to simulate the image quality of a typical 120 kVp acquisition [150]. The weighting factor is measured by the ratio of the central 35-cm image density in third-generation scanners (33 cm and 26 cm in second-generation and first-generation scanners respectively), that is contributed by the 80-kVp datasets. Dual energy post-processing software adjusts the weighting factor, but this option is not available with SS-DECT.

Some researchers have discussed the effect of weighting factors on radiation dose and image quality. Paul et al. [72] found that DECT in the carotid artery, employing different weighting factors from 0.0 to 1.0 of two datasets, affected both contrast enhancement and image quality. They also found that fused images with a weighting factor of 0.6 showed the highest CNR or SNR, compared to 80 or 140 images [72]. Behrendt et al. [133] also validated that using a weighting factor of 0.5 in aorta imaging with different weighting factors improved image quality. Other authors have reported that weighting factors of 0.3 and 0.4 achieved similar results in images, with characteristics comparable to those produced with 120 kVp [83, 89]. Consequently, the weighting factor of tube voltage has a direct impact on image quality. Optimum results may be obtained for peripheral angiography scanning, with 80 kVp and 140 kVp for small to medium-sized patients and 100 kVp and 140 kVp for large patients and, if possible, the usage of a weighting factor from 0.4 to 0.5.

2.10.1.4 Tube current

Another factor that compromises the radiation dose and enhances image quality is mA, although it is not as complicated as tube voltage. The tube current in most existing CT scanners can be adjusted up to 800 mA [37]. In third-generation DSCT scanners, mA up to 1300 can be used in combination with low kVp [62]. An increase in tube current has a positive effect on image quality, in that image noise will decrease when mA is increased

[151] because image noise is inversely proportional to the square root of dose and slice thickness. Using the same approach, both radiation dose and image quality are directly affected by scan time. Minimising the radiation dose delivered to the patient, and maintaining diagnostic image quality, are both very important because of radiation risk. A majority of scanners employ a modulated tube current to decrease radiation dose.

2.10.1.5 Tube current modulation

Automatic tube current modulation is a tool used to modulate the radiation dose according to the patient's body size in order to achieve optimal image quality relative to a specific body region. This concept was introduced in 1981 by Haaga et al. who used tube current variation to reduce the radiation dose, simultaneously maintaining image quality [152]. The first manufacturer who implemented this modulation technique was GE Healthcare in 1994, who effected a dose reduction of about 20% [132]. A further dose reduction from 40% to 50% was reported using the automatic tube current modulation in abdomen-pelvis adult CT [101]. The advantages of tube current modulation include control of radiation dose to the patient, limited artefacts from photon starvation, increased life of the X-ray tube, and control of image quality along the body region being scanned [37, 101].

Individual CT manufacturers have different definitions for automatic tube current modulation, but all of them share the same concept. Automatic tube current modulation can be defined as a device that works to adjust radiation dose by changing the mAs according to patient size and attenuation [100]. Consequently, the dose will increase on the greatest body thickness (shoulders and pelvis) and decrease on the thinnest body parts. The concept of using the automatic tube current modulation has been simplified by the major CT manufacturers for users as follows: on Toshiba CT scanners the CT user chooses the image quality based on a patient-equivalent water phantom and mAs is adjusted according to patient size to preserve image quality [153]. CT scanners from GE Healthcare have two methods for tube current modulation, auto mA and smart mA: auto mA adjusts mA only in the longitudinal direction to preserve a continuous noise index level, whereas smart mA adjusts mA on the x, y, and z axes to ensure a continuous noise index level [40]. Siemens CT scanners allow the CT user to specify mAs suited to the standard-sized patient, and also permit adjustment of tube current by angular modulation on the x, y, and z axes. On Philips CT scanners mA can be altered according to patient size to attain image noise levels similar to the defined reference image, prior to examination by the CT user.

Use of automated tube current modulation with DECT may reduce the radiation dose to patients, but in the first-generation DS-DECT scanner this option was not activated. In the

second-generation system, tube current could be individually optimised. In contrast, the fast kVp switching scanner does not permit modulation because the dose cannot be optimised for the low and high settings in the DECT mode.

2.10.1.6 X-ray beam, collimation, pitch and gantry rotation

Other parameters that have a direct impact on both radiation dose and image quality are X-ray beam, collimation, helical pitch and gantry rotation. The X-ray beam can be defined as an over-beaming effect. In this situation, the X-ray beam is extended to inactive detector areas, exposing patients to higher radiation doses [138]. The extended beam is not used for imaging purposes, compromising the procedural process in peripheral arteries, because, in MDCT, the radiation profile width is influenced by collimation and focal size [154]. Hence, collimation is determined based on specially chosen detector geometry or configuration to give shape to the X-ray beam. Thicker collimation decreases the over-beaming effect, while a narrower collimation leads to more over-beaming. Collimation should be as narrow as possible but must still allow for a reasonable table speed [151]. The compensation of a wide beam and a thinner slice optimise image quality and radiation dose efficiency [130]. In the post 64-slice CT era there is no longer a trade-off between resolution and scan speed, and this modality allows – even in obese patients – a fast, sub-millimetre scan protocol.

Pitch is another parameter that affects image quality and radiation dose. Frequently pitch values between 1 and 2 are preferred, but with CTA it is preferable to have a pitch value of less than 1 to get an overlap image for generating 3D images. Pitch can be defined as the ratio of table feed per gantry rotation [37]. A faster table speed results in a higher pitch, leading to a reduced radiation dose but at the same time lowering spatial resolution [138]. In addition, the scan duration is decreased with an increase in the level of pitch. Lowering the pitch results in better image quality but requires a longer scan time and hence a higher radiation dose [72]. For CTA examinations which focus on peripheral vessels stent evaluation, a pitch smaller than 1 is optimal to improve spatial resolution along the z-axis and obtain results that are as close to isotropic datasets as possible, for better multi-planar reconstructions.

Gantry rotation time is also related to radiation dose, and is defined as the time taken by the X-ray tube to complete a 360-degree revolution [138]. Correct usage of slip ring technology has made possible scanning of longer anatomic coverage with short time. The need for high temporal resolution has led to technical advances in MDCT for faster gantry rotation.

Decreasing gantry rotation time has a similar result when reducing mA, and the faster the

gantry rotation, the lower the radiation dose; however, the reduction in gantry rotation time has a direct effect on the spatial resolution [154].

2.10.2 Reconstruction parameters

The rapid advances in CT scanner technology are in alignment with Moore's law, which predicts the doubling of the density of transistors on integrated circuits approximately every two years [155]. Nowadays most CT manufacturers offer software that runs on economical computers and is capable of post-processing data with innovative lighting effects, based on multiples of contrast-enhanced CT images [40]. CT image reconstruction is a mathematical process that creates images from X-ray projection data obtained at various different angles around the patient. This has a vital impact on image quality and consequently on radiation dose. To maintain optimal image accuracy and spatial resolution for a particular radiation dose, it is appropriate to reconstruct images with the lowest possible noise. In CT scanners the mathematical procedures that are generally used include filtered back projection (FBP) and IR. With the currently available MDCT and DECT scanners, high-quality image reconstruction can be tolerated that allows for isotropic resolution; this can help reduce the number of scans needed and, accordingly, the radiation dose to the patient [138, 154]. The reconstruction parameters mostly depend on the system software and include slice thickness, reconstruction kernel, reconstruction FOV and iterative reconstruction.

2.10.2.1 Slice thickness

Slice thickness is also considered to affect image quality. When a smaller slice thickness is used in the imaging of peripheral arteries, image noise increases because the number of photons that reach each voxel in an image is reduced in quantity relative to slice thickness. This lowers the spatial resolution, affecting image clarity. The reverse takes place when slice thickness is increased. Choosing an appropriate slice thickness requires a balance between edge sharpness and noise. In some recent studies on peripheral DECTA, a slice thickness greater than 1 mm providing optimal image quality has been seen to reduce the radiation dose [78, 80].

2.10.2.2 Filtered back projection

Until recently, FBP was the common reconstruction algorithm widely used in CT scanners [116]. Its popularity may be attributed to the fact that FBP is an analytic reconstruction algorithm which expects the developed projection data to be noiseless in a high computational velocity and short time [156]. FBP initially filters data to improve certain image characteristics, then projects it back into the image space to re-create the image

volume. The underlying reason for using FBP is its computational simplicity, leading to fast image reconstruction. A drawback is that its image quality is limited, specifically with low radiation doses and with obese patients, because the back projection method and filtering involve noise, resulting in streak artefacts that cause degradation of the image [157, 158]. With the development of the computational capacity of CT reconstruction workstations, a new method of CT image reconstruction has emerged. The evaluation of these algorithms is done with a desire for further reduction in radiation dose without reducing image quality.

2.10.2.3 Iterative reconstruction

Over the last few years, rapid evolution of CT technology has led to the establishment of the IR algorithm in MDCT scanners, to overcome the image noise that occurs in some procedures and to reduce radiation dose [158, 159]. IR is an alternative to the conventional FBP method; it was primarily used in nuclear medicine studies [153]. All main vendors of CT scans offer IR algorithms with high velocity to be used in clinical practice, targeted to decrease image noise at lower doses [160-163]. The concept of IR, called algebraic reconstruction, was introduced before the FBP, but due to the limited computational power of CT it has been replaced by the FBP [153]. Primarily, IR algorithms are designed to improve the quality of reconstructed images, using two steps for reconstruction, namely, forward and backward. The backward step is made up of a standard FBP which generates images from the projection data; the forward step produces projection data from images. These iterations are repeated for a specific time period to reach the final step of optimal image quality comparable with the FBP [159]. Reconstruction algorithms, by themselves, do not directly affect radiation dose reduction, only succeeding in improving image quality when low-dose CT is used. These improvements affect only image noise and contrast; accordingly, CT dose reduction is achieved indirectly using IR. By using nonlinear image processing, especially at a low CT dose, the IR technique can avoid undesirable disharmony between image noise and contrast [164].

Ranges of iterative image reconstruction algorithms are commercially available from all major CT manufacturers as one of the strategies for radiation dose reduction [159, 165]. The use of IR varies from one manufacturer to another as all have different ways of implementing the IR technique in their scanners. The available techniques include iterative reconstruction in image space (IRIS), which is iterating on the image domain only; sinogram affirmed iterative reconstruction (SAFIRE), and advanced modelled iterative reconstruction (ADMIRE) strength 3 by Siemens Medical Solutions. SAFIRE requires longer a reconstruction time than IRIS [62]. Adaptive iterative dose reduction 3D (AIDR-3D) (Toshiba Medical Systems) and iDose (Phillips Healthcare) are iterating in both raw data and

image domains, while adaptive statistical iterative reconstruction (ASIR) (GE Healthcare) and model based iterative reconstruction (MBIR) (Veo, GE Healthcare) differ from the others by iterating with forward and backward reconstruction steps [159]. MBIR requires longer computational time than the other, simpler IR methods. All these initially reconstruct data with an FBP, and subsequently perform multiple iterations with IR algorithms [157].

Many researchers have discovered that using IR in many CT procedures can effectively reduce radiation doses by at least 25% and up to 60% without significantly affecting image quality [164-167]. According to Leipsic et al. [166], up to a 25% dose reduction has been achieved in CT chest examinations using ASIR reconstruction. Winklehner et al. [165] confirmed high image quality and dose reduction of more than 50% using SAFIRE, compared to FBP in body CTA. Some researchers have found that using IR reduced image noise leads to increased CNR [168, 169]. Beam hardening artefacts have been solved using IR techniques [116, 165, 170]. A recent study evaluated coronary stents using IR techniques, and showed a significant noise reduction with higher SNR compared to FBP [115]. The key advantage of IR in DECT is the reduction of radiation dose. Using these methods with peripheral arterial stents may improve image quality with a lower radiation dose. Using these techniques may also offset the negative effects of a lower radiation dose on image quality [171]. As has been mentioned, managing these techniques wisely may overcome the deleterious effects of a lower radiation dose on image quality, particularly with the advancement of technology that is evident in DECT scanners.

2.10.3 Image processing techniques

DECTA image processing includes image-re-formatting processes such as multiplanar re-formatting (MPR) in coronal, sagittal, oblique and curved planes, and specifically maximum intensity projection (MIP) and volume rendering (VR). It is difficult to evaluate vascular anatomy using axial reconstructions alone, but these reconstruction procedures allow better visualisation of the vessels' details.

2.10.3.1 Maximum intensity projection (MIP)

When a peripheral arterial tree is presented in an angiographic style, assessment of arterial abnormalities is simple. This approach can be achieved perfectly with MIP or VR techniques [46]. MIP displays vasculature in a manner similar to conventional angiography, mainly when vessels are free or have minimal calcification. MIP thus becomes useful to create a DSA-like image, providing a road map for planning the treatment of peripheral arteries.

2.10.3.2 Volume rendering (VR)

Volume rendering images are produced by an algorithm that builds 3D views by combining a set of axial CT images. VR is an essential tool for realistically analysing volume data, for describing complex vascular anatomy, and for recognising pathological changes [46]. It is the ideal tool for fast interactive exploration of peripheral CT angiography data sets.

The main disadvantage of MIP and VR is that the presence of bones, calcified tissues and stents may limit the vascular flow in datasets. In the presence of calcified plaque, severe vessel wall calcification or stents, 2D MPR is crucial to evaluate vascular flow. Axial images, and sagittal, coronal or oblique MPRs are all useful for vessel evaluation in conjunction with VR. With DECTA applications, this limitation can be substantially reduced when monochromatic imaging spectral is used [134]. High energy images in DECT contribute to the optimal assessment of stenosis in severely calcified vessels, metal artefact reduction, and, to an extent, improvement in stent evaluation. Low energy in conventional CTA, on the other hand, is associated with higher image noise; but this can be improved with iterative reconstruction to yield good quality images [119]. These properties are particularly useful when DECTA is used; therefore, it is one of the main benefits arising from the enhancement of iodine attenuation on low-energy DECT images.

2.11 Summary

The use of DECT in peripheral arterial disease and stent evaluation has many potential benefits. Radiation doses can be reduced without compromising image quality; spectral imaging is another advantages; and using iterative reconstruction techniques with DECT in peripheral arterial stents may improve the overall procedure by decreasing both the noise and the radiation dose. With the use of a low contrast medium, this modality may eventually lead to better evaluation of stent patency in peripheral arteries. Multi-energy CT is a promising technique to overcome the limitations of DECT and differentiating three or more materials.

2.12 References

1. Al-Sheikh SO, Aljabri BA, Al-Ansary LA, Al-Khayal LA, Al-Salman MM, Al-Omran MA. Prevalence of and risk factors for peripheral arterial disease in Saudi Arabia. A pilot cross-sectional study. *Saudi Med J* 2007; 28(3):412–4.
2. Fowkes FGR, Rudan D, Rudan I, Aboyans V, Denenberg JO, McDermott MM et al. Comparison of global estimates of prevalence and risk factors for peripheral artery disease in 2000 and 2010: a systematic review and analysis. *Lancet* 2013; 382(9901):1329–40.
3. Norgren L, Hiatt WR, Dormandy JA, Nehler MR, Harris KA, Fowkes FGR. Inter-Society consensus for the management of peripheral arterial disease (TASC II). *E J Vasc Endovasc Surg* 2007; 33(1, supplement):S1–S75.
4. Murray CJ, Lopez AD. Alternative projections of mortality and disability by cause 1990–2020: Global Burden of Disease Study. *Lancet* 1997; 349(9064):1498–504.
5. Golomb BA, Dang TT, Criqui MH. Peripheral Arterial disease: morbidity and mortality implications. *Circulation* 2006; 114(7):688–99.
6. Grundy SM, Cleeman JI, Daniels SR, Donato KA, Eckel RH, Franklin BA et al. Diagnosis and management of the metabolic syndrome: an American Heart Association/National Heart, Lung, and Blood Institute Scientific Statement. *Circulation* 2005; 112(17):2735–52.
7. Rooke TW, Hirsch AT, Misra S, Sidawy AN, Beckman JA, Findeiss LK et al. 2011 ACCF/AHA Focused update of the guideline for the management of patients with peripheral artery disease (updating the 2005 Guideline). *Vasc Med* 2011; 16(6):452–76.
8. Sorensen J, Wilks SA, Jacob AD, Huynh TTT. Screening for Peripheral artery disease. *Semin Roentgenol* 2015; 50(2):139–47.
9. Rofsky NM, Adelman MA. MR Angiography in the Evaluation of atherosclerotic peripheral vascular disease. *Radiology* 2000; 214(2):325–38.
10. Dormandy JA, Rutherford RB. Management of peripheral arterial disease (PAD). TASC Working Group. TransAtlantic Inter-Society Consensus (TASC). *J Vasc Surg* 2000; 31(1 Pt 2):S1–S296.
11. Tendera M, Aboyans V, Bartelink ML, Baumgartner I, Clement D, Collet J-P et al. ESC guidelines on the diagnosis and treatment of peripheral artery diseases. *Eur Heart J* 2011; 32(22):2851–906.
12. Layden J, Michaels J, Bermingham S, Higgins B. Diagnosis and management of lower limb peripheral arterial disease: summary of NICE guidance. *BMJ* 2012 345 doi: 10.1136/bmj.e4947
13. Olin JW, Allie DE, Belkin M, Bonow RO, Casey Jr DE, Creager MA et al. ACCF/AHA/ACR/SCAI/SIR/SVM/SVN/SVS 2010 performance measures for adults with peripheral artery disease. *J Vasc Nurs* 2011; 29(1):23–60.
14. Clair D. Pros and cons for intravascular ultrasound in stenting. *Phlebology* 2013; 28(suppl 1):129–34.

15. Pollak AW, Norton PT, Kramer CM. Multimodality imaging of lower extremity peripheral arterial disease: current role and future directions. *Circ-Cardiovasc Imag* 2012; 5(6):797–807.
16. Kawarada O, Higashimori A, Noguchi M, Waratani N, Yoshida M, Fujihara M et al. Duplex criteria for in-stent restenosis in the superficial femoral artery. *Cathet Cardiovasc Interv* 2013; 81(4):E199–E205.
17. Baril DT, Rhee RY, Kim J, Makaroun MS, Chaer RA, Marone LK. Duplex criteria for determination of in-stent stenosis after angioplasty and stenting of the superficial femoral artery. *J Vasc Surg* 2009;49(1):133-8; discussion 9.
18. Krnic A, Vucic N, Sucic Z. Duplex scanning compared with intra-arterial angiography in diagnosing peripheral arterial disease: three analytical approaches. *VASA Zeitschrift fur Gefasskrankheiten* 2006; 35(2):86–91.
19. Cowell GW, Reid AW, Roditi GH. Changing trends in a decade of vascular radiology: the impact of technical developments of non-invasive techniques on vascular imaging. *Insights into Imaging* 2012; 3(5):495–504.
20. Hingorani A, Ascher E, Marks N. Preprocedural imaging: new options to reduce need for contrast angiography. *Semin Vasc Surg* 2007; 20(1):15–28.
21. Josephs SC, Rowley HA, Rubin GD. Atherosclerotic peripheral vascular disease symposium II: vascular magnetic resonance and computed tomographic imaging. *Circulation*. 2008; 118(25):2837–44.
22. Kohler M, Burg MC, Bunck AC, Heindel W, Seifarth H, Maintz D. Dual-source CT angiography of peripheral arterial stents: in vitro evaluation of 22 different stent types. *Radiol Res Pract* 2011;2011:103873.
23. Langenberger H, Schillinger M, Plank C, Sabeti S, Dick P, Cejna M et al. Agreement of duplex ultrasonography vs. computed tomography angiography for evaluation of native and in-stent SFA re-stenosis: findings from a randomized controlled trial. *Eur J Radiol* 2012; 81(9):2265–9.
24. Ho KY, Leiner T, de Haan MW, Kessels AG, Kitslaar PJ, van Engelshoven JM. Peripheral vascular tree stenoses: evaluation with moving-bed infusion-tracking MR angiography. *Radiology* 1998; 206(3):683–92.
25. Visser K, Hunink MG. Peripheral arterial disease: gadolinium-enhanced MR angiography versus color-guided duplex US—a meta-analysis. *Radiology* 2000; 216(1):67–77.
26. Nelemans PJ, Leiner T, de Vet HC, van Engelshoven JM. Peripheral arterial disease: meta-analysis of the diagnostic performance of MR angiography. *Radiology* 2000; 217(1):105–14.
27. Prince MR, Yucel EK, Kaufman JA, Harrison DC, Geller SC. Dynamic gadolinium-enhanced three-dimensional abdominal MR arteriography. *J Magn Reson Imaging* 1993; 3(6):877–81.

28. Jens S, Koelemay MJ, Reekers JA, Bipat S. Diagnostic performance of computed tomography angiography and contrast-enhanced magnetic resonance angiography in patients with critical limb ischaemia and intermittent claudication: systematic review and meta-analysis. *Eur Radiol* 2013; 23(11):3104–14.
29. Koelemay MJ, Lijmer JG, Stoker J, Legemate DA, Bossuyt PM. Magnetic resonance angiography for the evaluation of lower extremity arterial disease: a meta-analysis. *JAMA* 2001; 285(10):1338–45.
30. Plank C, Wolf F, Langenberger H, Weber M, Beitzke D, Stadler A et al. Improved detection of in-stent restenosis by blood pool agent-enhanced, high-resolution, steady-state magnetic resonance angiography. *Eur Radiol* 2011; 21(10):2158–65.
31. Blum MB, Schmook M, Scherthaner R, Edelhauser G, Puchner S, Lammer J et al. Quantification and detectability of in-stent stenosis with CT angiography and MR Angiography in arterial stents in vitro. *Am J Roentgenol* 2007; 189(5):1238–42.
32. Li XM, Li YH, Tian JM, Xiao Y, Lu JP, Jing ZP et al. Evaluation of peripheral artery stent with 64-slice multi-detector row CT angiography: prospective comparison with digital subtraction angiography. *Eur J Radiol*. 2010; 75(1):98–103.
33. Tendera M, Aboyans V, Bartelink M-L, Baumgartner I, Clément D, Collet J-P et al. ESC Guidelines on the diagnosis and treatment of peripheral artery diseases *Eur Heart J* 2011; 32:2851–2906
34. Nielsen YW, Thomsen HS. Contrast-enhanced peripheral MRA: technique and contrast agents. *Acta Radiologica* 2012; 53(7):769–77.
35. Weinreb JC, Abu-Alfa AK. Gadolinium-based contrast agents and nephrogenic systemic fibrosis: why did it happen and what have we learned? *J Magn Reson Imaging* 2009; 30(6):1236–9.
36. Todd DJ, Kagan A, Chibnik LB, Kay J. Cutaneous changes of nephrogenic systemic fibrosis: predictor of early mortality and association with gadolinium exposure. *Arthritis Rheum* 2007; 56(10):3433–41.
37. Johnson TC, Kalender W. Physical background. In: Johnson T, Fink C, Schönberg SO, Reiser MF (eds) *Dual energy CT in clinical practice*. Medical Radiology: Springer, Berlin; 2011, pp. 3–9.
38. Duddalwar VA. Multislice CT angiography: a practical guide to CT angiography in vascular imaging and intervention. *Br J Radiol* 2004; 77 Spec No 1(suppl 1):S27–38.
39. Feuchtner GM, Schachner T, Bonatti J, Friedrich GJ, Soegner P, Klauser A et al. Diagnostic performance of 64-slice computed tomography in evaluation of coronary artery bypass grafts. *Am J Roentgenol* 2007; 189(3):574–80.
40. Flohr T. CT systems. *Curr Radiol Rep* 2013; 1(1):52–63.
41. Rubin GD, Leipsic J, Schoepf UJ, Fleischmann D, Napel S. CT angiography after 20 Years: a transformation in cardiovascular disease characterization continues to advance. *Radiology* 2014; 271(3):633–52.
42. Met R, Bipat S, Legemate DA, Reekers JA, Koelemay MJ. Diagnostic performance of computed tomography angiography in peripheral arterial disease: a systematic review and meta-analysis. *JAMA* 2009; 301(4):415–24.

43. Endo M, Mori S, Tsunoo T, Miyazaki H. Magnitude and effects of x-ray scatter in a 256-slice CT scanner. *Med Phys* 2006; 33(9):3359–68.
44. Flohr TG, Schaller S, Stierstorfer K, Bruder H, Ohnesorge BM, Schoepf UJ. Multi-Detector row ct systems and image-reconstruction techniques. *Radiology* 2005; 235(3):756–73.
45. Sun Z. Diagnostic accuracy of multislice CT angiography in peripheral arterial disease. *J Vasc Interv Radiol* 2006; 17(12):1915–21.
46. Fleischmann D, Hallett RL, Rubin GD. CT angiography of peripheral arterial disease. *J J Vasc Interv Radiol* 2006; 17(1):3–26.
47. Fleischmann D. Lower-extremity CTA. In: Reiser MF, Becker CR, Nikolaou K, Glazer G (eds) *Multislice CT*. Springer, Berlin, 2009, pp. 321–30.
48. Foley WD, Stonely T. CT angiography of the lower extremities. *Radiol Clin North Am* 2010; 48(2):367–96, ix.
49. Smith-Bindman R, Lipson J, Marcus R et al. Radiation dose associated with common computed tomography examinations and the associated lifetime attributable risk of cancer. *Arch Intern Med* 2009; 169(22):2078–86.
50. Laks S, Macari M, Chandarana H. Dual-energy computed tomography imaging of the aorta after endovascular repair of abdominal aortic aneurysm. *Semin Ultrasound CT MR* 2010; 31(4):292–300.
51. Shareghi S, Gopal A, Gul K, Matchinson JC, Wong CB, Weinberg N et al. Diagnostic accuracy of 64 multidetector computed tomographic angiography in peripheral vascular disease. *Catheter Cardiovasc Interv*. 2010; 75(1):23–31.
52. Schernthaner R, Stadler A, Lomoschitz F, Weber M, Fleischmann D, Lammer J et al. Multidetector CT angiography in the assessment of peripheral arterial occlusive disease: accuracy in detecting the severity, number, and length of stenoses. *Eur Radiol* 2008; 18(4):665–71.
53. Catalano C, Fraioli F, Laghi A, Napoli A, Bezzi M, Pediconi F et al. Infrarenal aortic and lower-extremity arterial disease: diagnostic performance of multi-detector row CT angiography. *Radiology* 2004; 231(2):555–63.
54. Ota H, Takase K, Igarashi K, Chiba Y, Haga K, Saito H et al. MDCT compared with digital subtraction angiography for assessment of lower extremity arterial occlusive disease: importance of reviewing cross-sectional images. *Am J Roentgenol* 2004; 182(1):201–9.
55. Laswed T, Rizzo E, Guntern D, Doenz F, Denys A, Schnyder P et al. Assessment of occlusive arterial disease of abdominal aorta and lower extremities arteries: value of multidetector CT angiography using an adaptive acquisition method. *Eur Radiol* 2008; 18(2):263–72.
56. Napoli A, Anzidei M, Zaccagna F, Marincola BC, Zini C, Brachetti G et al. Peripheral Arterial occlusive disease: diagnostic performance and effect on therapeutic management of 64-section CT angiography. *Radiology* 2011; 261(3):976–86.

57. Sabeti S, Schillinger M, Amighi J, Sherif C, Mlekusch W, Ahmadi R et al. Primary patency of femoropopliteal arteries treated with nitinol versus stainless steel self-expanding stents: propensity score-adjusted analysis. *Radiology* 2004; 232(2):516–21.
58. Halliburton SS, Abbara S, Chen MY, Gentry R, Mahesh M, Raff gl et al. SCCT guidelines on radiation dose and dose-optimization strategies in cardiovascular CT. *J Cardiovasc CT* 2011; 5(4):198–224.
59. Flohr TG, McCollough CH, Bruder H, Petersilka M, Gruber K, Suss C et al. First performance evaluation of a dual-source CT (DSCT) system. *Eur Radiol* 2006; 16(2):256–68.
60. Thorsten Johnson CF, Stefan O. Schönberg, Maximilian F. Reiser. *Dual energy CT in clinical practice*. Springer, Berlin, 2011.
61. Petersilka M, Bruder H, Krauss B, Stierstorfer K, Flohr TG. Technical principles of dual source CT. *Eur J Radiol* 2008; 68(3):362–8.
62. Siemens. Siemens SOMATOM Force. 2015. Available from: <http://www.healthcare.siemens.com/computed-tomography/dual-source-ct/somatom-force>
63. Yu L, Christner JA, Leng S, Wang J, Fletcher JG, McCollough CH. Virtual monochromatic imaging in dual-source dual-energy CT: radiation dose and image quality. *Med Phys* 2011; 38(12):6371–9.
64. Hounsfield GN. Computerized transverse axial scanning (tomography): part 1: description of system. *Br J Radiol* 1973; 46(552):1016–22.
65. Coursey CA, Nelson RC, Boll DT, Paulson EK, Ho LM, Neville AM et al. Dual-energy multidetector CT: how does it work, what can it tell us, and when can we use it in abdominopelvic imaging? *Radiographics* 2010; 30(4):1037–55.
66. Graser A, Johnson TR, Chandarana H, Macari M. Dual energy CT: preliminary observations and potential clinical applications in the abdomen. *Eur Radiol* 2009; 19(1):13–23.
67. Sengupta S, Jha S, Walter D, Du Y, Tkaczyk EJ, editors. *Dual energy for material differentiation in coronary arteries using electron-beam CT2005*. Proceedings of the SPIE 2005: 5745, pp. 1306–16
68. Silva AC, Morse BG, Hara AK, Paden RG, Hongo N, Pavlicek W. Dual-energy (spectral) CT: applications in abdominal imaging. *Radiographics* 2011; 31(4):1031–46; discussion 47–50.
69. Pessis E, Campagna R, Sverzut JM, Bach F, Rodallec M, Guerini H et al. Virtual monochromatic spectral imaging with fast kilovoltage switching: reduction of metal artifacts at CT. *Radiographics* 2013; 33(2):573–83.
70. Kaza RK, Platt JF, Cohan RH, Caoili EM, Al-Hawary MM, Wasnik A. Dual-energy CT with single- and dual-source scanners: current applications in evaluating the genitourinary tract. *Radiographics* 2012; 32(2):353–69.
71. Kang MJ, Park CM, Lee CH, Goo JM, Lee HJ. Dual-energy CT: clinical applications in various pulmonary diseases. *Radiographics* 2010; 30(3):685–98.

72. Paul J, Mbalisike EC, Nour-Eldin NE, Vogl TJ. Dual-source 128-slice MDCT neck: radiation dose and image quality estimation of three different protocols. *Eur J Radiol* 2013; 82(5):787–96.
73. Johnson TR. Dual-energy CT: general principles. *AJR Am J Roentgenol* 2012; 199(5 Suppl):S3–8.
74. McCollough CH, Leng S, Yu L, Fletcher JG. Dual- and Multi-Energy CT: Principles, Technical Approaches, and Clinical Applications. *Radiology*. 2015;276(3):637-53.
75. Marin D, Boll DT, Mileto A, Nelson RC. State of the Art: Dual-Energy CT of the Abdomen. *Radiology* 2014; 271(2):327–42.
76. Matsumoto K, Jinzaki M, Tanami Y, Ueno A, Yamada M, Kuribayashi S. Virtual monochromatic spectral imaging with fast kilovoltage switching: improved image quality as compared with that obtained with conventional 120–kVp CT. *Radiology* 2011; 259(1):257–62.
77. Bamberg F, Dierks A, Nikolaou K, Reiser MF, Becker CR, Johnson TR. Metal artifact reduction by dual energy computed tomography using monoenergetic extrapolation. *Eur Radiol* 2011; 21(7):1424–9.
78. Brockmann C, Jochum S, Sadick M, Huck K, Ziegler P, Fink C et al. Dual-energy CT angiography in peripheral arterial occlusive disease. *Cardiovasc Intervent Radiol* 2009; 32(4):630–7.
79. Apfaltrer P, Sudarski S, Schneider D, Nance Jr JW, Haubenreisser H, Fink C et al. Value of monoenergetic low-kVp dual energy CT datasets for improved image quality of CT pulmonary angiography. *Eur J Radiol* 2014; 83(2):322–8.
80. Kau T, Eicher W, Reiterer C, Niedermayer M, Rabitsch E, Senft B et al. Dual-energy CT angiography in peripheral arterial occlusive disease: accuracy of maximum intensity projections in clinical routine and subgroup analysis. *Eur Radiol* 2011; 21(8):1677–86.
81. Yamamoto S, McWilliams J, Arellano C, Marfori W, Cheng W, McNamara T et al. Dual-energy CT angiography of pelvic and lower extremity arteries: dual-energy bone subtraction versus manual bone subtraction. *Clin Radiol* 2009; 64(11):1088–96.
82. Meyer BC, Werncke T, Hopfenmuller W, Raatschen HJ, Wolf KJ, Albrecht T. Dual energy CT of peripheral arteries: effect of automatic bone and plaque removal on image quality and grading of stenoses. *Eur J Radiol* 2008; 68(3):414–22.
83. Huang SY, Nelson RC, Miller MJ, Kim CY, Lawson JH, Husarik DB et al. Assessment of vascular contrast and depiction of stenoses in abdominopelvic and lower extremity vasculature: comparison of dual-energy MDCT with digital subtraction angiography. *Acad Radiol* 2012; 19(9):1149–57.
84. De Zordo T, von Lutterotti K, Dejaco C, Soegner PF, Frank R, Aigner F, et al. Comparison of image quality and radiation dose of different pulmonary CTA protocols on a 128-slice CT: high-pitch dual source CT, dual energy CT and conventional spiral CT. *Eur Radiol* 2012;22(2):279-86.

85. de Broucker T, Pontana F, Santangelo T, Faivre JB, Tacelli N, Delannoy-Deken V, et al. Single- and dual-source chest CT protocols: levels of radiation dose in routine clinical practice. *Diagn Intervent Imag* 2012; 93(11):852-8.
86. Kamiya K, Kunimatsu A, Mori H, Sato J, Akahane M, Yamakawa T et al. Preliminary report on virtual monochromatic spectral imaging with fast kVp switching dual energy head CT: comparable image quality to that of 120-kVp CT without increasing the radiation dose. *Jpn J Radiol* 2013; 31(4):293-8.
87. Delesalle MA, Pontana F, Duhamel A, Faivre JB, Flohr T, Tacelli N et al. Spectral optimization of chest CT angiography with reduced iodine load: experience in 80 patients evaluated with dual-source, dual-energy CT. *Radiology* 2013; 267(1):256-66.
88. Maturen KE, Kaza RK, Liu PS, Quint LE, Khalatbari SH, Platt JF. 'Sweet SPOT' for Endoleak detection: optimizing contrast to noise using low keV Reconstructions from fast-switch kVp dual-energy CT. *J Comput Assist Tomogr* 2012; 36(1):83-7.
89. Sudarski S, Apfaltrer P, W. Nance J J, Schneider D, Meyer M, Schoenberg SO et al. Optimization of keV-settings in abdominal and lower extremity dual-source dual-energy CT angiography determined with virtual monoenergetic imaging. *Eur J Radiol* 2013; 82(10):e574-81.
90. Pinho DF, Kulkarni NM, Krishnaraj A, Kalva SP, Sahani DV. Initial experience with single-source dual-energy CT abdominal angiography and comparison with single-energy CT angiography: image quality, enhancement, diagnosis and radiation dose. *Eur Radiol* 2013; 23(2):351-9.
91. Anderson NG, Butler AP, Scott NJ, Cook NJ, Butzer JS, Schleich N et al. Spectroscopic (multi-energy) CT distinguishes iodine and barium contrast material in MICE. *Eur Radiol* 2010; 20(9):2126-34.
92. Fornaro J, Leschka S, Hibbeln D, Butler A, Anderson N, Pache G et al. Dual- and multi-energy CT: approach to functional imaging. *Insights into imaging* 2011; 2(2):149-59.
32. Schlomka JP, Roessl E, Dorscheid R, Dill S, Martens G, Istel T et al. Experimental feasibility of multi-energy photon-counting K-edge imaging in pre-clinical computed tomography. *Phys Med Biol* 2008; 53(15):4031-47.
94. Goldman LW. Principles of CT: radiation dose and image quality. *J Nucl Med Technol.* 2007; 35(4):213-25; quiz 26-8.
95. Bogaert E, Bacher K, Lemmens K, Carlier M, Desmet W, Wagter XD et al. A large-scale multicentre study of patient skin doses in interventional cardiology: dose-area product action levels and dose reference levels. *Br J Radiol* 2009; 82(976):303-12.
96. Preston DL, Ron E, Tokuoka S, Funamoto S, Nishi N, Soda M et al. Solid cancer incidence in atomic bomb survivors: 1958-1998. *Radiat Res* 2007; 168(1):1-64.
97. Pierce DA, Preston DL. Radiation-related cancer risks at low doses among atomic bomb survivors. *Radiat Res* 2000; 154(2):178-86.

98. Pierce DA, Shimizu Y, Preston DL, Vaeth M, Mabuchi K. Studies of the mortality of atomic bomb survivors. Report 12, Part I. Cancer: 1950–1990. *Radiat Res* 1996; 146(1):1–27.
99. Brenner DJ, Elliston CD, Hall EJ, Berdon WE. Estimated Risks of radiation-induced fatal cancer from pediatric CT. *Am J Roentgenol* 2001; 176(2):289–96.
100. Bauhs JA, Vrieze TJ, Primak AN, Bruesewitz MR, McCollough CH. CT Dosimetry: comparison of measurement techniques and devices. *RadioGraphics* 2008; 28(1):245–53.
101. Lee CH, Goo JM, Ye HJ, Ye SJ, Park CM, Chun EJ et al. Radiation dose modulation techniques in the multidetector CT era: from basics to practice. *Radiographics* 2008; 28(5):1451–9.
102. Hohl C, Muhlenbruch G, Wildberger JE, Leidecker C, Suss C, Schmidt T et al. Estimation of radiation exposure in low-dose multislice computed tomography of the heart and comparison with a calculation program. *Eur Radiol* 2006; 16(8):1841–6.
103. Huda W, Schoepf UJ, Abro JA, Mah E, Costello P. Radiation-related cancer risks in a clinical patient population undergoing cardiac CT. *Am J Roentgenol* 2011; 196(2):W159–65.
104. Dougeni E, Faulkner K, Panayiotakis G. A review of patient dose and optimisation methods in adult and paediatric CT scanning. *Eur J Radiol* 2012; 81(4):e665–83.
105. The 2007 recommendations of the International Commission on Radiological Protection. ICRP publication 103. *Annals of the ICRP*, 2007; 37(2–4):1–332.
106. Saltybaeva N, Jafari ME, Hupfer M, Kalender WA. Estimates of effective dose for CT Scans of the lower extremities. *Radiology* 2014; 273(1):153–9.
107. Werner M, Scheinert D. Drug eluting devices for critically ill patients: can we apply lessons learned from the treatment of peripheral artery disease? *Adv Drug Deliv Rev* 2014; 77:32–9.
108. Tapping CR, Ahmed M, Scott PM, Lakshminarayan R, Robinson GJ, Ettles DF et al. Primary infrarenal aortic stenting with or without iliac stenting for isolated and aortoiliac stenoses: single-centre experience with long-term follow-up. *Cardiovasc Intervent Radiol* 2013; 36(1):62–8.
109. Maurel B, Lancelevee J, Jacobi D, Bleuet F, Martinez R, Lermusiaux P. Endovascular treatment of external iliac artery stenoses for claudication with systematic stenting. *Ann Vasc Surg* 2009; 23(6):722–8.
110. Murphy TP, Ariaratnam NS, Wilfred I, Carney J, Marcaccio EJ, Slaiby JM, Soares GM et al. Aortoiliac Insufficiency: long-term experience with stent placement for treatment. *Radiology* 2004; 231(1):243–9.
111. Park SH, Rha SW, Choi CU, Kim EJ, Oh DJ, Cho YH et al. Efficacy of two different self-expanding nitinol stents for atherosclerotic femoropopliteal arterial disease (SENS-FP trial): study protocol for a randomized controlled trial. *Trials* 2014; 15:355.

112. Banerjee S, Das TS, Abu-Fadel MS, Dippel EJ, Shammam NW, Tran DL; et al. Pilot trial of cryoplasty or conventional balloon post-dilation of nitinol stents for revascularization of peripheral arterial segments: the COBRA trial. *J Am Coll Cardiol* 2012; 60(15):1352–9.
113. Liistro F, Grotti S, Porto I, Angioli P, Ricci L, Ducci K et al. Drug-Eluting balloon in peripheral intervention for the superficial femoral artery: the DEBATE-SFA randomized trial (drug eluting balloon in peripheral intervention for the superficial femoral artery). *JACC: Cardiovascular Interventions* 2013; 6(12):1295–302.
113. Ebersberger U, Tricarico F, Schoepf UJ, Blanke P, Spears JR, Rowe GW et al. CT evaluation of coronary artery stents with iterative image reconstruction: improvements in image quality and potential for radiation dose reduction. *Eur Radiol* 2013; 23(1):125–32.
114. Blum MB, Schmook M, Scherthaner R, Edelhauser G, Puchner S, Lammer J, et al. Quantification and detectability of in-stent stenosis with CT angiography and MR angiography in arterial stents in vitro. *Am J Roentgenol* 2007; 189(5):1238-42.
115. Ebersberger U, Tricarico F, Schoepf UJ, Blanke P, Spears JR, Rowe GW, et al. CT evaluation of coronary artery stents with iterative image reconstruction: improvements in image quality and potential for radiation dose reduction. *Eur Radiol* 2013; 23(1):125-32.
116. Nelson RC, Feuerlein S, Boll DT. New iterative reconstruction techniques for cardiovascular computed tomography: how do they work, and what are the advantages and disadvantages? *J Cardiovasc CT* 2011; 5(5):286–92.
117. Manousaki E, Perisinakis K, Karantanis A, Tsetis D. MDCT angiography assessment of renal artery in-stent restenosis: can we reduce the radiation exposure burden? A feasibility study. *Eur J Radiol* 2011; 79(2):224–31.
118. Zou Y, Silver MD Elimination of blooming artifacts off stents by dual energy CT In Samei E, Hsieh J (eds) *Medical imaging 2009: Physics of Medical Imaging*. Proceedings of SPIE, 13 March 2009. doi: 10.1117/12.811696
119. Gassenmaier T, Petri N, Allmendinger T, Flohr T, Maintz D, Voelker W et al. Next generation coronary CT angiography: in vitro evaluation of 27 coronary stents. *Eur Radiol* 2014; 24(11):2953–61.
120. Richenberg J. How to reduce nephropathy following contrast-enhanced CT: a lesson in policy implementation. *Clin Radiol* 2012; 67(12):1136–45.
121. Bae KT, Heiken JP. Scan and contrast administration principles of MDCT. *Eur Radiol* 2005; 15 Suppl 5:E46–59.
122. Hallett RL, Fleischmann D. Tools of the trade for CTA: MDCT scanners and contrast medium injection protocols. *Tech Vasc Interv Radiol* 2006; 9(4):134–42.
123. Utsunomiya D, Oda S, Funama Y, Awai K, Nakaura T, Yanaga Y et al. Comparison of standard- and low-tube voltage MDCT angiography in patients with peripheral arterial disease. *Eur Radiol* 2010; 20(11):2758–65.

124. Nakayama Y, Awai K, Funama Y, Liu D, Nakaura T, Tamura Y et al. Lower tube voltage reduces contrast material and radiation doses on 16-MDCT aortography. *Am J Roentgenol* 2006; 187(5):W490–7.
125. Iezzi R, Santoro M, Marano R, Di Stasi C, Dattesi R, Kirchin M et al. Low-dose multidetector CT angiography in the evaluation of infrarenal aorta and peripheral arterial occlusive disease. *Radiology* 2012; 263(1):287–98.
126. Megibow AJ, Sahani D. Best practice: implementation and use of abdominal dual-energy CT in routine patient care. *Am J Roentgenol* 2012; 199(5 Suppl):S71–7.
127. Yuan R, Shuman WP, Earls JP, Hague CJ, Mumtaz HA, Scott-Moncrieff A et al. Reduced iodine load at CT pulmonary angiography with dual-energy monochromatic imaging: comparison with standard CT pulmonary angiography—a prospective randomized trial. *Radiology* 2012; 262(1):290–7.
128. Dong J, Wang X, Jiang X, Gao L, Li F, Qiu J et al. Low-contrast agent dose dual-energy CT monochromatic imaging in pulmonary angiography versus routine CT. *J Comput Assist Tomogr* 2013; 37(4):618–25.
129. Månsson LG. Methods for the evaluation of image quality: a review. *Radiat Prot Dosim* 2000; 90(1–2):89–99.
130. European Commission. European Guidelines on quality Criteria for Computed Tomography: Report. Brussels European Commission; 1999. EUR 16262.
131. Primak AN, McCollough CH, Bruesewitz MR, Zhang J, Fletcher JG. Relationship between noise, dose, and pitch in cardiac multi-detector row CT. *Radiographics* 2006; 26(6):1785–94.
132. McCollough CH, Bruesewitz MR, James M, Kofler J. CT dose reduction and dose management tools: overview of available options. *RadioGraphics* 2006; 26(2):503–12.
133. Behrendt FF, Schmidt B, Plumhans C, Keil S, Woodruff SG, Ackermann D et al. Image fusion in dual energy computed tomography: effect on contrast enhancement, signal-to-noise ratio and image quality in computed tomography angiography. *Invest Radiol* 2009; 44(1):1–6.
134. Vlahos I, Chung R, Nair A, Morgan R. Dual-energy CT: vascular applications. *Am J Roentgenol* 2012; 199(5):S87–S97.
135. Gramer BM, Muenzel D, Leber V, von Thaden AK, Feussner H, Schneider A et al. Impact of iterative reconstruction on CNR and SNR in dynamic myocardial perfusion imaging in an animal model. *Eur Radiol* 2012; 22(12):2654–61.
136. Holmes DR, Fletcher JG, Apel A, Huprich JE, Siddiki H, Hough DM et al. Evaluation of non-linear blending in dual-energy computed tomography. *Eur J Radiol* 2008; 68(3):409–13.
137. Li S, Wang C, Jiang X, Xu G. Effects of dual-energy CT with non-linear blending on abdominal CT angiography. *Korean J Radiol* 2014; 15(4):430–8.
138. Singh S, Kalra MK. Scan parameters and CT Radiation dose. In: Tack D, Kalra MK, Gevenois PA (eds) *Radiation Dose from Multidetector CT*. Medical Radiology: Springer, Berlin, 2012, pp. 119–29.

139. Wintersperger B, Jakobs T, Herzog P, Schaller S, Nikolaou K, Suess C et al. Aorto-iliac multidetector-row CT angiography with low kVp settings: improved vessel enhancement and simultaneous reduction of radiation dose. *Eur Radiol* 2005; 15(2):334–41.
140. Iezzi R, Cotroneo AR, Giammarino A, Spigonardo F, Storto ML. Low-dose multidetector-row CT-angiography of abdominal aortic aneurysm after endovascular repair. *Eur J Radiol* 2011; 79(1):21–8.
141. Apfaltrer P, Hanna EL, Schoepf UJ, Spears JR, Schoenberg SO, Fink C et al. Radiation dose and image quality at high-pitch CT angiography of the aorta: intraindividual and interindividual comparisons with conventional CT angiography. *Am J Roentgenol* 2012; 199(6):1402–9.
142. Goetti R, Winklehner A, Gordic S, Baumueller S, Karlo CA, Frauenfelder T et al. Automated attenuation-based kilovoltage selection: preliminary observations in patients after endovascular aneurysm repair of the abdominal aorta. *Am J Roentgenol* 2012; 199(3):W380–5.
143. Mayer C, Meyer M, Fink C, Schmidt B, Sedlmair M, Schoenberg SO et al. Potential for radiation dose savings in abdominal and chest CT using automatic tube voltage selection in combination with automatic tube current modulation. *Am J Roentgenol* 2014; 203(2):292–9.
144. Schindera ST, Winklehner A, Alkadhi H, Goetti R, Fischer M, Gnannt R et al. Effect of automatic tube voltage selection on image quality and radiation dose in abdominal CT angiography of various body sizes: a phantom study. *Clin Radiol* 2013; 68(2):e79–e86.
145. Eller A, May MS, Scharf M, Schmid A, Kuefner M, Uder M et al. Attenuation-based automatic kilovolt selection in abdominal computed tomography: effects on radiation exposure and image quality. *Invest Radiol* 2012; 47(10):559–65.
146. Eller A, Wuest W, Scharf M, Brand M, Achenbach S, Uder M et al. Attenuation-based automatic kilovolt (kVp)-selection in computed tomography of the chest: effects on radiation exposure and image quality. *Eur J Radiol* 2013; 82(12):2386–91.
147. Krazinski A, Meinel F, Schoepf UJ, Silverman J, Canstein C, De Cecco C et al. Reduced radiation dose and improved image quality at cardiovascular CT angiography by automated attenuation-based tube voltage selection: intra-individual comparison. *Eur Radiol* 2014; 24(11):2677–84.
148. Hough DM, Fletcher JG, Grant KL, Fidler JL, Yu L, Geske JR et al. Lowering kilovoltage to reduce radiation dose in contrast-enhanced abdominal CT: initial assessment of a prototype automated kilovoltage selection tool. *Am J Roentgenol* 2012; 199(5):1070–7.
149. Macari M, Spieler B, Kim D, Graser A, Megibow AJ, Babb J et al. Dual-source dual-energy MDCT of pancreatic adenocarcinoma: initial observations with data generated at 80 kVp and at simulated weighted-average 120 kVp. *Am J Roentgenol* 2010; 194(1):W27–W32.

150. Chandarana H, Godoy MC, Vlahos I, Graser A, Babb J, Leidecker C et al. Abdominal aorta: evaluation with dual-source dual-energy multidetector CT after endovascular repair of aneurysms—initial observations. *Radiology* 2008; 249(2):692–700.
151. Keeling AN, Farrelly C, Carr JC, Yaghmai V. Technical considerations for lower limb multidetector computed tomographic angiography. *Vasc Med* 2011; 16(2):131–43.
152. Haaga JR, Miraldi F, MacIntyre W, LiPuma JP, Bryan PJ, Wiesen E. The effect of mAs variation upon computed tomography image quality as evaluated by in vivo and in vitro studies. *Radiology* 1981; 138(2):449–54.
153. Fleischmann D, Boas FE. Computed tomography: old ideas and new technology. *Eur Radiol* 2011; 21(3):510–7.
154. Smith AB, Dillon WP, Gould R, Wintermark M. Radiation dose-reduction strategies for neuroradiology CT protocols. *Am J Neuroradiol* 2007; 28(9):1628–32.
153. Beister M, Kolditz D, Kalender WA. Iterative reconstruction methods in X-ray CT. *Physica Medica* 2012; 28(2):94–108.
156. Li X, Luo S. A compressed sensing-based iterative algorithm for CT reconstruction and its possible application to phase contrast imaging. *Biomed Eng Online* 2011; 10:73.
157. Baek J, Pelc NJ. The noise power spectrum in CT with direct fan beam reconstruction. *Med Phys* 2010; 37(5):2074–81.
158. Pan X, Sidky EY, Vannier M. Why do commercial CT scanners still employ traditional, filtered back-projection for image reconstruction? *Inverse Problems* 2009; 25(12):1230009.
159. Willemink MJ, de Jong PA, Leiner T, de Heer LM, Nievelstein RA, Budde RP et al. Iterative reconstruction techniques for computed tomography part 1: technical principles. *Eur Radiol* 2013; 23(6):1623–31.
160. Korn A, Bender B, Fenchel M, Spira D, Schabel C, Thomas C et al. Sinogram affirmed iterative reconstruction in head CT: improvement of objective and subjective image quality with concomitant radiation dose reduction. *Eur J Radiol* 2013; 82(9):1431–5.
161. Bittencourt M, Schmidt B, Seltmann M, Muschiol G, Ropers D, Daniel W et al. Iterative reconstruction in image space (IRIS) in cardiac computed tomography: initial experience. *Int J Cardiovasc Imaging* 2011; 27(7):1081–7.
162. Silva AC, Lawder HJ, Hara A, Kujak J, Pavlicek W. Innovations in CT Dose reduction strategy: application of the adaptive statistical iterative reconstruction algorithm. *Am J Roentgenol* 2010; 194(1):191–9.
163. Katsura M, Matsuda I, Akahane M, Yasaka K, Hanaoka S, Akai H et al. Model-based iterative reconstruction technique for ultralow-dose chest CT: comparison of pulmonary nodule detectability with the adaptive statistical iterative reconstruction technique. *Invest Radiol* 2013; 48(4):206–12.

164. Hara AK, Paden RG, Silva AC, Kujak JL, Lawder HJ, Pavlicek W. Iterative reconstruction technique for reducing body radiation dose at CT: feasibility study. *Am J Roentgenol* 2009; 193(3):764–71.
165. Winklehner A, Karlo C, Puipe G, Schmidt B, Flohr T, Goetti R et al. Raw data-based iterative reconstruction in body CTA: evaluation of radiation dose saving potential. *Eur Radiol* 2011; 21(12):2521–6.
166. Leipsic J, Nguyen G, Brown J, Sin D, Mayo JR. A prospective evaluation of dose reduction and image quality in chest CT using adaptive statistical iterative reconstruction. *Am J Roentgenol* 2010; 195(5):1095–9.
167. Desai GS, Uppot RN, Yu EW, Kambadakone AR, Sahani DV. Impact of iterative reconstruction on image quality and radiation dose in multidetector CT of large body size adults. *Eur Radiol* 2012; 22(8):1631–40.
168. Yin WH, Lu B, Li N, Han L, Hou ZH, Wu RZ et al. Iterative reconstruction to preserve image quality and diagnostic accuracy at reduced radiation dose in coronary CT angiography: an intraindividual comparison. *JACC Cardiovasc Imaging* 2013; 6(12):1239–49.
169. Wang R, Schoepf UJ, Wu R, Reddy RP, Zhang C, Yu W et al. Image quality and radiation dose of low dose coronary CT angiography in obese patients: sinogram affirmed iterative reconstruction versus filtered back projection. *Eur J Radiol* 2012; 81(11):3141–5.
170. Raman SP, Johnson PT, Deshmukh S, Mahesh M, Grant KL, Fishman EK. CT dose reduction applications: available tools on the latest generation of CT scanners. *J Am Coll Radiol* 2013; 10(1):37–41.
171. Renker M, Geyer LL, Krazinski AW, Silverman JR, Ebersberger U, Schoepf UJ. Iterative image reconstruction: a realistic dose-saving method in cardiac CT imaging? *Expert Rev Cardiovasc Ther* 2013; 11(4):403–9.

Every reasonable effort has been made to acknowledge the owners of copyright material. I would be pleased to hear from any copyright owner who has been omitted or incorrectly acknowledged.

Chapter 3 Dual energy computed tomography angiography in the peripheral arterial imaging: A systematic review of image quality, radiation dose and diagnostic value¹

The usefulness of DECT technologies and how their application in lower extremities could improve the image quality was presented in Chapter 2. This chapter is a systematic review conducted to identify the factors affecting the image quality and radiation dose of DECTA in peripheral stenting. It also illustrates the diagnostic value of DECTA and the use of contrast mediums in peripheral arterial imaging.

3.1 Introduction

The recent development of dual-energy computed tomography (DECT) allows the utilisation of this technology for differentiation of materials, enhancing diagnostic accuracy when compared to conventional CT [1, 2]. The main advantage of DECT is the use of various kiloelectron volt (keV) values ranging from 40 to 190 keV, which leads to improvement in differentiating different materials, such as iodine mapping, and improvement in diagnosis of cardiovascular disease [3]. The main characteristics of DECT lie in its ability to produce and display either monochromatic or material differentiation in an image [4], such as separating iodine from calcification and other materials [5], a process beyond traditional single-energy CT. Use of DECT in clinical practice provides better image quality and may lower the radiation dose by eliminating the true unenhanced series as shown in DECT abdominal protocols [6–10]. The lower tube potential (kVp) in DECT not only has higher contrast

¹ This chapter is a version of Almutairi A, & Sun Z, Dual energy computed tomography angiography in peripheral arterial imaging: a systematic review of image quality, radiation dose and diagnostic value, accepted 14 April, 2016 by Current Medical Imaging Reviews.

attenuation than the high kVp images, but is associated with a high contrast-to-noise ratio (CNR), achieving higher vascular enhancement with lower image noise [4].

The concept of using low kVp in DECT can be applied to evaluate peripheral arterial disease (PAD). Cardiovascular structure can also be assessed with improved accuracy when bone removal application is used in DECT [3, 11]. Virtual monochromatic images (MEIs) at the desired energy level can be produced by subtracting the iodine from the images [12].

Accurate detection and analysis of vessel wall calcification in the cardiovascular system, especially in lower extremities, is one of the main challenges for conventional CT angiography (CTA) due to blooming artefacts arising from heavy calcification [13, 14]; the use of DECT may overcome this limitation. Despite the advantages of DECT, the associated radiation dose is still a major concern in the medical field [15]. Furthermore, use of contrast mediums leads to the potential risk of contrast-induced acute kidney injury. Reduction of contrast medium during DECT is another research direction in the current literature [2, 16].

Although a number of studies of the use of DECT in lower extremities have been reported in the literature with promising results, their findings are variable. To the best of our knowledge there is no systematic review of the diagnostic value, image quality or radiation dose associated with DECT angiography (DECTA) in peripheral arterial disease; thus, this systematic review is conducted to determine the diagnostic performance of DECT in PAD, based on analysis of the current literature.

3.2 Materials and methods

3.2.1 Literature searching and data selection criteria

The literature search was performed by using different databases including PubMed, ProQuest, Medline and ScienceDirect. The keywords used for searching the eligible references included dual energy computed tomography, DECT and cardiovascular disease, dual source computed tomography and cardiovascular disease, DECT and peripheral angiography, DECT and radiation dose and image quality, diagnostic value of DECT in cardiovascular disease. The reference lists of identified articles were checked manually to obtain additional relevant articles. Article inclusion criteria were: 1) published between 2006 and October 2015 (DECT was introduced in 2006); 2) published in the English language; 3) prospective and retrospective studies with at least 10 patients and with one DECT series performed and with (a) radiation dose or image quality comparison with conventional CTA or invasive angiography or (b) diagnostic value (in terms of sensitivity and specificity) in

comparison with conventional CTA or DSA. Exclusion criteria were review articles, comments to the editor, phantom studies, case reports and conference abstracts.

3.2.2 Study selection

Two reviewers independently assessed the title and abstract of the identified articles for eligibility based on the study design and procedure techniques. After this initial selection, the full texts of the potentially eligible articles were retrieved and assessed for eligibility by the both authors of this article independently. Agreement on the final data and results were resolved by consensus. Potentially missed relevant articles were identified by checking the reference lists of the included articles.

3.2.3 Data extraction

A data extraction sheet was developed, including the year of publication, number of subjects, their age, gender, body mass index (BMI), type of CT scanner, section thickness, reconstruction interval, gantry rotation time, beam collimation, pitch, tube voltage, and current. Radiation dose parameters were volume CT dose index ($CTDI_{vol}$), dose length product (DLP), and effective dose (E). Image quality based on the image noise, signal-to-noise ratio (SNR), and CNR data was also extracted. The accuracy of DECTA based on sensitivity and specificity was extracted from each study. Additionally, the use of contrast material for DECTA was extracted, including the following details: contrast medium type, contrast concentration mg/ml, flow rate mL/s, method of dose calculation, and CT threshold (HU) for scan initiation.

3.2.4 Data analysis

Data was entered into SPSS V 22.0 for statistical analysis (SPSS Inc, Chicago, IL, USA). Categorical variables were presented as percentages or frequencies. Diagnostic value of sensitivity, specificity, image quality and radiation dose were analysed with mean values reported and compared using the student T test.

3.3 Results

3.3.1 Study selection

The initial search yielded 335 articles from all the databases examined in this study. A total of 18 studies met the selection criteria and nine [11, 14, 17–23] were found to be eligible for analysis. Four studies were excluded as they evaluated the venography system, while another

three evaluating the upper extremities were excluded as well; the remaining two did not use a dual energy mode. Figure 1 is the flow chart showing the search process for identifying eligible studies. Two types of CT scanner were used in these studies, with eight studies using the Somatom definition 64-slice dual-source CT [11, 14, 17–22], and one using a fast kilovoltage-switching 64-slice CT scanner [23]. The total number of patients included in these studies was 286, with a mean age of 67.5 years. Of these nine studies, only four reported the radiation dose [14, 17, 19, 24]; none compared the radiation dose with that of conventional CTA. For the scanning parameters used in these studies, the section thickness ranged from 1 mm to 1.5 mm and the reconstruction interval ranged from 0.65 mm to 1.5 mm, with a pitch value from 0.55 to 0.984. Patients’ characteristics and scan parameters of DECT protocols are summarised in Table 1.

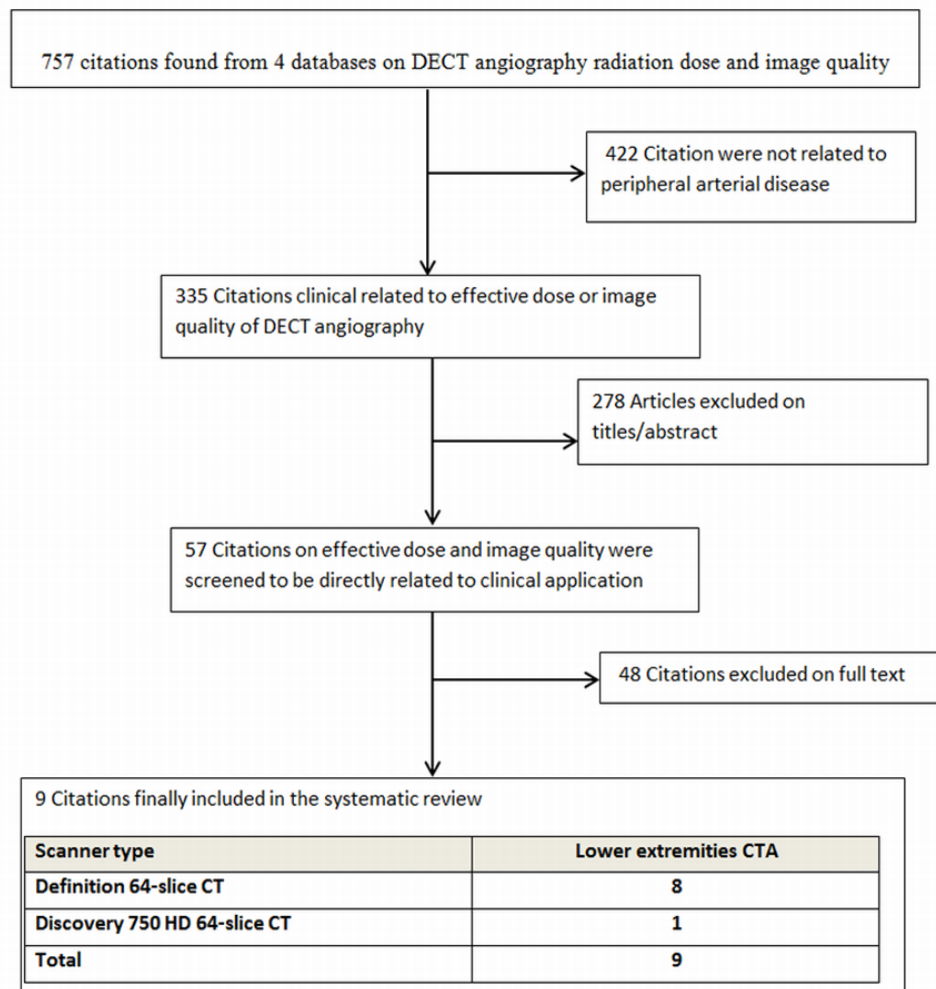


Figure 3.1.Flow chart showing search strategy for identifying eligible studies

Table 3.1. Study characteristics of dual energy CT angiography in peripheral arterial disease

Study /Year	Body part	No of patients	Mean age (yrs)	Male %	Scanner type	Technique used for DECT	Collimator Setting	Section thickness (mm)	Recon. interval (mm)	Pitch	Algorithm	mA	Dose modulation	Rotation time (msec)
Meyer et al. 2008 [11]	Lower extremity	50	67	68	64 DSCT	2 tubes	2 x 32 x 0.6	1	0.6	0.7	NA	56/238	NA	500
Brockmann et al. 2008 [14]	Lower extremity	20	67	80	64 DSCT	2 tubes	14 x 1.2	1.2	1	0.6	D30f	90/382	NA	500
Yamamoto et al. 2009 [17]	Lower extremity	20	73	55	64 DSCT	2 tubes	2 x 32 x 0.6	1	0.65	NA	D30f	95/405	Yes	500
Sommer et al. 2009 [18]	Lower extremity	51	70.8	72	64 DECT	2 tubes	2 x 32 x 0.6	1.5	1	0.7	NA	80/340	Yes	500
Kau et al. 2011 [19]	Lower extremity	58	72	60	64 DSCT	2 tubes	14 x 1.2	1.5	1	0.6	NA	90/390	NA	500
Huang et al. 2012 [20]	Abdomen and lower extremity	25	64.7	52	64 DSCT	2 tubes	14 x 1.2	1.2	1.5	0.55	D20f	115/448	NA	500
Sudarski et al. 2013 [21]	Abdomen and lower extremity	18	67	72	64 DSCT	2 tubes	14 x 1.2	1	1.5	0.6	NA	80/440	NA	500
Swanberg et al. 2014 [22]	Lower extremity	10	73	9	64 DECT	2 tubes	2 x 32 x 0.6	1.5	1	0.7	D30f	55/Auto	No	500
Abdulrahman et al. 2015 [23]	Lower extremity	34	52.1	25	64 DECT	Fast kVp switching	64 x 0.625	1	1	0.984	Standard	600	Yes	500

Recon = reconstruction, NA = not available, mA = Milliampere

3.3.2 Image quality assessment

Image quality parameters evaluated in these studies included image noise, SNR, CNR and ranking scales. Qualitative assessment of image quality using a four- and three-point ranking scale was performed in four studies, a three-point scale was used in three studies, in one study a four-point scale was used, and in the remaining study information about qualitative assessment was unavailable. For quantitative evaluation of the lower extremities, of the nine studies only three reported the SNR and CNR, comparing MEIs with polychromatic images [20, 21, 23]. A study by Sudarski et al. concluded that using a low keV of 60 resulted in higher attenuation and CNR and SNR (513 HU, 87, 13.2, respectively) compared to the polychromatic images (333 HU, 57, and 8.75, respectively). However, a recent study by Almutairi et al. found that 65 keV yielded the highest SNR and CNR (14.61 and 21.75) when peripheral arterial trees were evaluated [23]. One study reported the CNR was only additional to the coefficient of variance as another parameter to evaluate the image quality compared to DSA and CTA [18]; in this study the CNR ranged from 45 to 64.6 for vessels above the knee, which was claimed to be higher than those in DSA and CTA; however, for the subjective image evaluation of image quality on a 3-point scale in two other studies a higher value using DECTA was achieved [20, 23]. The quality of bone removal using a DECT application was reported in five studies, with general agreement that bone removal with DECT scored higher than with conventional CTA.

3.3.3 Radiation dose

The radiation dose was reported in three studies [11, 14, 23] with different approaches to calculating effective dose. Effective dose was estimated by multiplying the DLP with a conversion factor of 0.015 in two studies [11, 14], while the third used a conversion factor of 0.0056 [23]. The mean effective dose for DECT protocols from these three studies was 9.51 mSv, ranging from 7.56 to 11.18 mSv. The reported CTDI_{vol} was 6.6, and 7.48 mGy for studies using Somatom definition 64 DSCT scanners and 9.05 mGy for the fast kilovoltage-switching 64-slice CT scanner. Tube current modulation was applied in three studies, but none reported the radiation dose.

3.3.4 Diagnostic value of DECTA

The diagnostic value of DECTA was reported in four studies [11, 14, 19, 22]. Comparison of diagnostic values between DECTA and conventional CTA was reported in one study [14], so only analysis of the mean diagnostic value of DECTA in PAD was conducted. Summary estimates of the overall sensitivity and specificity of DECTA were 95.87% (95% CI: 84 to

97.2%) and 79.8% (95% CI: 78 to 97%) respectively. With regard to diagnostic performance in the four subdivisions of the arterial tree in the three studies that reported the data, the pooled sensitivity and specificity for aorta were 94.5% (95% CI: 89 to 100%) and 94% (95% CI: 88 to 100%), 88.4% (95% CI: 81 to 94.4%) and 92.9% (95% CI: 88 to 96.2%) for pelvis, 84.5% (95% CI: 67 to 100%) and 93.3% (95% CI: 88 to 97.8%) for thigh, and 95.9% (95% CI: 91 to 100%) and 58.9% (95% CI: 38.7 to 86.9%) for calf. Two studies evaluated the accuracy of the bone removal algorithm, with sensitivity and specificity ranging from 84% to 97.2% and 67% to 94% for stenosis greater than 50–74%. One study evaluated the accuracy of maximum intensity projections and found that DECTA had 84% sensitivity and 67% specificity when compared with DSA [19]. Another study evaluated the accuracy of selective CTA for below-knee arteries as a sensitivity of 100% and specificity of 89% [22].

3.3.5 Contrast medium assessment

Table 2 shows details of the contrast mediums used in these studies during DECTA examinations. As shown in the table, the mean contrast volume and flow rate were 108.94 ml (66.47–160 ml) and 4.22 ml/s (3–5.5 ml/s) respectively. The contrast concentration used in DECTA was between 300 mg/ml and 400 mg/ml in all studies, and eight followed the protocol of using a saline chaser following administration of the contrast medium. Two approaches were used to monitor the contrast flow: by bolus tracking in two studies [18, 23], and specific threshold levels in six studies [11, 14, 17, 9–21] with CT attenuation between 100 and 250 HU as the triggering threshold. Only one study offered a comparison of the effect of different contrast volumes [23]. The remaining study used a selective CTA and injection of contrast medium directly via catheter into the external iliac artery using an ultra-low contrast volume (17.5 mL) [22].

Table 3.2. Contrast protocols used in dual-energy CT angiography in peripheral arterial disease

Study /Year	Body part	No of patients	Mean age (yrs)	Male %	Scanner type	Technique used for DECT	Collimator Setting	Section thickness (mm)	Recon. Interval (mm)	Pitch	Algorithm	mA	Dose modulation	Rotation time (msec)
Meyer et al. 2008 [11]	Lower extremity	50	67	68	64 DSCT	2 tubes	2 x 32 x 0.6	1	0.6	0.7	NA	56/238	NA	500
Brockmann et al. 2008 [14]	Lower extremity	20	67	80	64 DSCT	2 tubes	14 x 1.2	1.2	1	0.6	D30f	90/382	NA	500
Yamamoto et al. 2009 [17]	Lower extremity	20	73	55	64 DSCT	2 tubes	2 x 32 x 0.6	1	0.65	NA	D30f	95/405	Yes	500
Sommer et al. 2009 [18]	Lower extremity	51	70.8	72	64 DECT	2 tubes	2 x 32 x 0.6	1.5	1	0.7	NA	80/340	Yes	500
Kau et al. 2011 [19]	Lower extremity	58	72	60	64 DSCT	2 tubes	14 x 1.2	1.5	1	0.6	NA	90/390	NA	500
Huang et al. 2012 [20]	Abdomen and lower extremity	25	64.7	52	64 DSCT	2 tubes	14 x 1.2	1.2	1.5	0.55	D20f	115/448	NA	500
Sudarski et al. 2013 [21]	Abdomen and lower extremity	18	67	72	64 DSCT	2 tubes	14 x 1.2	1	1.5	0.6	NA	80/440	NA	500
Swanberg et al. 2014 [22]	Lower extremity	10	73	9	64 DECT	2 tubes	2 x 32 x 0.6	1.5	1	0.7	D30f	55/Auto	No	500
Abdulrahman et al. 2015 [23]	Lower extremity	34	52.1	25	64 DECT	Fast kVp switching	64 x 0.625	1	1	0.984	Standard	600	Yes	500

CM= contrast medium, HU = Hounsfield unit, NS = normal saline

3.4 Discussion

Four key findings were found in this systematic review: first, improved image quality can be achieved with use of DECTA in PAD compared to conventional CTA. Second, there is good accuracy of DECTA in the diagnostic assessment of PAD. Third, the contrast medium can be reduced by up to 50% without compromising image quality. Finally, radiation dose may be higher in DECTA despite its improved diagnostic performance.

Image quality degradation in conventional CT is caused by the polychromatic fauna of the x-ray source and the ability of the CT detector to distinguish the energy. Currently there are two types of DECT in clinical practice: single source dual energy (achieving dual energy imaging with the use of fast kilovolt dynamic switching) and dual source dual energy (achieving dual energy imaging with the use of two x-ray tubes with different kVp). DECT is based on the MEI, and may be able to overcome the limitations of conventional CT and improve image quality. The post-processing flexibility of DECT data permits a wide range of monochromatic energy levels so that image contrast and noise can be balanced to obtain the best diagnostic information for the clinicians. The evaluation of peripheral arterial disease by DECT allows for acquisition of image quality beyond what has been obtained by conventional CTA. Huang et al. [20] reported that DECT improved vascular enhancement with the ability to assess the severity of stenosis beyond CTA and DSA in peripheral disease. For MEIs, lower keV was found to improve the image quality of enhanced vessels because it is close to the K-shell of iodine material, which is 33keV [4].

Several studies have been published on image quality using different keV settings in the evaluation of PAD. Almutairi et al. [23] reported that 65 keV produced optimal image quality in peripheral DECTA, which is in accordance with a phantom study that evaluated peripheral arterial stents [24]. A study by Sudarski et al. [21] demonstrated the best image quality of MEI was at 60 keV for lower extremities. This is supported by studies investigating spectral imaging in thoracic arteries, with results showing that MEIs from 55 keV provide better image quality than a standard chest CTA [2, 17, 25]. A recent study evaluating abdominal aorta aneurysms found higher accuracy at 55 keV than with standard CTA; while Pinho et al. [9] and Sudarski et al. [21] found optimal image quality was obtained at 70 keV in abdominal artery imaging. Improvement of the noise and contrast in a pixel-by-pixel way can be achieved using non-linear image blending techniques in vascular imaging [26]. A recent study by Lv et al. [27] reported that in a non-linear blending image in abdominal CTA the contrast enhancement was improved at a lower energy protocol. Despite

these encouraging results, more studies are needed to confirm the use of MEIs and non-linear blending images in peripheral arterial imaging protocols.

The diagnostic value for CTA in the assessment of peripheral arteries has been reported with high accuracy [28–30]; recent advances in CT technology may further improve the diagnostic value. Using DECT applications for bone removal is more accurate and time efficient than conventional CTA applications, and several studies have concluded that DECT bone removal applications are superior [11, 14, 20, 23]. None of these studies investigated the use of MEIs with bone removal in peripheral arterial protocols. so further research is needed to clarify the quality of MEIs with bone removal application in the lower extremities.

The analysis of the available data in this review shows that DECTA is an accurate diagnostic tool compared with the standard reference DSA or CTA for detecting arterial lesions of the lower extremities, with overall good sensitivity and specificity. The results from most of the individual studies show that improvement of image quality using DECTA in peripheral arteries is highly significant. Brockmann et al. [14] reported a sensitivity of 97.2% and specificity of 94% when compared with DSA and CTA for diagnosing $\geq 50\%$ stenosis. This is supported by Meyer et al. [11] who evaluated peripheral arteries by DECT, with a reported sensitivity of 93.1% and specificity of 78.2%. The lower accuracy of this review was mainly due to the results of the study by Kau et al. [19], who reported lower sensitivity of 84% (95% CI, 80–88%) and specificity of 67% (95% CI, 62–71%) when maximum intensity projections in DECT were compared with DSA. Thus, the results of the diagnostic value of DECTA in this review need to be interpreted with caution.

Although diagnostic accuracy was moderate, as shown in this analysis, the selective CTA for assessing popliteal arteries conducted by Swanberg et al. [22] was reported to achieve a sensitivity of 100% and specificity of 89% at an ultra-low contrast medium volume. This new approach may lead to better evaluation of specific arteries and stents with minimum radiation dose and contrast medium.

This review finds no consistency in these studies in terms of contrast flow rate and contrast monitoring. Baxa et al. [31] assessed the use of a low volume of the contrast material with a double-level test bolus method and concluded that this method could achieve high image quality with low contrast material volume. Another study compared different volumes of contrast medium and concluded that using a low contrast volume was no different from the usual contrast volume regarding image quality [23]. Reducing the contrast medium volume by up to 50% with DECT was found to be useful and did not affect the overall image quality. Therefore, low contrast volume is highly recommended at low kVp during DECTA in PAD.

This approach is supported by studies evaluating the contrast medium volume in pulmonary CTA [32, 33] and abdominal CTA [9], as low contrast and high contrast volumes return similar image quality. To reduce variances between patients, an individual contrast medium and scan time optimisation in lower extremities is recommended.

Although the radiation dose associated with CT is always a main concern, dose reduction technique was not evaluated in most of the studies analysed in this review. However, the obtainable dose values mentioned in some studies are found to be similar to or even lower than those of conventional CTA. Applying the latest methods of calculating the effective dose with DECT in peripheral arterial studies may significantly reduce the radiation dose [23, 34]. A low effective dose in peripheral arterial protocol was achieved by using the new method of estimating the lower limb area with conversion coefficient k (0.0056 mSv/mGy) in DECTA. This approach was only recently applied to the clinical area, and the calculated dose in the other studies seems similar to those recorded in abdominal protocols. Further studies with a focus on dose reduction are indicated.

There are some limitations in this review that should be acknowledged. First, the limited number of studies of DECTA in PAD did not allow us to perform a meta-analysis, so only a systematic review could be conducted. Second, insufficient information was provided in some studies, which lacked such things as dose reports or the diagnostic value of DECTA in PAD. Furthermore, different ranking scales were used in the various studies, and objective assessment of image quality was available in only a few. Third, inconsistent protocols among these studies represent another important limitation of our analysis. Finally, the heterogeneity that exists in these studies with various types of DECT scanning is another important limitation of our analysis.

3.5 Conclusion

This systematic review shows that DECT angiography may achieve optimal image quality at low keV values. DECT is an accurate diagnostic imaging technology in the assessment of peripheral arterial disease, with moderate diagnostic value but lower contrast medium, therefore reducing the risk of contrast-induced acute kidney injury. Reduction of the contrast medium volume up to 50% can achieve an adequate image quality at the optimal keV setting.

3.6 References

- 1 Coursey CA, Nelson RC, Boll DT, Paulson EK, Ho LM, Neville AM et al. Dual-energy multidetector CT: how does it work, what can it tell us, and when can we use it in abdominopelvic imaging? *Radiographics* 2010; 30(4):1037–55.
- 2 Delesalle M-A, Pontana F, Duhamel A, Faivre J-B, Flohr T, Tacelli N et al. Spectral optimization of chest CT angiography with reduced iodine load: experience in 80 patients evaluated with dual-source, dual-energy CT. *Radiology* 2013; 267(1):256–66.
- 3 Vlahos I, Chung R, Nair A, Morgan R. Dual-energy CT: vascular applications. *Am J Roentgenol* 2012; 199(5):S87–S97.
- 4 Johnson TC, Kalender W. Physical background. In: Johnson T, Fink C, Schönberg SO, Reiser MF (eds) *Dual Energy CT in clinical Practice*. Medical Radiology: Springer, Berlin, 2011, pp. 3–9.
- 5 Matsumoto K, Jinzaki M, Tanami Y, Ueno A, Yamada M, Kuribayashi S. Virtual monochromatic spectral imaging with fast kilovoltage switching: improved image quality as compared with that obtained with conventional 120-kVp CT. *Radiology* 2011; 259(1):257–62.
- 6 Ascenti G, Mazziotti S, Mileto A, Racchiusa S, Donato R, Settineri N et al. Dual-source dual-energy CT evaluation of complex cystic renal masses. *Am J Roentgenol* 2012; 199(5):1026–34.
- 7 Liu X, Zhou J, Zeng MS, Ma Z, Ding Y. Homogeneous high attenuation renal cysts and solid masses—differentiation with single phase dual energy computed tomography. *Clin Radiol* 2013; 68(4):e198–205.
- 8 Mileto A, Mazziotti S, Gaeta M, Bottari A, Zimbaro F, Giardina C et al. Pancreatic dual-source dual-energy CT: is it time to discard unenhanced imaging? *Clin Radiol* 2012; 67(4):334–9.
- 9 Pinho DF, Kulkarni NM, Krishnaraj A, Kalva SP, Sahani DV. Initial experience with single-source dual-energy CT abdominal angiography and comparison with single-energy CT angiography: image quality, enhancement, diagnosis and radiation dose. *Eur Radiol* 2013; 23(2):351–9.
- 10 Toepker M, Moritz T, Krauss B, Weber M, Euller G, Mang T et al. Virtual non-contrast in second-generation, dual-energy computed tomography: reliability of attenuation values. *Eur J Radiol* 2012; 81(3):e398–405.
- 11 Meyer BC, Werncke T, Hopfenmuller W, Raatschen HJ, Wolf KJ, Albrecht T. Dual energy CT of peripheral arteries: effect of automatic bone and plaque removal on image quality and grading of stenoses. *Eur J Radiol* 2008; 68(3):414–22.
- 12 Pessis E, Campagna R, Sverzut JM, Bach F, Rodallec M, Guerini H et al. Virtual monochromatic spectral imaging with fast kilovoltage switching: reduction of metal artifacts at CT. *Radiographics* 2013; 33(2):573–83.

- 13 Ouwendijk R, Kock MCJM, van Dijk LC, van Sambeek MRHM, Stijnen T, Hunink MGM. Vessel wall calcifications at multi-detector row CT angiography in patients with peripheral arterial disease: effect on clinical utility and clinical predictors. *Radiology* 2006; 241(2):603–8.
- 14 Brockmann C, Jochum S, Sadick M, Huck K, Ziegler P, Fink C et al. Dual-energy CT angiography in peripheral arterial occlusive disease. *Cardiovasc Interv Radiol* 2009; 32(4):630–7.
- 15 Smith-Bindman R, Lipson J, Marcus R, Kim KP, Mahesh M, Gould R, et al. Radiation dose associated with common computed tomography examinations and the associated lifetime attributable risk of cancer. *Arch Intern Med* 2009; 169(22):2078–86.
- 16 Shen Y, Sun Z, Xu L, Li Y, Zhang N, Yan Z et al. High-pitch, low-voltage and low-iodine-concentration CT angiography of aorta: assessment of image quality and radiation dose with iterative reconstruction. *PloS One* 2015; 10(2):e0117469.
- 17 Yamamoto S, McWilliams J, Arellano C, Marfori W, Cheng W, McNamara T et al. Dual-energy CT angiography of pelvic and lower extremity arteries: dual-energy bone subtraction versus manual bone subtraction. *Clin Radiol* 2009; 64(11):1088–96.
- 18 Sommer WH, Johnson TR, Becker CR, Arnoldi E, Kramer H, Reiser MF et al. The value of dual-energy bone removal in maximum intensity projections of lower extremity computed tomography angiography. *Invest Radiol* 2009; 44(5):285–92.
- 19 Kau T, Eicher W, Reiterer C, Niedermayer M, Rabitsch E, Senft B et al. Dual-energy CT angiography in peripheral arterial occlusive disease-accuracy of maximum intensity projections in clinical routine and subgroup analysis. *Eur Radiol* 2011; 21(8):1677–86.
- 20 Huang SY, Nelson RC, Miller MJ, Kim CY, Lawson JH, Husarik DB et al. Assessment of vascular contrast and depiction of stenoses in abdominopelvic and lower extremity vasculature: comparison of dual-energy MDCT with digital subtraction angiography. *Acad Radiol* 2012; 19(9):1149–57.
- 21 Sudarski S, Apfaltrer P, W. Nance J, Schneider D, Meyer M, Schoenberg SO et al. Optimization of keV-settings in abdominal and lower extremity dual-source dual-energy CT angiography determined with virtual monoenergetic imaging. *Eur J Radiol* 2013; 82(10):e574–81.
- 22 Swanberg J, Nyman R, Magnusson A, Wanhainen A. Selective intra-arterial dual-energy CT angiography (s-CTA) in lower extremity arterial occlusive disease. *Eur J Vasc Endovasc Surg* 2014; 48(3):325–9.
- 23 Almutairi A, Sun Z, Poovathumkadavi A, Assar T. Dual energy CT angiography of peripheral arterial disease: feasibility of using lower contrast medium volume. *PloS One* 2015; 10(9):e0139275.
- 24 Almutairi A, Sun Z, Al Safran Z, Poovathumkadavi A, Albader S, Ifdailat H. Optimal scanning protocols for dual-energy CT angiography in peripheral arterial stents: an in vitro phantom study. *Int J Mol Sci* 2015; 16(5):11531–49.

- 25 Cheng J, Yin Y, Wu H, Zhang Q, Hua J, Hua X et al. Optimal monochromatic energy levels in spectral CT pulmonary angiography for the evaluation of pulmonary embolism. *PloS One* 2013; 8(5).
- 26 Eusemann C, Holmes Iii DR, Schmidt B, Flohr TG, Robb R, McCollough C et al., eds. Dual energy CT: How to best blend both energies in one fused image? *Proc. SPIE 6918, Medical Imaging 2008: Visualization, Image-guided Procedures, and Modeling*, 691803.
- 27 Lv P, Liu J, Wu R, Hou P, Hu L, Gao J. Use of non-linear image blending with dual-energy CT improves vascular visualization in abdominal angiography. *Clin Radiol* 2014; 69(2):e93–e9.
- 28 Met R, Bipat S, Legemate DA, Reekers JA, Koelemay MJ. Diagnostic performance of computed tomography angiography in peripheral arterial disease: a systematic review and meta-analysis. *JAMA* 2009; 301(4):415–24.
- 29 Heijnenbrok-Kal MH, Kock MC, Hunink MG. Lower extremity arterial disease: multidetector CT angiography meta-analysis. *Radiology* 2007; 245(2):433–9.
- 30 Sun Z. Diagnostic accuracy of multislice CT angiography in peripheral arterial disease. *J Vasc Interv Radiol* 2006; 17(12):1915–21.
- 31 Baxa J, Vendis T, Molacek J, Stepankova L, Flohr T, Schmidt B et al. Low contrast volume run-off CT angiography with optimized scan time based on double-level test bolus technique: feasibility study. *Eur J Radiol* 2014; 83(3):e147–55.
- 32 Dong J, Wang X, Jiang X, Gao L, Li F, Qiu J et al. Low-contrast agent dose dual-energy CT monochromatic imaging in pulmonary angiography versus routine CT. *J Comput Assist Tomogr* 2013; 37(4):618–25.
- 33 Gorgos A, Remy-Jardin M, Duhamel A, Faivre JB, Tacelli N, Delannoy V et al. Evaluation of peripheral pulmonary arteries at 80 kVp and at 140 kVp: dual-energy computed tomography assessment in 51 Patients. *J Comput Assist Tomogr* 2009; 33(6):981–6.
- 34 Saltybaeva N, Jafari ME, Hupfer M, Kalender WA. Estimates of effective dose for CT scans of the lower extremities. *Radiology* 2014; 273(1):153–9.

Every reasonable effort has been made to acknowledge the owners of copyright material. I would be pleased to hear from any copyright owner who has been omitted or incorrectly acknowledged.

Chapter 4 Optimal scanning protocols for dual-energy CT angiography in peripheral arterial stenting: An in vitro phantom study²

The factors that affect the image quality and radiation dose of peripheral arterial imaging has been presented in previous chapters. This chapter exploits these outcomes to address the third objective of this study, which is to test the quality of images that are produced using the advised imaging protocol. It is demonstrated by using a phantom to simulate the anatomical arteries with the use of different stents in different locations. Technical approaches to dose optimisation and image quality evaluation are covered in this chapter.

4.1 Introduction

The increasing prevalence of peripheral artery disease (PAD) is an important cardiovascular disease risk factor [1–3]. Stent placement for occlusive vascular disease is recognised as a safe and effective alternative treatment for PAD [4]. The main concern of stent implantation is the development of in-stent restenosis. Recent studies have shown a 30–55% restenosis rate after the first year of stent implementation [5–7], indicating that a follow-up examination for the patency of implanted stents is important. A number of imaging techniques have been used to evaluate stent patency, including digital subtraction angiography (DSA), multi-detector computed tomography (MDCT), doppler ultrasound and magnetic resonance imaging. DSA is the standard follow-up procedure for PAD, but it has gradually been replaced by less invasive techniques such as MDCT [8] which is associated with fewer procedure-related complications, shorter procedural time, and fewer motion artefacts [8]. Despite these advantages, MDCT has its weaknesses, including a higher rate of

² This chapter is a version of the article by Almutairi et al., Optimal scanning protocols for dual-energy CT angiography in peripheral arterial stents: an in vitro phantom study. *Int J Mol Sci* 2015; 16(5):11531–49.

nephrotoxicity, a problem with blooming artefact caused by stent struts, and radiation-induced malignancy.

The latest MDCT systems such as DSCT and dual-energy computed tomography (DECT) are capable of addressing these weaknesses [9]. In particular, DECT has the ability to distinguish different materials at high density – for example, separating iodinated contrast from other materials [10]. In addition, beam-hardening artefacts, which usually result from the polychromatic energy of the X-ray spectrum, can be eliminated by using the monochromatic energy images (MEI) spectrum. Furthermore, suitable rotation time and use of iterative reconstruction can reduce the radiation dose [11]. Although extensive studies have been conducted on the use of DECT for cardiovascular disease, there is a paucity of literature focusing on the lower extremities, especially for stent patency evaluation [12–15].

Most previous studies of DECT were performed on dual-source DECT, which uses two x-ray tubes [8, 15–18]. However, the fast kilovoltage switching CT scanner, using one x-ray tube and a full field of view (FOV) with the special detector gemstone spectral image (GSI) of GE medical systems, represents another advantage of DECT as it can improve image quality by reducing beam-hardening artefacts associated with stents. Furthermore, it can distinguish between materials such as contrast and soft tissue or other constituents by suppressing one material and enhancing the other with better temporal registration [19]. To the best of our knowledge, there is no report available in the literature on using the fast kilovoltage switching GE scanner for evaluating peripheral arterial stenting; thus, the purpose of this study is to identify an optimal DECT scanning protocol that provides a lower radiation dose and maintains image quality in peripheral arterial stents, based on an in vitro phantom study.

4.2 Experimental Section

4.2.1 Peripheral artery phantom design and stent placement

The custom-made peripheral arterial phantom consisting of a main peripheral arterial tree and arterial branches was developed with use of a computer-aided design program to represent realistic anatomic dimensions. The phantom was made of poly methyl methacrylate with anatomical dimensions similar to the normal anatomy of a peripheral arterial tree, as shown in Figure 4.1.



Figure 4.1. Photograph of the phantom with stent insertions

A total of 15 expired stents of different size, material and design was used in the experiments. Details of the stents are shown in Table 4.1. Of these fifteen stents, ten were of stainless steel (316 L), three of a platinum chromium alloy, one of Nitinol and one of cobalt-superalloy. Stents were deployed into the simulated peripheral arteries modelled within the phantom. Stents with lumen diameters ranging from 2.75 to 3, 4, 5, 6, 7, and 8 mm, which closely matched their nominal diameter, were inserted into the arteries with two exceptions: the two Taxus Element stents with nominal diameters of 3mm were inserted into simulated arteries with a diameter of 2.5mm.

Table 4.1. Details of the examined stents

Model	Material	Manufacturer	Diameter (mm)	Length (mm)	Stent No.
Express LD	316L stainless steel	Boston Scientific	7–8	27–37	(1,2,9,10)
Absolute .035	Nitinol	Abbott	6	40	3
Wallstent-Uni Endoprosthesis	Cobalt-superalloy	Boston Scientific	5	40	4

Palmaz Genesis	316L stainless steel	Cordis	5	14	(5,6,11)
Taxus Element	316L Stainless steel	Boston Scientific	2.75	32	(7,14)
Taxus Liberté 2 nd Generation	Platinum Chromium	Boston Scientific	3	28	8
Promus Element	Platinum Chromium	Boston Scientific	4	16	12
Express Vascular SD	316L stainless steel	Boston Scientific	4	15	13
Monorail Liberté	316L Stainless steel	Boston Scientific	3	28	15

4.2.2 DECT scanning protocols and image reconstruction

DECT scans were performed with a fast kilovoltage-switching 64-slice CT scanner (Discovery CT750 HD; GE Healthcare). Of the GSI-protocols that the manufacturer has developed as default settings, three (protocols 36, 48, and 51) were selected for this study, based on the lowest CTDI_{vol} with acceptable diagnostic image quality to evaluate peripheral arterial stents. These protocols have been preset by the manufacturer to maintain constant tube power when switching the tube voltage back and forth, so changing the radiation dose was only possible by adjusting the pitch and/or rotation time. As a result, the three available pitch values, 0.516, 0.984, and 1.375, were tested, with the same beam collimation of 40 mm in all and fixed rotation times of 0.5, 0.7, and 0.8 seconds per rotation, respectively. The phantom was then positioned in the gantry in an orientation parallel to the z-axis of the scanner.

The scanning parameters for the selected preset GIS-protocols are summarised in Table 4.2. Images were acquired with a coverage of 30 cm, ranging from aortic bifurcation to arteries below the knee. The raw data obtained from each scan was reconstructed in four image sets with five levels of adaptive statistical iterative reconstruction (ASIR): 0%, 30%, 40%, 50%, and 60%, and four kiloelectron volts (keV) of 60, 65, 70, and 75, with slice thicknesses of 1 mm and 50% reconstruction overlap. Tube current modulation was not available in dual energy acquisition in this system for all protocols.

A simulated intravenous contrast medium (Omnipaque 350, GE Healthcare, Milwaukee, WI) was used to represent the actual contrast-enhanced CT angiography. The contrast medium was diluted with normal saline to reach the attenuation of 250 Hounsfield units (HU), which

is the acceptable CT attenuation in peripheral CT angiography. The contrast medium was injected into the simulated arteries, which were sealed at both ends [20].

Table 4.2. Details of scan parameters by protocol

Scan parameters	Protocol 1	Protocol 2	Protocol 3
GSI protocol	GSI- 36	GSI -48	GSI -51
Scan mode	Dual-energy	Dual-energy	Dual-energy
Tube potential	80/140 kVp	80/140 kVp	80/140 kVp
Tube current	260 mAs	260 mAs	360 mAs
Rotation time (s)	0.8	0.7	0.5
Detector collimation (mm)	64 × 0.625	64 × 0.625	64 × 0.625
Pitch	0.516, 0.984 and 1.375	0.516, 0.984 and 1.375	0.516, 0.984 and 1.375
Table speed (mm/R)	20.62	39.37	55
Reconstruction kernel	Standard		
Section thickness (mm)	1	1	1
Interval	0.5	0.5	0.5
keV	(60, 65, 70, and 75)		
ASIR	(30, 40, 50, and 60)		

keV = kiloelectron volt, ASIR = adaptive statistical iterative reconstruction

4.2.3 Quantitative image assessment

Quantitative measurements were performed for DECT images at 1 mm slice thickness on a separate independent workstation with the GSI Viewer (ADW 4.6 General Electric Healthcare). The mean HU was obtained by placing a circular region of interest (ROI) in selected areas of the phantom for the 15 stents (iliac arteries, common femoral arteries, superficial femoral arteries, popliteal arteries, anterior tibial arteries, peroneal arteries, and posterior tibial arteries). Two ROIs were selected; the first was in the common femoral artery to measure the noise on an unstented area of the phantom. The second was in the stented lumen area on the axial images to measure the noise for all stents without inclusion of stent struts, as shown in Figure 4.2. Two stents – no. 7 and no. 14 – were difficult to place the ROI because of their small size with a limited lumen area being visualised; therefore we excluded them from the analysis.

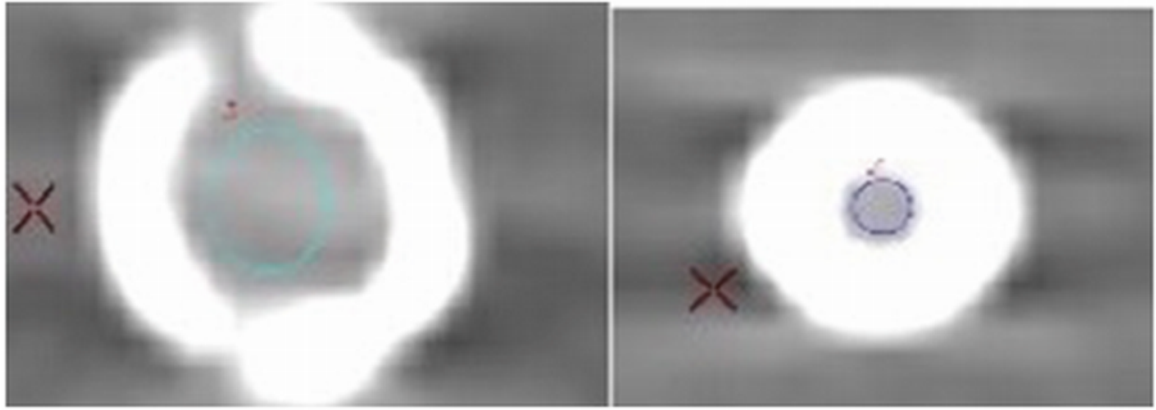


Figure 4.2. The region of interest was placed in the inner stent lumen for measurement of image noise

The selected ROI in an unstented area was in the femoral artery and within each stent at the same location for all protocols to measure the mean CT attenuation and image noise that was defined as the standard deviation (SD). The signal-to-noise ratio (SNR) for both the stented and unstented areas was calculated with the following formula:

$$\text{SNR} = \text{in stent lumen or nonstented area of CT attenuation in HU} / \text{SD} \quad (3)$$

4.2.4 Qualitative assessment of image quality

Three radiologists with 5, 15, and 20 years of experience in CT imaging performed a qualitative evaluation of the GSI viewer with identical window width, window level, and FOV. Different MEI series from each GSI protocol were evaluated randomly (between 60, 65, 70 and 75 keV within each ASIR), with a total of 180 series reviewed by each radiologist. It was considered unnecessary to blind readers to the different energies because different values could easily be determined by visual inspection of the images[12]; however, they were blinded to other parameters. Intraobserver variability was not estimated because each radiologist assessed the images only once. Visualisation of the stent lumen was assessed using a 3-point scale (1 = poor image quality and non-diagnostic; 2 = adequate image quality; 3 = good image quality).

4.2.5 CT dose

A fixed scan length of 29.9 cm was used for all examinations. The volume CT dose index (CTDI_{vol}) and dose-length products (DLP) were recorded for the calculation of effective dose, as shown in Table 4.3. Effective dose (E) was calculated for each protocol using a conversion factor of 0.015, taken from the normalised value of the effective dose per dose-length product for peripheral arteries [21].

Table 4.3. Summary of CTDI_{vol} values, dose-length products, and effective doses across the protocols

GE protocol	Pitch	CTDI _{vol}	DLP	Effective Dose
GSI-36	0.516	39.33	863.86	12.96
GSI-36	0.984	10.30	457.56	6.86
GSI-36	1.375	7.73	341.00	6.47
GSI-48	0.516	17.28	759.13	11.39
GSI-48	0.984	9.05	402.10	6.03
GSI-48	1.375	6.48	299.72	4.50
GSI-51	0.516	19.74	867.57	13.01
GSI-51	0.984	10.34	459.66	6.89
GSI-51	1.375	7.40	342.69	5.14

GSI = gemstone spectral imaging, CTDI_{vol} = computed tomography volume dose index; DLP = dose-length product

4.2.6 Statistical Analysis

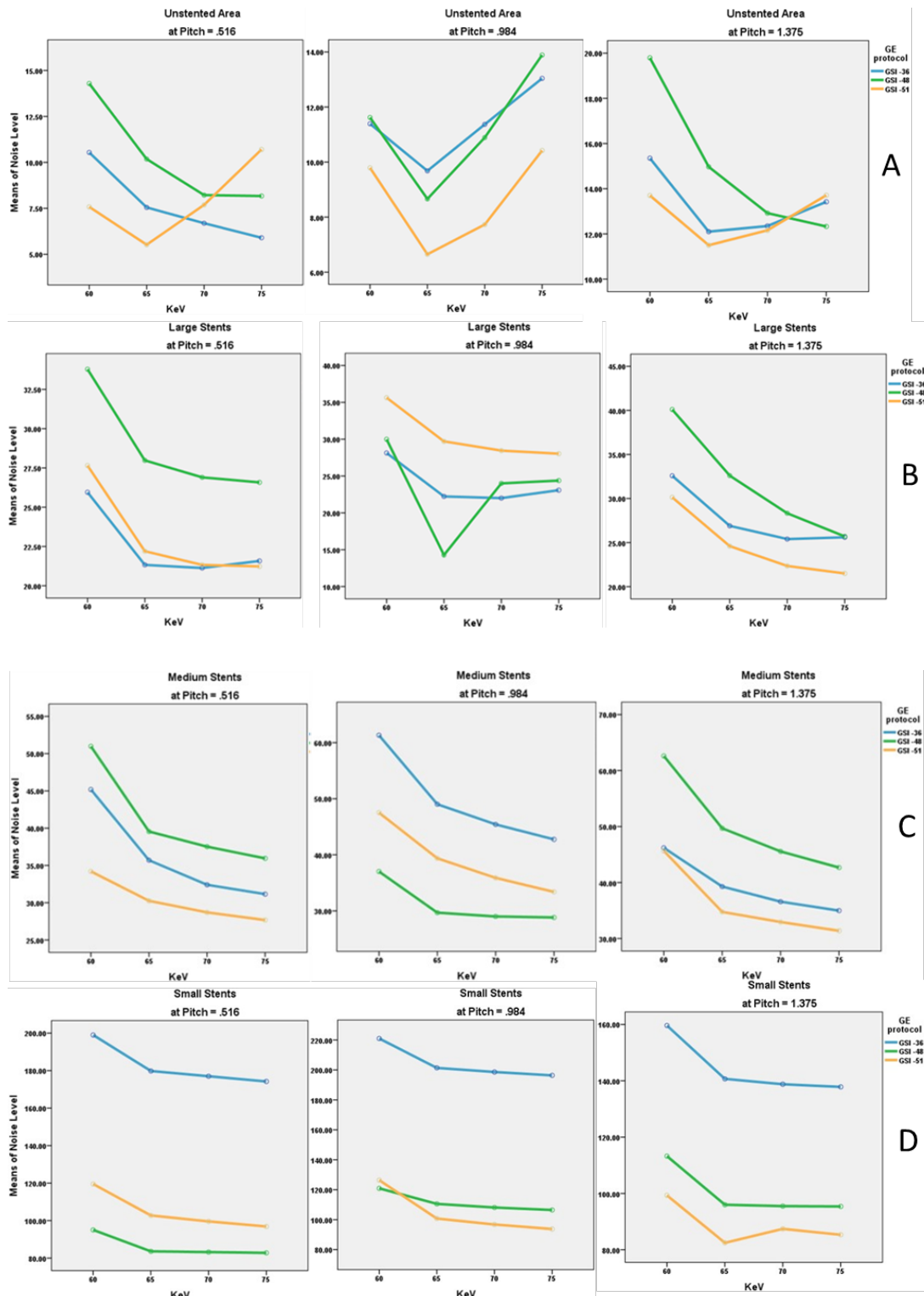
All the data was entered into SPSS Statistics version 22.0 (SPSS Inc., Chicago, IL) for statistical analysis. Two data sets – the noise level and SNR (independent variable) responses obtained when ASIR = 0 – were used to produce 36 observations in a three-factor factorial analysis of variance (univariate ANOVA) model: GSI (three levels: GSI-36, GSI-48, GSI-51), pitch (three levels: 0.516, 0.984, 1.375), and keV (four levels: 60, 65, 70, 75).

The second part of the statistical analysis relates to the noise level and SNR in the nonstented area when ASIR > = 40; three levels, 40, 50, 60, were used to produce 108 observations in a four-factor factorial model. The highest order interaction in each analysis was employed as an estimate of residual (error) variation; when there was no significant interaction, the main effect was considered. Statistical significance was assessed by comparing the *p* values obtained in the F-tests corresponding to the main effect of GSI as well as to the interaction effect of pitch, keV, and ASIR. All tests were performed at the 5% significance level.

4.3 Results and Discussion

A total of 180 series acquired with virtual MEI imaging at 4-keV and 5-ASIR levels were reconstructed to determine the interaction between peripheral arterial stent image quality factors and scanning protocols. There was a significant reduction of image noise with MEI between 65 keV and 70 keV in all investigated preset GSI protocols (*p* < 0.05). A significant reduction was observed at 65 keV for the unstented area, and for large stents and small stents

with both GSI48 and GSI-51. However, the mean HU was reduced as the keV increased for all protocols, as shown in Figure 4.3 (F). Results indicate that the preset GSI-48 scanning protocol with a pitch value of 0.984, 65 keV, and ASIR $\leq 50\%$ achieved the optimal image quality compared with other protocols, as shown in Figure 4.3 (A–E). Figure 4.4 shows an example of a series of images acquired with protocols using 65 keV and three GSI settings.



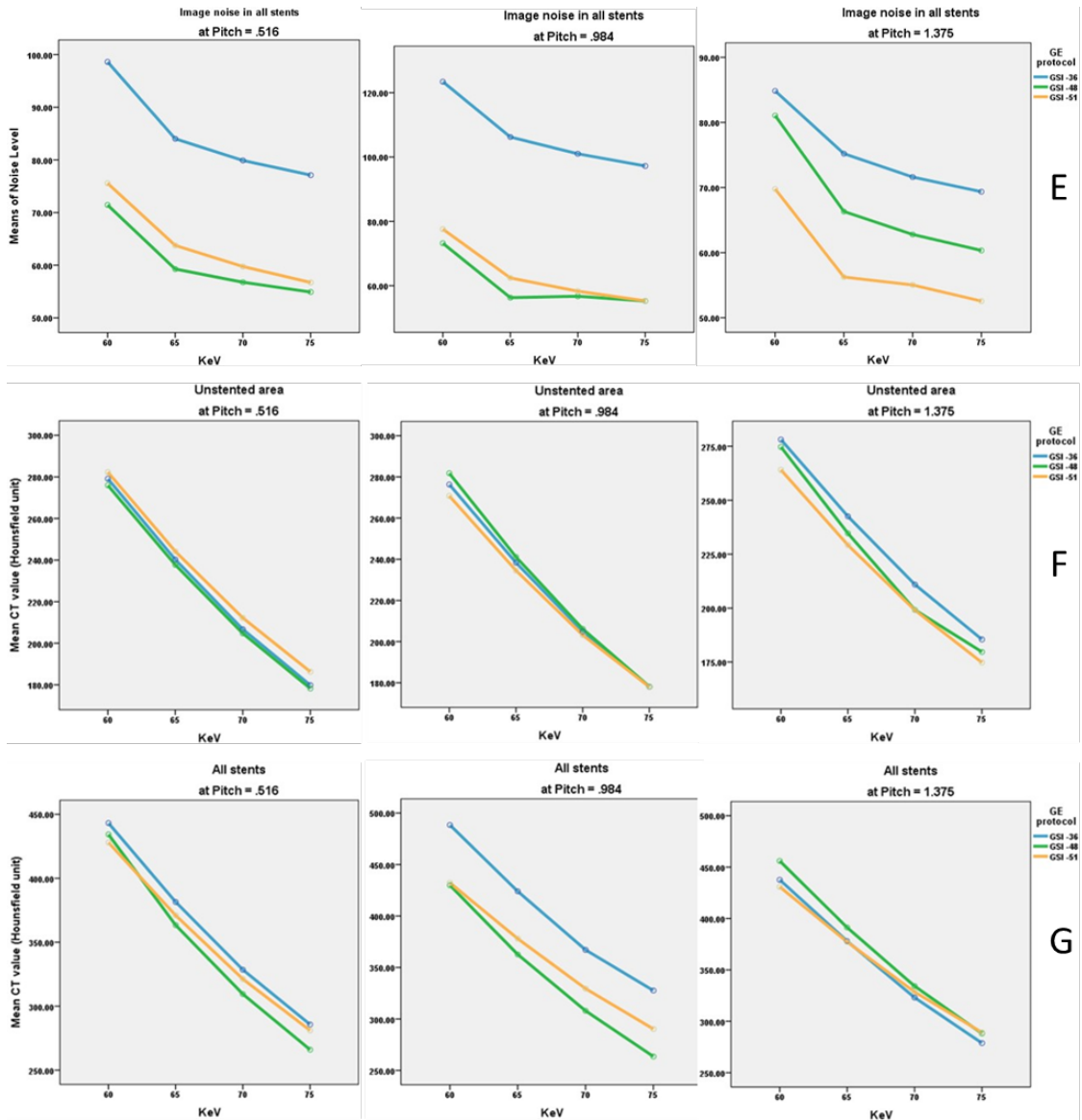
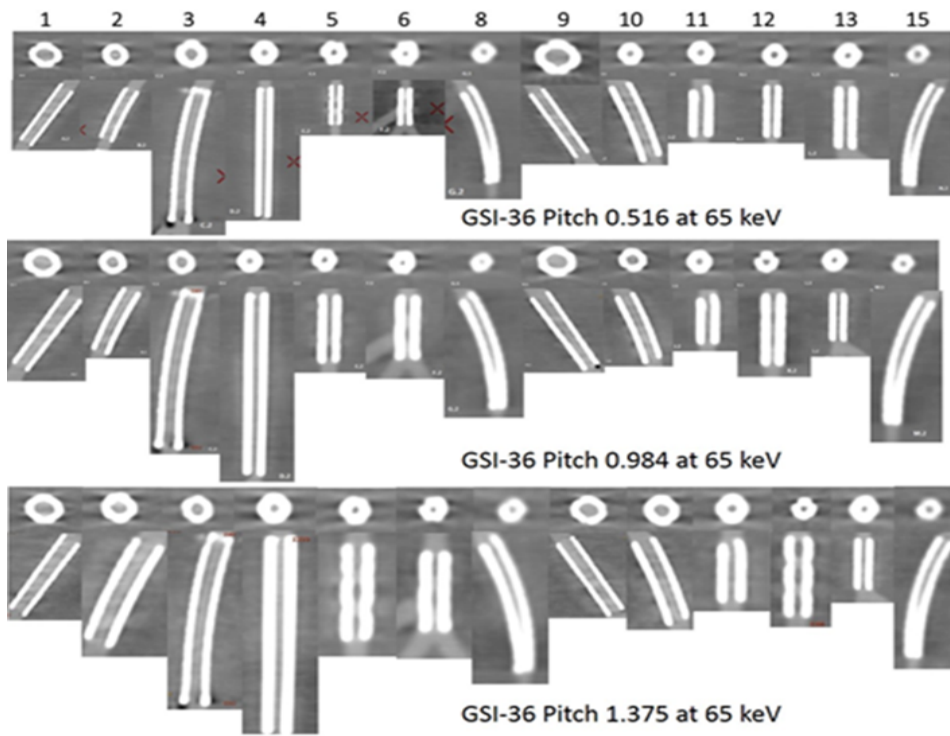
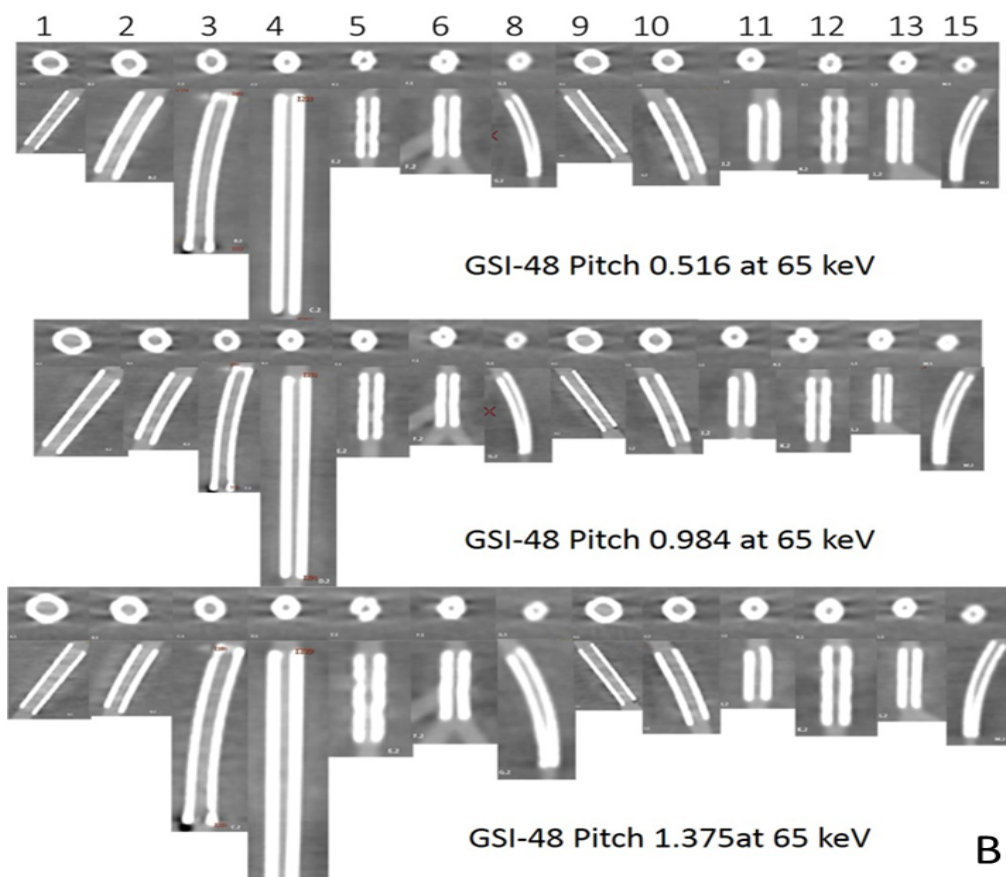


Figure 4.3. Figures A-E show the comparison of noise level at different kiloelectron voltage (keV) with the three preset GSI protocols and three pitch values. Figures F and G represent the mean of CT value in unstented area and all stents with these scanning protocols.



A



B

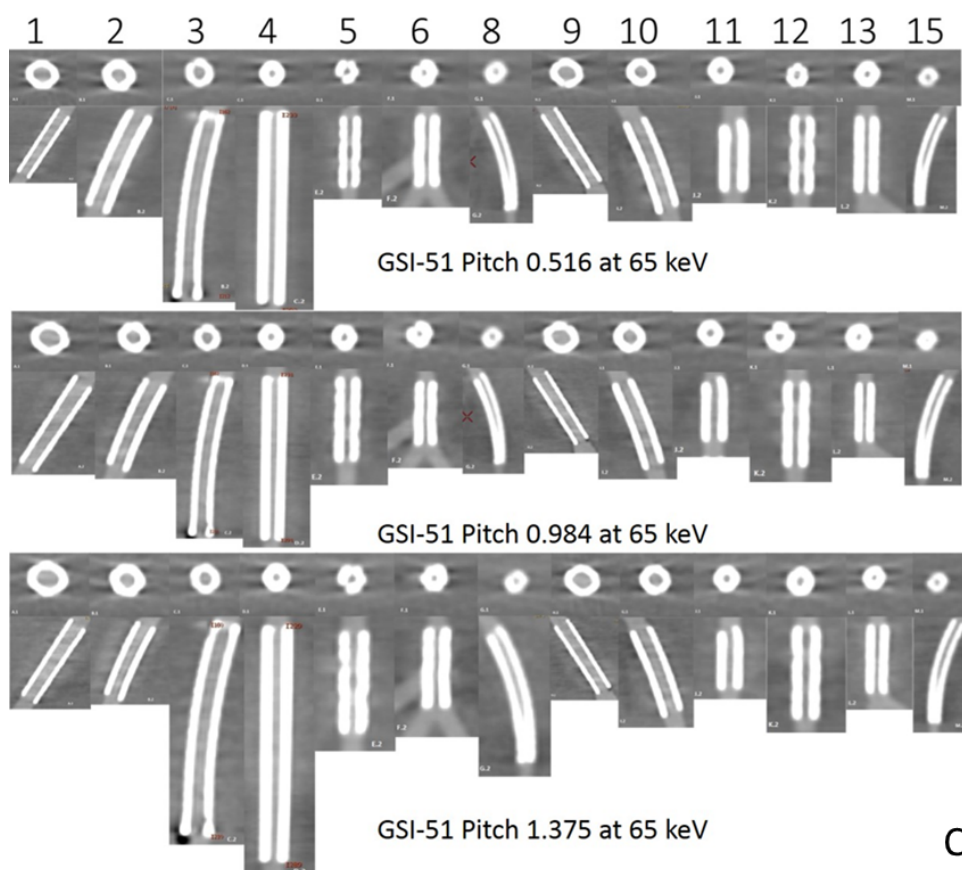


Figure 4.4. A total of 13 stents (No. 7 and 14 were not included due to difficulty placing the region of interest in the area) with axial and coronal reformatted images demonstrated with three GSI protocols and three pitch values at a keV of 65.

4.3.1 Image quality assessment

The phantom data was analysed with a 3-GSI x 3-pitch x 4-keV factorial ANOVA. Each effect was tested with a mean standard error (MSE) of 71.27. There was a highly significant interaction of image noise and SNR with the GSI and pitch ($p = 0.001$). Similar findings were observed in the unstented area with highly significant effects. In addition, significant effects were found for these factors: GSI, pitch, and keV ($p = 0.001$). In contrast there was a significant interaction on the unstented area between GSI and ASIR ($p = 0.015$) and a very highly significant difference between keV and ASIR ($p < 0.001$). For noise level, two of the 3-way interactive terms were statistically significant, namely GSI, pitch and keV; and GSI, pitch, and ASIR $p < 0.001$; the main effects and interactions for these are shown in Table 4.4. The noise level (MSE = 89.04) was higher in GSI-36 than in the other two GSIs, as shown in Figure 4.3 (A-E) above.

4.3.2 Effect of keV on image quality

There was no significant interaction between keV and GSI or pitch factors in the stented area. This does not mean that there was no effect of keV on image quality, but that the effect of keV on image noise was not dependent on GSI or pitch. The four noise-level means for keV range from 83.94 to 64.30 HU – and, incidentally, decreasing image noise occurred monotonically with increasing keV; the effect of keV on image noise was therefore independent of any other design effect. A similar effect was observed with the SNR. Unlike its effect on the unstented area, keV was found to be highly significant for both image noise and SNR ($p = 0.001$). Figure 4.5 compares the selected keV in different GSIs for both unstented and stented areas with different ASIR values.

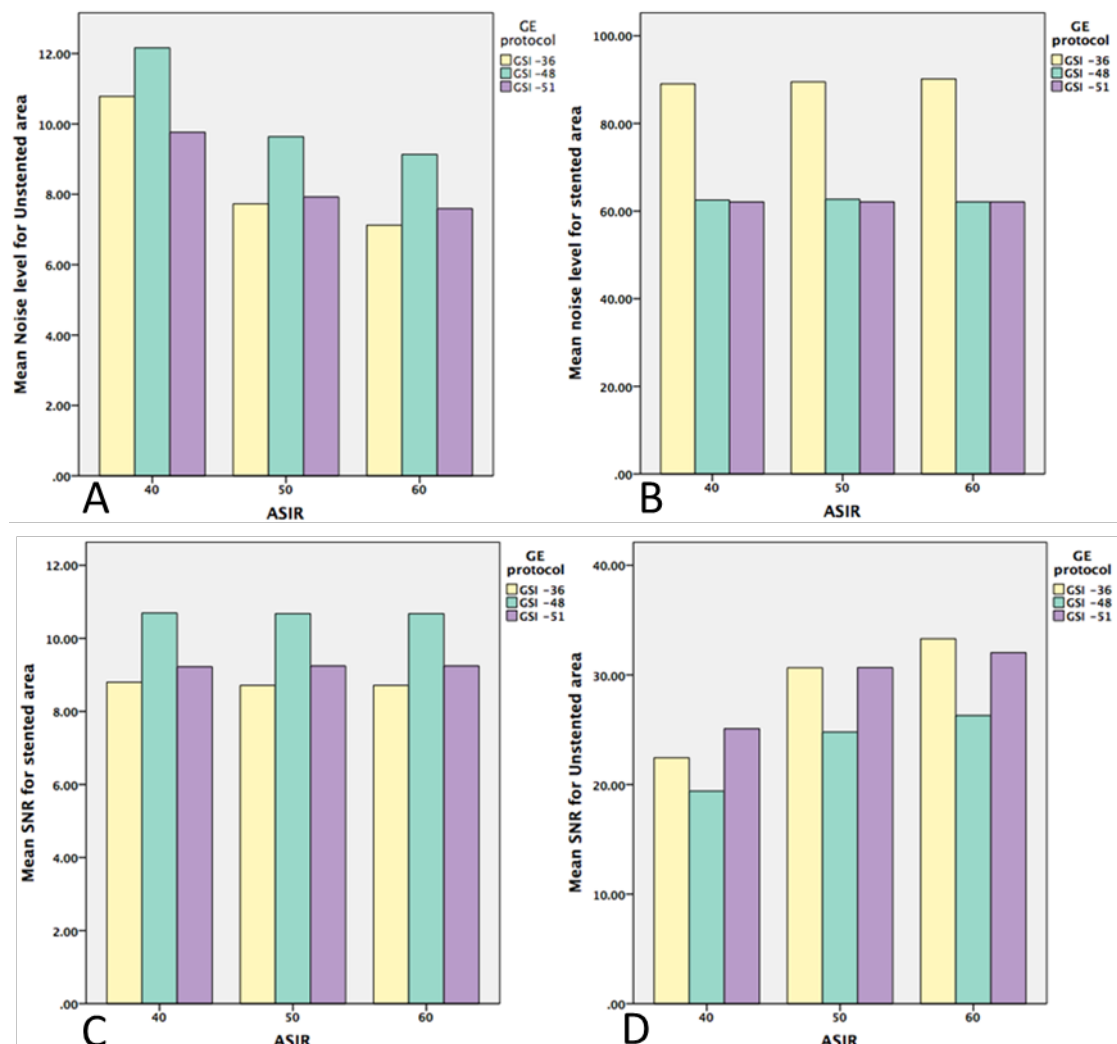


Figure 4.5.A and B are graphic representations showing the noise level when ASIR is used within the both unstented and stented areas, while C and D represent the means of SNR when ASIR is used.

4.3.3 Effect of GSI and pitch on image quality

The interaction of GSI by pitch is highly statistically significant ($p < 0.001$). A significance interaction was observed on the unstented area. The main effects of GSI and pitch on noise level are also highly significant ($p < 0.001$), as shown in Table 4.4 (below).

The marginal noise level means for the 3-GSI categories were 89.03, 62.86, and 61.92, indicating significant differences with the first GSI and with both the second and third GSI of around 27.11 and 0.94 HU, respectively. However, when the three GSI means were investigated for the first pitch category (84.90, 60.60, and 63.95), significant changes were observed. These changes varied with respect to both magnitude and direction, and presented as the significant interaction of GSI by pitch.

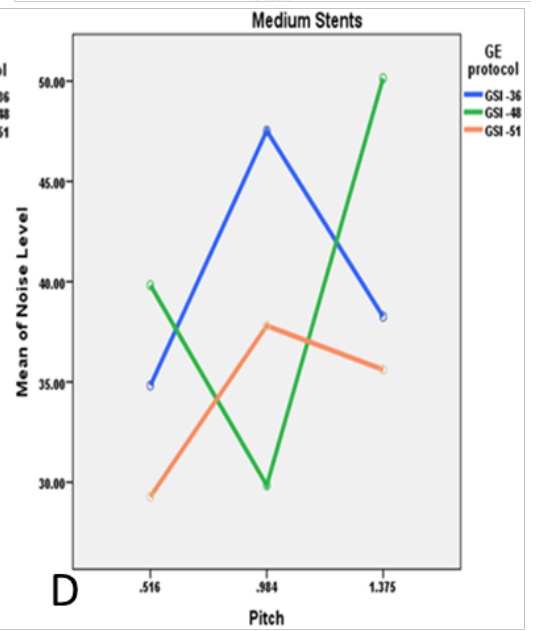
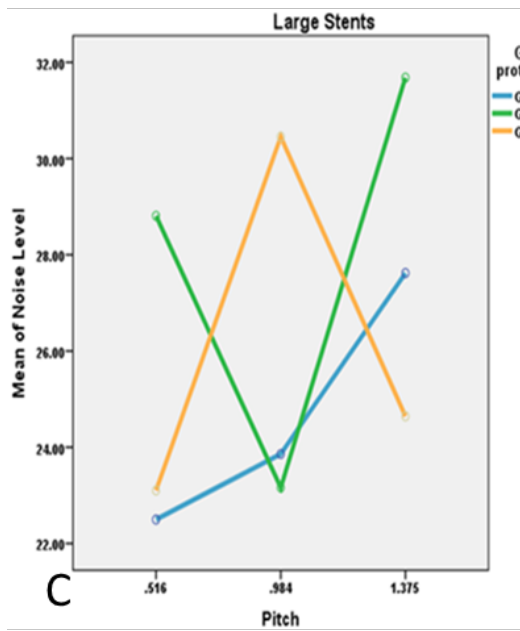
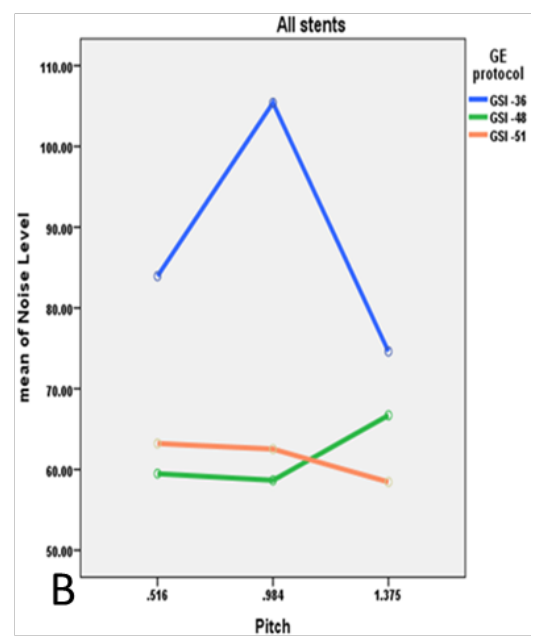
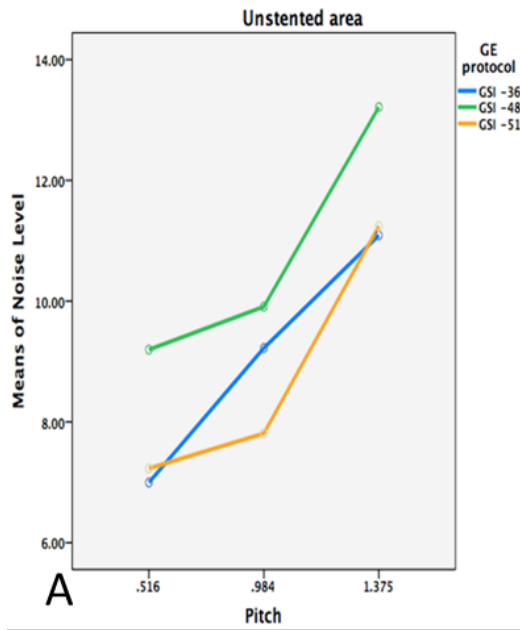
4.3.4 Effect of stents on image quality

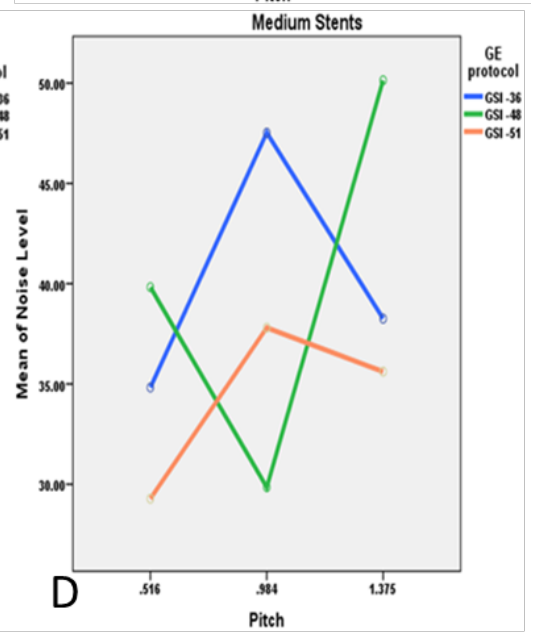
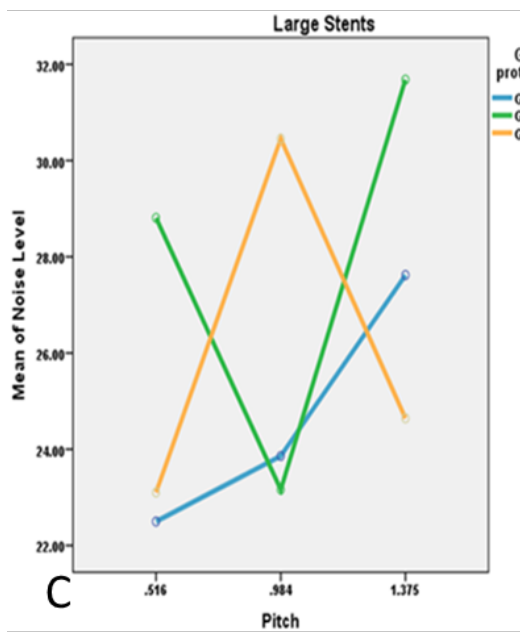
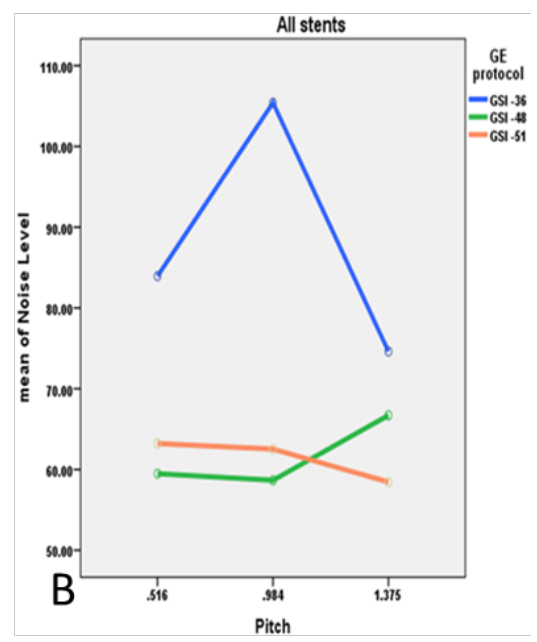
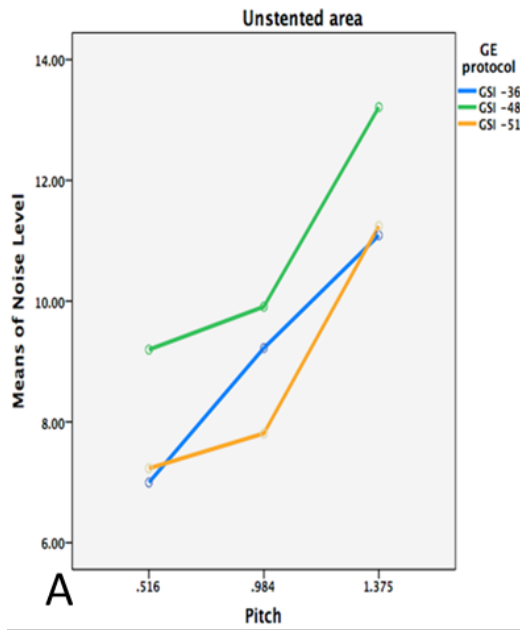
The noise level in the unstented area showed a direct relationship between image noise and pitch value, with noise increasing when pitch increased. However, with large stents, lower image noise was found in GSI-36 and GSI-48 protocols, with a pitch value of 0.984. The medium-sized stent showed a lower noise achieved by a GSI-48 pitch of 0.984, a result different from that of the small stents where the best visualisation was achieved with the use of GSI-51 and a pitch of 0.516, as shown in Figure 4.6.

A radiation dose reduction of about 50% was achieved in all protocols when the pitch value 0.984 was used; a minimal reduction was observed when the pitch value was changed from 0.984 to 1.375.

4.3.5 Subjective image quality assessment

The subjective grading of image quality showed a discrepancy between the readers of kappa = 0.24, which might be explained by the limited experience of those readers in clinical research. The box plots of the noise level for the three radiologists are shown in Figure 4.7.





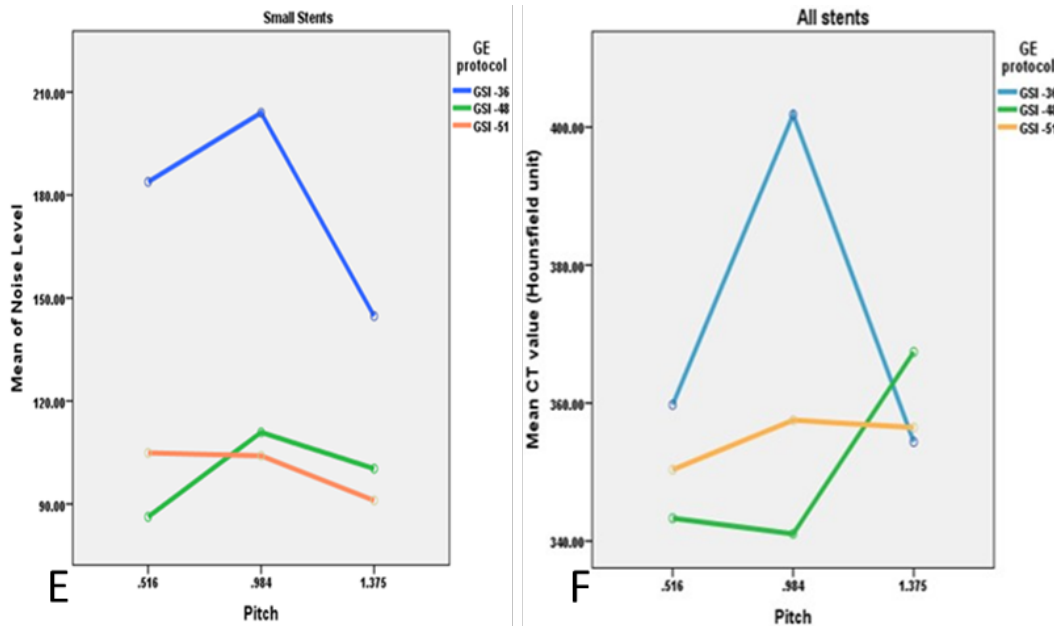


Figure 4.6.A-E: A comparison of relationship between noise levels measured with different GSI protocols and pitch values at 65 keV with different diameters of stents. **F** represents the mean of CT values measured in all stents with the use of three GSI and pitch protocols

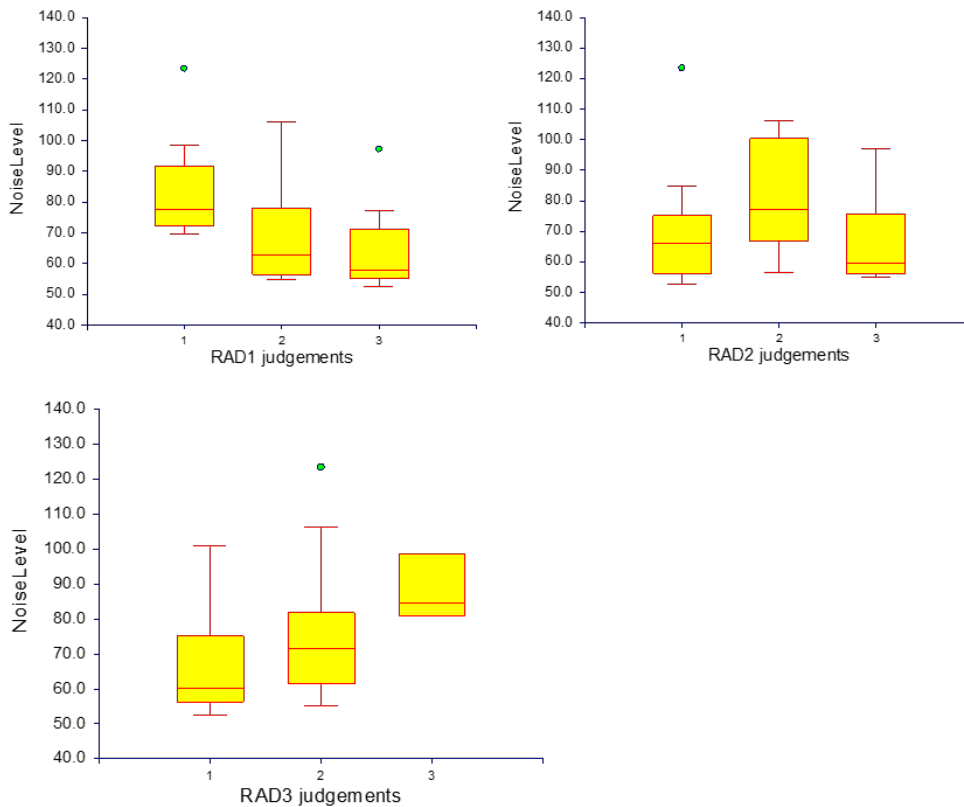


Figure 4.7. Box plots demonstrate the radiologist's evaluation of the image quality using a 3-point scale

Table 4.4. Results of factorial ANOVA

Effects		SNR		SNR2		NL		NL2	
		F	P	F	P	F	P	F	P
GSI	Main effect	11.806	0.001	86.658	0.000	947.509	0.000	572.661	0.000
Pitch	Main effect	10.992	0.002	302.411	0.000	102.664	0.000	1883.182	0.000
KeV	Main effect	13.424	0.000	192.161	0.000	230.042	0.000	894.644	0.000
ASIR	Main effect	NA	NA	157.416	0.000	NA	NA	1291.264	0.000
GSI * ASIR	Two-factor interaction effect	NA	NA	3.823	0.015	NA	NA	27.164	0.000
KeV * ASIR	Two-factor interaction effect	NA	NA	6.133	0.001	NA	NA	3.652	0.010
Pitch * ASIR	Two-factor interaction effect	NA	NA	1.877	0.147	NA	NA	68.25	0.000
GSI * KeV	Two-factor interaction effect	0.454	0.829	16.528	0.000	0.649	0.691	120.311	0.000
GSI * Pitch	Two-factor interaction effect	13.708	0.000	12.793	0.000	142.367	0.000	30.586	0.000
Pitch * KeV	Two-factor interaction effect	0.419	0.853	18.778	0.000	1.189	0.375	120.391	0.000
GSI * KeV * ASIR	Three-factor interaction effect	NA	NA	0.457	0.920	NA	NA	1.727	0.123
GSI * Pitch * ASIR	Three-factor interaction effect	NA	NA	0.634	0.742	NA	NA	9.842	0.000
Pitch * KeV * ASIR	Three-factor interaction effect	NA	NA	0.558	0.853	NA	NA	1.326	0.268
GSI * Pitch * KeV	Three-factor interaction effect	NA	NA	21.545	0.000	NA	NA	118.371	0.000

SNR: Signal to noise ratio in the stented area, SNR2: Signal to noise ratio in the unstented area, NL: noise level in the stented area, NL3 noise level in the unstented area, F: value of test statistic of F-test for corresponding effect; p: corresponding p value, GSI; gemstone spectral image protocol, keV: kiloelectron volt, and ASIR: adaptive statistical iterative reconstruction

4.3.6 Discussion

This phantom study indicates that the effect of the pitch factor on keV and radiation dose is an important indicator for determining both radiation dose and image quality, as the lowest pitch is associated with the highest radiation dose and vice versa. The lowest radiation dose with sufficient image noise was obtained with the GSI-48 protocol with a pitch of 0.984 and 65 keV. Overall, the GSI-51 protocol achieved the highest SNR and lowest noise level values with pitch values of 0.516 and 1.375. A pitch value of 0.516 was associated with the highest radiation dose, whereas a pitch value of 1.375 was associated with the highest image noise. To our knowledge, no study has been published comparing different DECT protocols with different pitch values. Results of this study show that the effect of the pitch value on image noise is strongly dependent on rotation time, as the protocol with the lowest rotation time (GSI-36) achieved both the highest SNR and the lowest image noise, and the protocol with the highest rotation time (GSI-51) achieved the highest image noise even when mAs was higher than that of the other protocols.

It was found that the images acquired with approximately 65–70 keV had less image noise and higher SNR than other energies with lower noise levels and a lower SNR. Our results are similar to those reported from a chest study by Cheng et al. [14], who found that the MEI images at 65–70 keV resulted in less image noise and a better contrast-to-noise ratio. The findings of the current study are consistent with those of Yu et al. [22] who studied various phantom sizes to evaluate MEI at multiple keV levels to optimise chest image quality. They found that the best image quality was obtained with energies of 66 keV for small phantoms, 68 keV for medium, 70 keV for large, and 72 keV for extra-large phantoms [22]. Similarly, Matsumoto et al. [23] reported that using 70 keV achieved the lowest image noise in a phantom study. Pehno et al. [12] compared the subjective and objective image quality of virtual MEI DECTA to PEI in aortoiliac arteries, demonstrating optimal contrast enhancement and improved image quality using 70 keV MEI compared with single-energy CTA. However, our findings show that the highest image noise was found with 60 keV, which differs from the finding of Sudarski et al. [24] that the use of 60 keV for lower extremities led to the best image quality when compared with the quality of conventional polyenergetic images (PEIs). These findings can be justified because the effect of stents on image noise is clearly evident when comparing small, medium, and large stents with different keV, as shown in Figure 5.4. The findings from these studies suggest that using keV between 65 and 70 with a pitch value of 0.984 achieves optimal image quality with a lower radiation dose in peripheral arterial DECT.

When iterative reconstruction is evaluated there is a significant difference between the unstented and stented areas. In the unstented area the image quality was improved when the ASIR was increased from 40% to 50%. This is similar to previous studies that showed that an ASIR of less than 40% did not improve image quality when compared with conventional PEIs [13, 25–27]. However, the current study shows that images with stents are not affected by any level of ASIR when they are applied with all the preset GSI protocols: therefore, based on the unstented area results, we recommend the use of 50% ASIR, with 65 to 70 keV in the peripheral arterial stent protocol with preset GSI-48 as the optimal protocol to replace conventional CTA.

Our study has some limitations. First, although the experimental setup simulated a peripheral vascular tree, the idealised anatomic environment did not have surrounding organs, vessel walls or tissues. The nature of body vessels varies from those in a phantom, and this could affect the visualisation of stents to some extent. Another limitation is that this custom-made phantom represented only an average-sized adult, and absorption of low-energy radiation will differ for large- or small-sized patients. Finally, although the default manufacturer's setting of 0.3 as the weighting factor for the low-energy tube was used to create virtual 120 kilovolt reconstructions, there have been reports that a weighting factor of 0.5 improves image quality and would be better for vascular imaging [28]. This suggests that further studies are necessary to confirm our findings.

4.4 Conclusions

All preset GSI protocols were found to be suitable for the evaluation of peripheral arterial stents. This study recommends use of the faster rotation time with a pitch value of 0.984 and keV of 65–70 with 50% ASIR for peripheral arterial stent visualisation with DECT, as this protocol results in lower image noise and a lower radiation dose, but with acceptable diagnostic images.

4.5 References

1. Rosamond, W, Flegal, K, Furie, K, Go, A, Greenlund, K, Haase, N et al. Heart disease and stroke statistics—2008 update: a report from the American Heart Association Statistics Committee and Stroke Statistics Subcommittee. *Circulation* 2008; 117(4), e25–146.
2. Norgren, L, Hiatt, WR, Dormandy, JA, Nehler, MR, Harris, A, Fowkes, FGR et al. In: *Inter-Society Consensus for the Management of Peripheral Arterial Disease (TASC II)*, England, 2007; S1–75.
3. Fowkes, FGR, Rudan, D, Rudan, I, Aboyans, V, Denenberg, JO, McDermott, MM et al. Comparison of global estimates of prevalence and risk factors for peripheral artery disease in 2000 and 2010: a systematic review and analysis. *Lancet* 2013; 382(9901), 1329–1340.
4. Napoli, A, Anzidei, M, Zaccagna, F, Cavallo Marincola, B, Zini, C, Brachetti, G et al. Peripheral arterial occlusive disease: diagnostic performance and effect on therapeutic management of 64-section ct angiography. *Radiology* 2011; 261(3), 976–986.
5. Rastan, A, Krankenberg, H, Baumgartner, I, Blessing, E, Müller-Hülsbeck, S, Pilger, E et al. Stent placement versus balloon angioplasty for the treatment of obstructive lesions of the popliteal artery: a prospective, multicenter, randomized trial. *Circulation*. 2013; 127(25), 2535–2541.
6. Iida, O, Yokoi, H, Soga, Y, Inoue, N, Suzuki, K, Yokoi, Y et al. Cilostazol reduces angiographic restenosis after endovascular therapy for femoropopliteal lesions in the sufficient treatment of peripheral intervention by cilostazol study. *Circulation*. 2013; 127(23), 2307–2315.
7. Tendera, M, Aboyans, V, Bartelink, M-L, Baumgartner, I, Clément, D, Collet, J-P et al. ESC Guidelines on the diagnosis and treatment of peripheral artery diseases: document covering atherosclerotic disease of extracranial carotid and vertebral, mesenteric, renal, upper and lower extremity arteries. *Eur Heart J* 2011; 32(22), 2851–2906.
8. Brockmann, C, Jochum, S, Sadick, M, Huck, K, Ziegler, P, Fink, C et al. Dual-energy CT angiography in peripheral arterial occlusive disease. *Cardiovasc Intervent Radiol* 2009; 32(4), 630–7.
9. Coursey, CA, Nelson, RC, Boll, DT, Paulson, EK, Ho, LM, Neville, A et al. Dual-energy multidetector CT: how does it work, what can it tell us, and when can we use it in abdominopelvic imaging? *Radiographics* 30(4), 1037–1055.
10. Graser, A, Johnson, TC, Chandarana, H, Macari, M. Dual energy CT: preliminary observations and potential clinical applications in the abdomen. *Eur Radiol*. 2009; 19(1), 13-23.
11. Silva, AC, Morse, BG, Hara, AK, Paden, RG, Hongo, N, Pavlicek, W. Dual-energy (spectral) CT: applications in abdominal imaging. *Radiographics* 2011; 31(4), 1031–1046.

12. Pinho, DF, Kulkarni, NM, Krishnaraj, A, Kalva, SP, Sahani, DV. Initial experience with single-source dual-energy CT abdominal angiography and comparison with single-energy CT angiography: image quality, enhancement, diagnosis and radiation dose. *Eur Radiol* 2013; 23(2), 351–9.
13. Fuchs, TA, Stehli, J, Fiechter, M, Dougoud, S, Gebhard, C, Ghadri, JR et al. First experience with monochromatic coronary computed tomography angiography from a 64-slice CT scanner with Gemstone Spectral Imaging (GSI). *J Cardiovasc CT* 2013; 7(1), 25–31.
14. Cheng, J, Yin, Y, Wu, H, Zhang, Q, Hua, J, Hua, X et al. Optimal monochromatic energy levels in spectral CT pulmonary angiography for the evaluation of pulmonary embolism. *PLoS One* 2013; 8(5).
15. Huang, SY, Nelson, C, Miller, MJ, Kim, CY, Lawson, JH, Husarik, DB et al. Assessment of vascular contrast and depiction of stenoses in abdominopelvic and lower extremity vasculature: comparison of dual-energy MDCT with digital subtraction angiography. *Acad Radiol* 2012; 19(9), 1149–1157.
16. Maaß, C, Baer, M, Kachelrieß, M. Image-based dual energy CT using optimized pre-correction functions: a practical new approach of material decomposition in image domain. *Med Phys* 2009; 36(8), 3818–3829.
17. Kau, T, Eicher, W, Reiterer, C, Niedermayer, M, Rabitsch, E, Senft, B et al. Dual-energy CT angiography in peripheral arterial occlusive disease—accuracy of maximum intensity projections in clinical routine and subgroup analysis. *Eur Radiol* 2011; 21(8), 1677–1686.
18. Yamamoto, S, McWilliams, J, Arellano, C, Marfori, W, Cheng, W, McNamara, T et al. Dual-energy CT angiography of pelvic and lower extremity arteries: dual-energy bone subtraction versus manual bone subtraction. *Clin Radiol* 2009; 64(11), 1088–1096.
19. Krasnicki, T, Podgorski, P, Guzinski, M, Czarnecka, A, Tupikowski, K, Garcarek, J et al. Novel clinical applications of dual energy computed tomography. *Advan Clin Exp Med* 2012; 21(6), 831–41.
20. Köhler, M, Burg, MC, Bunck, AC, Heindel, W, Seifarth, H, Maintz, D. Dual-Source CT angiography of peripheral arterial stents: in vitro evaluation of 22 different stent types. *Radiol Res Pract* 2011; 103873. doi:10.1155/2011/103873.
21. Valentin, J, International Commission on Radiation, P. Managing patient dose in multi-detector computed tomography (MDCT). ICRP Publication 102, *Ann ICRP* 2007; 37(1), 1–79, iii.
22. Yu, L, Christner, JA, Leng, S, Wang, J, Fletcher, JG, McCollough, CH. Virtual monochromatic imaging in dual-source dual-energy CT: radiation dose and image quality. *Med Phys* 2011; 38(12), 6371–9.
23. Matsumoto, K, Jinzaki, M, Tanami, Y, Ueno, A, Yamada, M, Kuribayashi, S., Virtual monochromatic spectral imaging with fast kilovoltage switching: improved image quality as compared with that obtained with conventional 120-kVp CT. *Radiology* 2011; 259(1), 257–262.

24. Sudarski, S, Apfaltrer, PW, Nance JJ, Schneider, D, Meyer, M, Schoenberg, SO et al. Optimization of keV-settings in abdominal and lower extremity dual-source dual-energy CT angiography determined with virtual monoenergetic imaging. *Eur J Radiol* 2013; 82(10), e574-81.
25. Marin, D, Choudhury, K, Gupta, R, Ho, L, Allen, B, Schindera, S et al. Clinical impact of an adaptive statistical iterative reconstruction algorithm for detection of hypervascular liver tumours using a low tube voltage, high tube current MDCT technique. *Eur Radiol* 2013; 23(12), 3325–3335.
26. Kulkarni, NM, Uppot, RN, Eisner, BH, Sahani, DV. Radiation dose reduction at multidetector ct with adaptive statistical iterative reconstruction for evaluation of urolithiasis: how low can we go? *Radiology* 2012; 265(1), 158–166.
27. Vardhanabhuti, V, Olubaniyi, B, Loader, R, Riordan, RD, Williams, MP, Roobottom, CA. Image quality assessment in torso phantom comparing effects of varying automatic current modulation with filtered back projection, adaptive statistical, and model-based iterative reconstruction techniques in CT. *JMIRS* 2012; 43(4), 228–238.
28. Behrendt, FF, Schmidt, B, Plumhans, C, Keil, S, Woodruff, SG, Ackermann, D et al. Image fusion in dual energy computed tomography: effect on contrast enhancement, signal-to-noise ratio and image quality in computed tomography angiography. *Invest radiol* 2009; 44(1), 1–6.

Every reasonable effort has been made to acknowledge the owners of copyright material. I would be pleased to hear from any copyright owner who has been omitted or incorrectly acknowledged.

Chapter 5 Dual energy CT angiography of peripheral arterial disease: feasibility of using lower contrast medium volume³

Defining the optimal DECTA scanning protocol for peripheral arterial stents has been discussed in Chapter 4. This chapter focuses on contrast medium optimisation for lower extremities when DECTA is used, attempting to approach part of the final objective of our study, which is to apply the devised scanning protocol in experimental and clinical settings. It compares the use of routine contrast volume with reduced contrast volume in patient with peripheral arterial disease.

5.1 Introduction

Computed tomography angiography (CTA) has, over the last decade, become the preferred choice for diagnosing and evaluating peripheral arterial disease (PAD) in a manner comparable to invasive angiography [1]. Patients diagnosed with PAD are usually evaluated with CTA, which requires administration of iodinated contrast medium. The patient exposed to this technique faces the risk of developing contrast-induced nephropathy (CIN) [2–4]. With the onset of the 64-slice and post 64-slice CT era, scanning of the lower extremities could be achieved routinely in less than ten seconds. As this fast a scan may outrun the contrast bolus, large quantities of contrast volume are not essential for vascular studies [5]. Furthermore, low kilovoltage (kVp) levels have been shown to improve contrast enhancement in CTA [6, 7]. The disadvantages of this procedure lie in the beam hardening artefacts and the increase of image noise.

Dual energy CT (DECT) is a recently developed form of multidetector CT (MDCT) scanners with the capability of compounding two different tube voltages (kVp range 80–140). The

³ This chapter is a version of the article by Almutairi A, Sun Z, Poovathumkadavi A, Assar T. Dual Energy CT angiography of peripheral arterial disease: feasibility of using lower contrast medium volume. PLoS ONE 2015; 10(9): e0139275.

main advantage of DECT is represented by material decomposition, by acquiring two image series at the same anatomic location simultaneously with use of different kVp (80 and 140 kVp). Currently there are three systems available for the simultaneous acquisition of dual-energy images during a single breath-hold: 64-slice dual-source CT, 128-slice dual-source CT (Definition and Definition Flash, Siemens Medical Systems) and high-definition 64-MDCT (Discovery 750 HD, GE Healthcare) [8]. In the Siemens CT scanners, the two x-ray tubes use different kVp (80 and 140 kVp), while in the 64-MDCT, dual-energy imaging can be achieved with a single x-ray tube with fast kilovolt dynamic switching (from 80 to 140 kVp) between two different energy levels of x-ray from view to view during a single rotation. This improved technique overcomes the disadvantages of a single kVp which is inherent in traditional MDCT scanners. The modification is brought about by combining the high and low kVp voltages to generate a variety of monochromatic CT images at multiple kilo-electron voltages (keV) ranging from 40 to 190 [9]. In this operation the contrast volume is utilised most efficiently. Additional benefits of DECT include the facilitation of a number of post-processing opportunities such as the reduction of contrast material dose given to patients when a low keV is applied [10, 11]. Applying the monochromatic images allows for the optimisation of image quality parameters like image noise and CT attenuation, with a low volume of contrast medium [11, 12].

Several reports have been published on the benefits of using (a) DSCT that employs low contrast medium volume and/or concentration protocols for imaging different body regions including coronary artery, thoracic and abdominal aorta, and lower extremities; and (b) low-iodine concentration or low volume CTA showing good diagnostic images [13–21]. However, to the best of our knowledge, with respect to the diagnosis and assessment of PAD, the application of DECT and comparison of different amounts of both contrast medium volume and keV values have not been fully reported. The present study aims to determine the optimal scanning protocol for DECTA in peripheral arterial imaging by comparing two groups of patients who were administered either a routine or a lower contrast medium volume during DECTA scanning of the lower extremities. It is hypothesised that when weighed against the routine approach, lowering of the contrast medium volume will produce acceptable diagnostic images while reducing the risk of CIN.

5.2 Materials and methods

5.2.1 Patient population

Thirty-four patients (25 male and 9 female) between 27 and 73 years of age, with a mean age of 52.73 ± 11.37 years, who had been advised to undergo peripheral arterial DECTA, were

selected for the study. The duration of the study period was September 2014 to March 2015. These subjects were randomly assigned to two groups as follows:

Group 1, the routine contrast volume group, consisting of 17 patients (11 male and 6 female), with a mean age of 52.21 ± 13.55 years, falling within the age range of 27–73 years.

Group 2, the low contrast volume group, consisting also of 17 patients (14 male and 3 female), with a mean age of 53.35 ± 9.48 years, falling within the age range of 32–67 years.

Exclusion criteria for subjects included contraindication to intravenous administration of iodine contrast medium, and presence of renal dysfunction or renal failure. The study was approved by the Curtin Human Research Ethics (HR 167/2013) and King Fahad Specialist Hospital Committees (IRB-RAD029-FB). Informed written consent was obtained from all patients participating in the study. These consent forms were kept in a secure location which could only be accessed by investigators. The Institutional Review Boards (IRBs) approved this procedure.

5.2.2 CT scanning protocol

All CT examinations were performed on a fast kilovoltage-switching 64-slice CT scanner (Discovery CT HD 750; Gemstone Spectral Imaging, GE Healthcare, Milwaukee, WI) in the DE mode. The following features of GSI (Gemstone Spectral Imaging)-48 protocol were used:

- collimation – 64×0.625 mm
- pitch – 0.984
- gantry rotation time – 0.7s
- slice thickness – 1 mm
- reconstruction interval – 1 mm
- alternated 80 kVp and 140 kVp with the same X-ray tube by fast kVp switching
- a constant tube current of 600 mAs, (tube current modulation is not available in DE acquisition in this system).

Six sets of monochromatic images at 50, 55, 60, 65, 70 and 75 keV were reconstructed with adaptive statistical iterative reconstruction (ASIR) at 50%.

The non-ionic intravenous contrast medium called Xenetix 350® (350 mg. Iodine/mL, Guerbet, Sulzbach, Germany), was injected using a power injector (Envision CT injector, Medrad) through an 18–20G catheter inserted into the median cubital vein. A bolus tracking

technique was used to initiate the scan in the abdominal aorta at the level of the celiac trunk with a threshold of 150 HU. Group 1 (routine group) was administered 1.5 mL/kg body weight and Group 2 (low contrast group) 0.75mL/kg body weight (a reduction of about 50%) of Xenetix, followed by 40 ml of a saline flush. The injection rate of contrast medium and saline solution was 4–5 ml/s for all subjects in both groups

5.2.3 Qualitative assessment of image quality

Two radiologists with 20 years and 15 years of experience in body imaging and CTA interpretation performed qualitative evaluations separately on a workstation with dedicated software (Gemstone Spectral Imaging Viewer, GE). The different virtual monochromatic spectral (VMS) image sets of each individual patient were evaluated randomly at 50, 55, 60, 65, 70 and 75 keV energy levels, by each reader. It was deemed unnecessary to blind the readers to the altered energy levels because the different values could easily be detected by visual inspection of the images.

The image quality of the different VMS series, as well as the 2D and 3D reformations (Maximum-Intensity Projection (MIP) and Multiplanar Reformations (MPR)), were subjectively analysed using a 4-point scale, where the scores were interpreted as follows: 1 – poor vessel opacification and non-diagnostic; 2 – fair vessel opacification; 3 – good vessel opacification; 4 – excellent vessel opacification. The evaluation was carried out for three body regions, the pelvic, thigh and leg regions. A score of 2 or above was considered clinically diagnostic.

5.2.4 Quantitative assessment of image quality

A single reviewer performed quantitative analysis on the same workstation. The CT attenuation (mean CT number in Hounsfield units) and noise (computed as standard deviation of the CT number in Hounsfield units) were calculated for the main peripheral arteries, including the common iliac, superficial, femoral and tibial arteries, by placing a defined Region of Interest (ROI) on all VMS series. ROIs were marked as large as possible in the vessel lumen. Areas with wall calcification that might cause artefacts were avoided. The CT attenuation of the background was also measured for all patients at the region of the muscle closest to the arteries under investigation. The mean CT attenuation and noise were calculated for individual subjects by averaging the values derived from both sides of the arteries under study. The signal-to-noise ratio (SNR) was calculated as mean CT value of ROI divided by the mean image noise (SD), while the contrast-to-noise ratio (CNR) was

calculated as mean CT value of vessel minus CT value of background muscle divided by the mean image noise (SD) of vessel, which is:

$$\text{CNR} = (\text{Mean}_{\text{vessel}} - \text{Mean}_{\text{muscle}}) / \text{SD}_{\text{vessel}} \quad (4)$$

5.2.5 Radiation dose estimation

To arrive at the most effective radiation dose, the scan length was documented for each patient. Thereafter, the volume CT dose index (CTDI_{vol}) and dose length product (DLP) were recorded from the CT console following individual examination of subjects. The multiplication product of DLP and a conversion factor for peripheral arteries examinations in the lower extremities [$k = 0.0056 \text{ mSv} / (\text{mGy} \times \text{cm})$] yielded the effective dose of radiation [22].

5.2.6 Statistical analysis

Statistical analysis was performed with the help of commercial software SPSS version 22.0, (SPSS Inc., Chicago, IL). Quantitative variables were expressed as the mean \pm SD and categorical variables as frequencies or percentages. Repeated measures (split plot) Analysis of Variance (ANOVA) was used to compare the CT value, noise, SNR and CNR of the VMS images at varying monochromatic energy levels. The analysis of covariance (ANCOVA) was used to compare six factors (group, gender, hypertension, smoking, diabetes and hyperlipidemia) with dependent variables such as scan time, scan range, DLP and effective dose. At the main plot level, the design was simple and fully randomised. Subsequently each participant was 'split' into 18 sub-plots, corresponding to the 18 combinations of three body regions with six voltage settings, to enable the application of 18 regimes to each of the participants and to facilitate recording of the output measure again, for each regime (hence the name, repeated measures). This experimental design produced a total of $34 \times 18 = 612$ sub plots. A high degree of calcification in the arteries of the thigh and leg regions of two patients in Group 2 (low contrast medium group) made it necessary to exclude them from the analysis of quantitative image quality. A measure of the concurrence between the two radiologists for various parameters was elicited with the kappa coefficient of concordance, which provides information about inter-observer variability. Probability values of less than 0.05 were considered statistically significant.

5.3 Results

Scans were successfully completed for each of the 34 enrolled patients. Table 5.1 displays patient characteristics and contrast protocols.

5.3.1 Scan time

Analysis of risk factors demonstrated that four factors affected scan time:

- (a) Hypertension – a significant effect ($p = 0.013$) was seen to be exerted by hypertension, with the scanning time increasing from 23.5 seconds (non-hypertensives) to 24.5 seconds (hypertensives).
- (b) Diabetes – a highly significant effect ($p = 0.004$) was observed in the presence of Diabetes (diabetics vs non-diabetics 24.9 secs vs 23.4 secs).
- (c) Age – every additional year of age was reflected in a reduction of scanning time by 0.038 seconds. The statistical test of significance was positive with p value being 0.032.
- (d) Body weight – a highly significant difference ($p < 0.001$), was noted with each additional kilogram of body weight with an increase of 0.47 seconds (S 1–3 Tables).

Table 5.1. Patient characteristics and contrast protocols

	Routine contrast volume (n = 17)	Low contrast volume (n = 17)
Patient characteristics		
Male: Female	11:6	14:3
Age (yrs)	52.12 ± 13.17	53.35 ± 9.21
Weight (kg)	77.07 ± 15.56	71.49 ± 13.87
Height (cm)	162.65 ± 7.78	163.68 ± 8.55
BMI (kg/m ²)	29.84 ± 5.77	26.79 ± 5.49
Contrast medium		
Contrast volume (mL)	116.00 ± 16.09	66.47 ± 6.83***
Flow rate (mL/sec)	4.74 ± 0.35	4.76 ± 0.39
Contrast duration (sec)	25.01 ± 3.37	14.69 ± 2.34***
Scanning parameters and radiation dose		
Scanning time (sec)	24.27 ± 1.52	24.64 ± 1.16
Scanning range (mm)	1244.18 ± 103.03	1272.12 ± 67.09
DLP) (mGy*cm)	1238.52 ± 73.25	1257.53 ± 58.45
Effective dose (mSv)	7.56 ± 0.53	7.57 ± 0.80
Conversion factor for peripheral CTA = 0.0056 mSv/mGy*cm		

BMI = body mass index; DLP = dose length product

*** $p < 0.001$, highly significant

Table 5.2.Results of factorial ANOVA

Source		CT value		Image noise		SNR		CNR	
		F	p-value	F	p-value	F	p-value	F	p-value
Group	Hypothesis	67.898	0.001	19.115	0.001	15.897	0.001	20.976	0.001
Body Part	Hypothesis	18.240	0.001	45.943	0.001	42.011	0.001	172.846	0.001
KeV	Hypothesis	597.903	0.001	97.788	0.001	4.863	0.001	19.767	0.001
Group * Body Part	Hypothesis	6.352	0.002	2.684	0.072	3.071	0.047	5.904	0.003
Body Part * keV	Hypothesis	1.021	0.424	1.066	0.387	0.671	0.751	0.660	0.762
Group * keV	Hypothesis	17.543	0.001	0.863	0.506	0.169	0.974	0.092	0.993
Group * Body Part * keV	Hypothesis	0.362	0.962	0.039	1.000	0.077	1.000	0.041	1.000

Group: routine contrast volume and low contrast volume, CT value: CT number in Hounsfield units, SNR: Signal to noise ratio in the stented area, CNR: Contrast to noise ratio, F: value of test statistic of F-test for corresponding effect; P: corresponding p-value, keV: kiloelectron volt.

Table 5.3.Objective and subjective image quality

Body Part	Contrast groups	Kiloelectron volt (keV)	CT value	Image noise	SNR	CNR	Likert score	
1 Pelvis	1 Routine contrast volume	50	737.29 ± 138.88	62.56 ± 19.77	12.59 ± 3.44	13.37 ± 4.80	3.88 ± 0.33	
		55	614.29 ± 115.27	53.05 ± 16.72	12.36 ± 3.36	12.91 ± 4.51	3.32 ± 0.67	
		60	510.37 ± 94.07	37.44 ± 11.37	14.51 ± 3.68	15.90 ± 5.55	3.32 ± 0.72	
		65	426.08 ± 77.49	30.17 ± 8.31	14.89 ± 3.69	15.36 ± 4.79	3.20 ± 0.82	
		70	363.98 ± 64.53	27.70 ± 7.56	13.82 ± 3.43	13.89 ± 4.46	2.88 ± 1.10	
		75	316.16 ± 57.68	29.59 ± 7.91	11.20 ± 2.92	10.49 ± 3.65	2.82 ± 1.11	
	2 Low contrast volume	50	536.26 ± 157.29	55.13 ± 17.78	10.20 ± 3.22	10.60 ± 4.10	3.64 ± 0.55	
		55	447.18 ± 130.39	47.09 ± 14.96	9.98 ± 3.23	10.07 ± 3.73	2.73 ± 0.96	
		60	373.45 ± 106.48	32.22 ± 11.66	12.37 ± 4.17	12.32 ± 5.60	3.14 ± 0.95	
		65	312.60 ± 87.29	25.61 ± 9.28	13.18 ± 4.73	12.48 ± 6.59	2.82 ± 0.97	
		70	267.08 ± 74.83	24.17 ± 7.83	11.85 ± 4.33	10.28 ± 4.41	2.53 ± 1.02	
		75	230.74 ± 64.61	26.17 ± 7.68	9.58 ± 4.11	7.73 ± 3.15	1.91 ± 0.97	
	2 Thigh	1 Routine contrast volume	50	745.29 ± 184.23	56.04 ± 28.81	15.42 ± 6.30	24.07 ± 11.70	3.61 ± 0.58
			55	622.78 ± 150.15	47.19 ± 24.28	15.26 ± 6.05	23.24 ± 11.05	3.05 ± 0.80
60			517.80 ± 122.39	36.52 ± 19.57	16.67 ± 6.64	28.04 ± 12.67	3.44 ± 0.70	
65			432.90 ± 101.88	30.16 ± 15.95	17.09 ± 7.39	28.96 ± 12.97	2.99 ± 0.90	
70			368.04 ± 97.45	26.18 ± 14.29	16.75 ± 6.94	25.98 ± 11.84	2.85 ± 1.00	
75			328.29 ± 74.25	25.01 ± 12.75	15.11 ± 5.55	19.88 ± 9.39	3.02 ± 1.18	
2 Low contrast volume		50	508.48 ± 178.71	40.04 ± 12.06	13.57 ± 5.57	16.77 ± 7.49	3.41 ± 0.79	
		55	430.54 ± 146.11	33.68 ± 10.31	13.70 ± 5.46	16.30 ± 6.96	2.38 ± 0.93	
		60	360.21 ± 121.88	25.05 ± 9.36	16.08 ± 7.23	20.98 ± 9.73	3.11 ± 1.05	
		65	304.78 ± 102.39	20.65 ± 9.24	17.36 ± 8.38	22.43 ± 11.20	2.47 ± 0.99	
		70	266.48 ± 86.83	17.87 ± 6.63	16.55 ± 6.93	17.99 ± 8.21	2.67 ± 1.07	
		75	235.53 ± 74.43	17.55 ± 5.48	14.49 ± 5.65	13.34 ± 5.54	2.05 ± 0.97	

3 Legs	1 Routine contrast volume	50	665.62 ± 185.87	72.80 ± 31.41	11.27 ± 6.72	24.43 ± 11.81	3.29 ± 0.94
		55	566.85 ± 155.02	61.67 ± 26.63	11.32 ± 6.66	23.64 ± 11.39	3.49 ± 0.74
		60	460.82 ± 131.12	48.06 ± 20.94	11.99 ± 7.38	28.33 ± 13.76	3.29 ± 0.92
		65	385.55 ± 114.27	38.75 ± 16.99	12.51 ± 7.83	28.96 ± 13.81	3.11 ± 0.78
		70	342.71 ± 97.26	35.08 ± 15.53	12.29 ± 7.49	24.72 ± 12.64	2.82 ± 0.84
		75	311.92 ± 86.02	32.43 ± 14.33	11.94 ± 6.81	20.27 ± 10.44	2.35 ± 1.02
	2 Low contrast volume	50	500.62 ± 147.36	61.14 ± 43.33	11.39 ± 8.40	18.63 ± 7.31	3.50 ± 0.89
		55	425.86 ± 124.15	51.68 ± 36.71	11.62 ± 8.55	18.11 ± 7.03	2.64 ± 0.88
		60	348.15 ± 99.60	39.74 ± 28.57	11.99 ± 7.21	21.83 ± 8.43	2.96 ± 1.15
		65	289.41 ± 82.79	32.00 ± 23.72	12.60 ± 7.17	22.29 ± 8.74	2.65 ± 0.82
		70	257.90 ± 74.52	29.25 ± 21.98	12.62 ± 7.71	18.84 ± 7.56	2.29 ± 1.12
		75	232.62 ± 68.02	27.55 ± 23.72	12.38 ± 8.18	15.01 ± 6.23	2.11 ± 0.98

5.3.2 Image quality assessment

Assessment of image quality was carried out by taking the overall mean CT value and mean noise for all body regions. It was seen to be significantly lower for the low volume contrast group than for the routine contrast group ($p < 0.001$). A more detailed account of this parameter follows.

In both groups, the CT value in the pelvis, thighs, and legs for all the keV ranges was >230 HU, which is considered sufficient opacification for CTA examination. CT attenuation varied significantly within groups ($p = 0.001$), body parts ($p < 0.001$) and keVs ($p < 0.001$). The interaction between group and body part in terms of CT attenuation and CNR was significant ($p = 0.002$ and $p = 0.003$ respectively; Table 5.2). However, the mean CT attenuation was lower for the low contrast volume group than for the routine contrast volume group, recording statistically significant figures ($p = 0.001$). The marked difference in interaction between body parts in the two contrast groups was reflected in a huge drop from 494 HU (routine/pelvis) to 361 HU (low/pelvis). An even larger drop was observed for the thigh region, and the largest drop was noticed for legs. These results were similar for both groups. The SNR, in contrast, remained slightly different, with a marginally significant p value (0.047) (Tables 5.3 and 5.4).

No evidence of interaction effects was observed between body part and keV, nor between groups and body part by keV for the entire range of quality variables. The interaction between group by keV was highly significant ($p < 0.001$). Reduction in CT values between routine and low contrast groups, with increase in voltage, were 28.1%, 27.8%, 27.3%, 27.1%, 26.3% and 26.9% HU respectively, so it can be inferred that the difference between routine and low contrast uniformly came down with each rise in voltage.

Table 5.4. CT value, image noise, SNR and CNR

Body part	Contrast group	CT value	Image noise	SNR	CNR
1 Pelvis	1 Routine contrast volume	494.69 ^a	40.07 ^a	13.23 ^a	13.66 ^a
	2 Low contrast volume	361.22 ^a (428) ^b	35.07 ^a (37.6) ^b	11.19 ^a (12.2) ^b	10.58 ^a (12.1) ^b
2 Thigh	1 Routine contrast volume	502.52 ^a	36.85 ^a	16.05 ^a	25.03 ^a
	2 Low contrast volume	351.00 ^a (427) ^b	25.81 ^a (31.3) ^b	15.29 ^a (15.7) ^b	17.97 ^a (21.5) ^b
3 Legs	1 Routine contrast volume	455.58 ^a	48.13 ^a	11.89 ^a	25.06 ^a
	2 Low contrast volume	342.43 ^a (399) ^b	40.23 ^a (44.2) ^b	12.10 ^a (12) ^b	19.12 ^a (22.1) ^b
Total	1 Routine contrast volume	484.30 ^a	41.70 ^a	13.70 ^a	21.30 ^a
	2 Low contrast volume	351.60 ^a	33.70 ^a	12.90 ^a	15.90 ^a

^a Based on modified population marginal mean.

^b The marginal body part means.

Image noise was found to be lower in the low contrast volume group at 65 to 70 keV, but at the 70 keV energy level the noise either remained unchanged or increased to a small extent in the pelvic area (Figure 5.1). The highest values of SNR and CNR were obtained at 65 keV for both groups. Figure 5.1 portrays an example of image quality with different keV ranges, and Figure 5.2 displays the comparison of SNR and CNR figures across the keV ranges. Figure 5.3 shows an example of DECTA images acquired with different keV ranges.

With respect to qualitative analysis, the mean scores of the CTA image quality indices for routine contrast and low contrast groups were 3.24 and 2.80 respectively. The lowest quality in both groups was attained in the leg region due to the incidence of severe calcification. The inter-reader concurrence for image quality grading was moderate ($k = 0.33$). Overall the qualitative assessment of image quality indicated that all the images were acceptable for clinical diagnosis.

5.3.3 Radiation dose

The difference in radiation dose was not statistically significant (DLP and effective dose) between the routine contrast and low contrast cohorts ($p = 0.07$). Routine contrast group figures were 1238.52 ± 73.25 mGy*cm and 7.56 ± 0.53 mSv (male: 7.36 ± 0.53 mSv, female: 7.93 ± 0.24 mSv), while the low contrast group readings were 1257.53 ± 58.45 mGy*cm and 7.57 ± 0.67 mSv (male: 7.46 ± 0.78 mSv, female: 8.12 ± 0.68 mSv).

5.4 Discussion

The present study compares low volume with routine volume contrast medium for assessment of peripheral arteries using DECT on a clinical patient population, with the aim of evaluating the optimal contrast protocol of image quality, using virtual manipulation of keV-settings. To the best of our knowledge, no studies have been published comparing different contrast volumes with varying keV settings in DECTA of lower extremities. Results of the investigation demonstrate that contrast medium volume may be reduced by as much as 50% without compromising vascular visualisation. DECTA protocol of 65-keV with 50% ASIR resulted in the highest degree of CT attenuation and lowest image noise with a resultant increase in SNR and CNR, in comparison with the other VMS levels attained in both the groups.

The findings of this study are consistent with previous reports in a phantom study [23], which illustrated the achievement of optimal image quality between 65 and 70 keV [23]. The results of the present experiment make obvious that a lower keV in peripheral DECTA

produces higher vascular enhancement in both groups, irrespective of contrast volume. The investigation reiterates the feasibility of reducing contrast medium volume by 50% without negatively altering diagnostic image quality. These findings are supported by Baxa et al. [17], who used only 40mL in their study of lower extremity DECTA imaging; they did not, however, make evaluate spectral imaging because they were assessing contrast delivery rather than scanning techniques. The reduction of contrast medium volume was not a priority in their study, and therefore, there was no significant difference in contrast medium volume between control (routine) and experimental (low dose) groups. The image quality at 65 keV, for both groups, was found to be optimal for lower extremity CTA with Dual Energy CT. This protocol could greatly minimise the risk of CIN in patients with renal insufficiency.

In recent years a number of studies have focused on image quality using different virtual keV-values in imaging body vasculature [9, 24, 25]. Of them, only one study pertains to the evaluation of peripheral arteries through DECT at varying keV levels [9]. The authors discovered that best image quality for lower extremity CTA was attainable at 60 keV. Another study on abdominal CTA imaging with altered contrast volumes showed that up to 70% of contrast volume could be used successfully with DECT. Other research has reported that contrast medium volume determines the optimal keV level [25]. Contrary to these findings, the present investigation demonstrates that an inferior image quality is produced at 60 keV compared to 65 keV. This observation is supported by the postulation that 60 keV is the outcome of the 80 kVp, which corresponds to higher image noise [26].

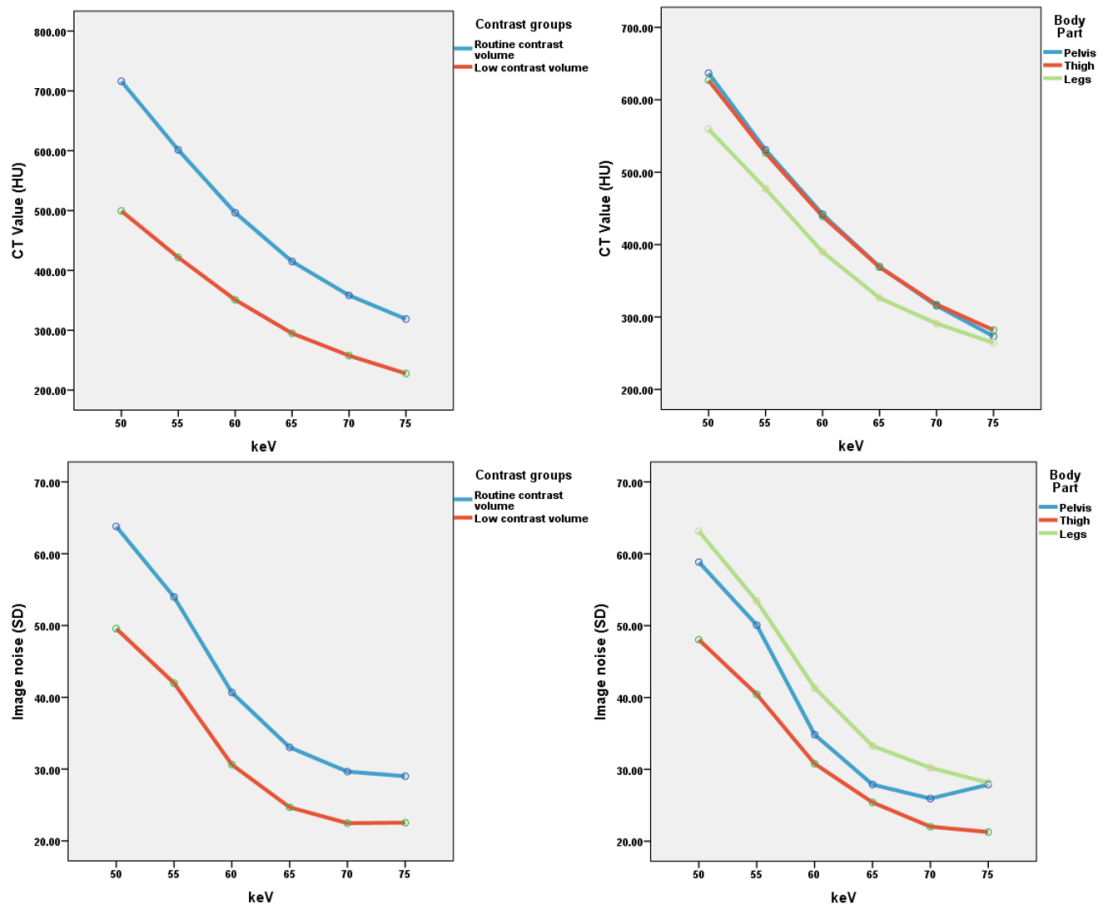


Figure 5.1. Comparison of CT attenuation and image noise measured at two contrast groups at different body parts with variable keV sets.

A: Comparison of the measured CT values in the monochromatic images for the two contrast groups.

B: comparison of the measured CT values of three body parts at different keV sets.

C: image noise values in the monochromatic images for the two contrast groups.

D: comparison of image noise of different body parts at different keV sets.

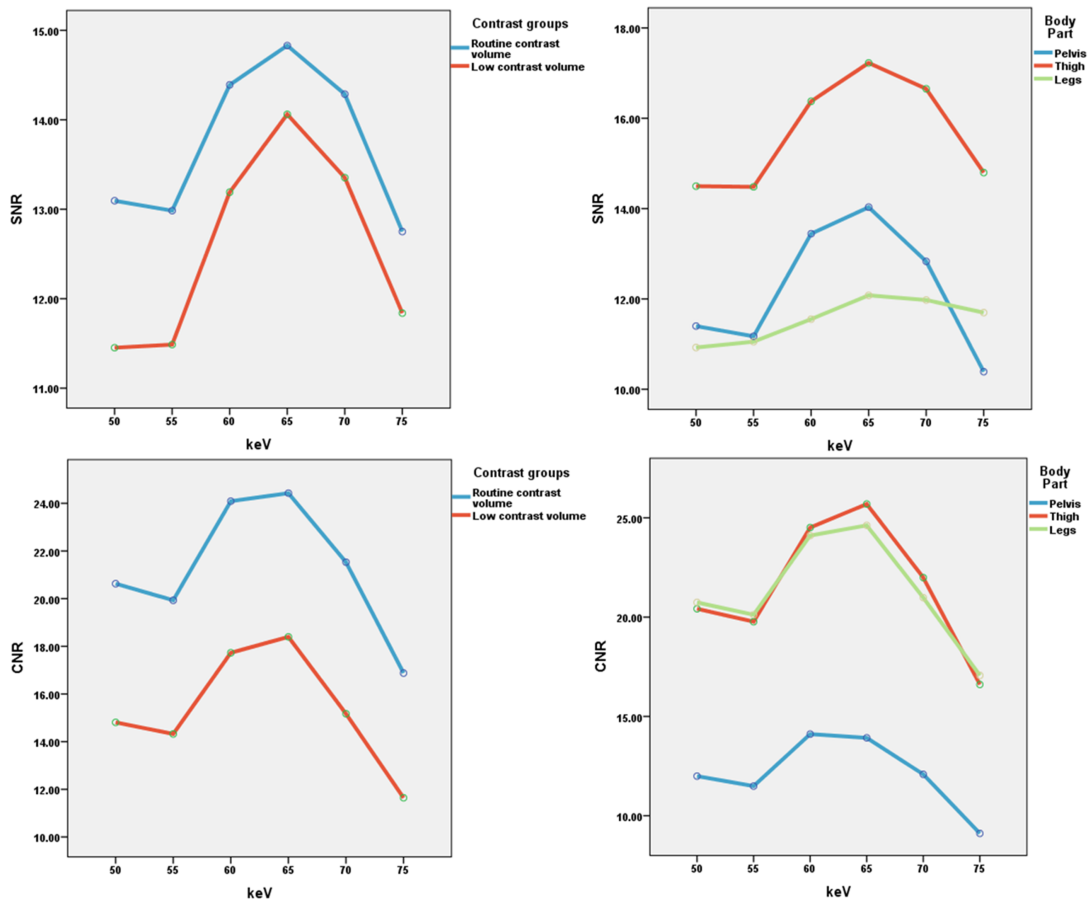


Figure 5.2. Comparison of SNR and CNR measured at two contrast groups at different body parts with variable keV sets. Comparison of calculated and measured SNR in monochromatic images with A showing the differences between the two contrast groups at different keV sets, B representing the SNR values of keV sets with three body parts, C showing the comparison of calculated and measured CNR in monochromatic images for the two contrast groups, and D demonstrating the CNR values of three body parts at different keV sets. In the range of 55–65 keV, both of the two curves increase sharply with the gradual rise in keV. Between 65 and 75 keV, both curves of the contrast values decrease sharply with 65 keV, resulting in the highest value.

Several researchers have worked on the efficacy of VMS for visualising thoracic and abdominal arteries. Delesalle et al. studied the spectral optimisation of thoracic arteries and found that 60 keV and 100 keV produced either identical or better image quality than standard chest CTA [18]. Maturen et al., in their investigation of endovascular aneurysms of the aorta, established high sensitivity in the detection of endoleaks at 55 keV compared to standard CTA [27]. In another study, Sudarski et al. recommended that using 70 keV might achieve a higher CNR in abdominal arteries [9]. Pehno et al. compared the image quality of VMS DECTA with standard CTA in aortoiliac arteries and demonstrated that optimal contrast enhancement improved image quality at 70 keV [24]. Applying these values for lower extremity DECTA may not be feasible because of inherent structural differences in

body regions. The present undertaking used 65 keV to attain a lower image noise and higher CNR and SNR, in order to promote efficient imaging of peripheral arteries.

The type and severity of vascular disease have an enormous impact on blood flow velocity and contrast delivery. Improved image quality has been achieved in patients with PAD by employing faster table speed. In contrast, a lower table speed gives rise to better image quality in patients with abdominal aortic aneurysm [28]. It has been reported that aneurismal patients exhibit longer aortic peaks than non-aneurismal subjects [17]. With regard to the duration of the scan period, it was found in the present investigation that hypertensive patients need a lower scan time than non-hypertensives, while non-diabetic patients require a significantly shorter scan time than diabetic patients. Age and body weight were seen to be important influencing factors, producing significantly different readings for scan time. Clinicians need to consider all these findings while scanning patients with different risk factors so that the best possible desired CTA images may be obtained. More in-depth studies in this area are recommended due to the limited number of respondents participating in the present study.

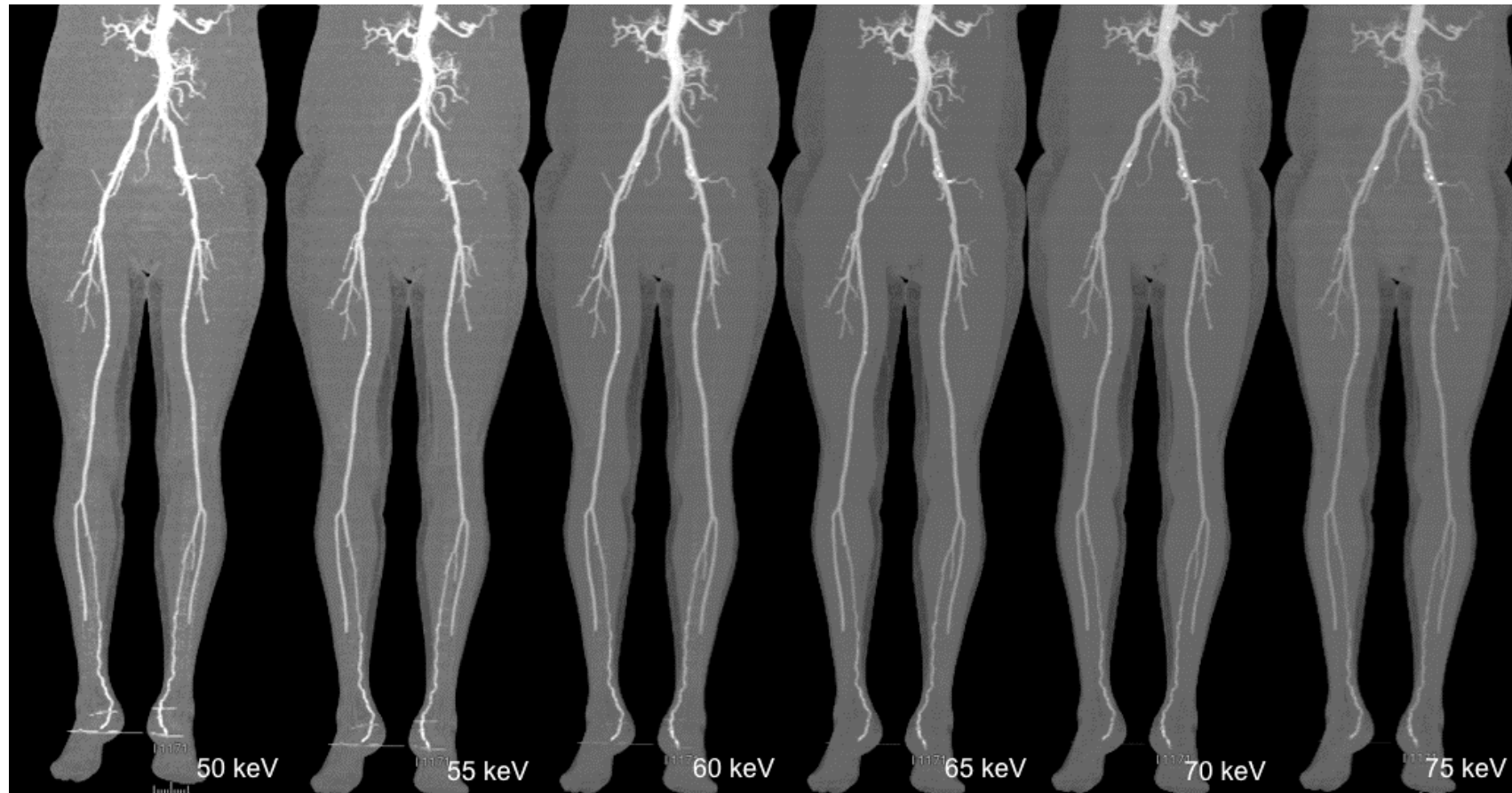


Figure 5.3. DECTA images acquired with different keV values using routine contrast medium. Examples of image quality of DECTA maximum-intensity projection (MIP) are shown in a 53-year-old female with a body weight of 54 kg, using 80 ml of contrast medium. Comparison among DECTA acquisitions in the different virtual monochromatic energies (50, 55, 60, 65, 70 and 75 keV) shows higher image noise at 50 and 55 keV which affects visualisation of the vascular lumen details. VMS images acquired at 65 keV were shown to have better image quality (higher SNR and CNR) than other keVs.

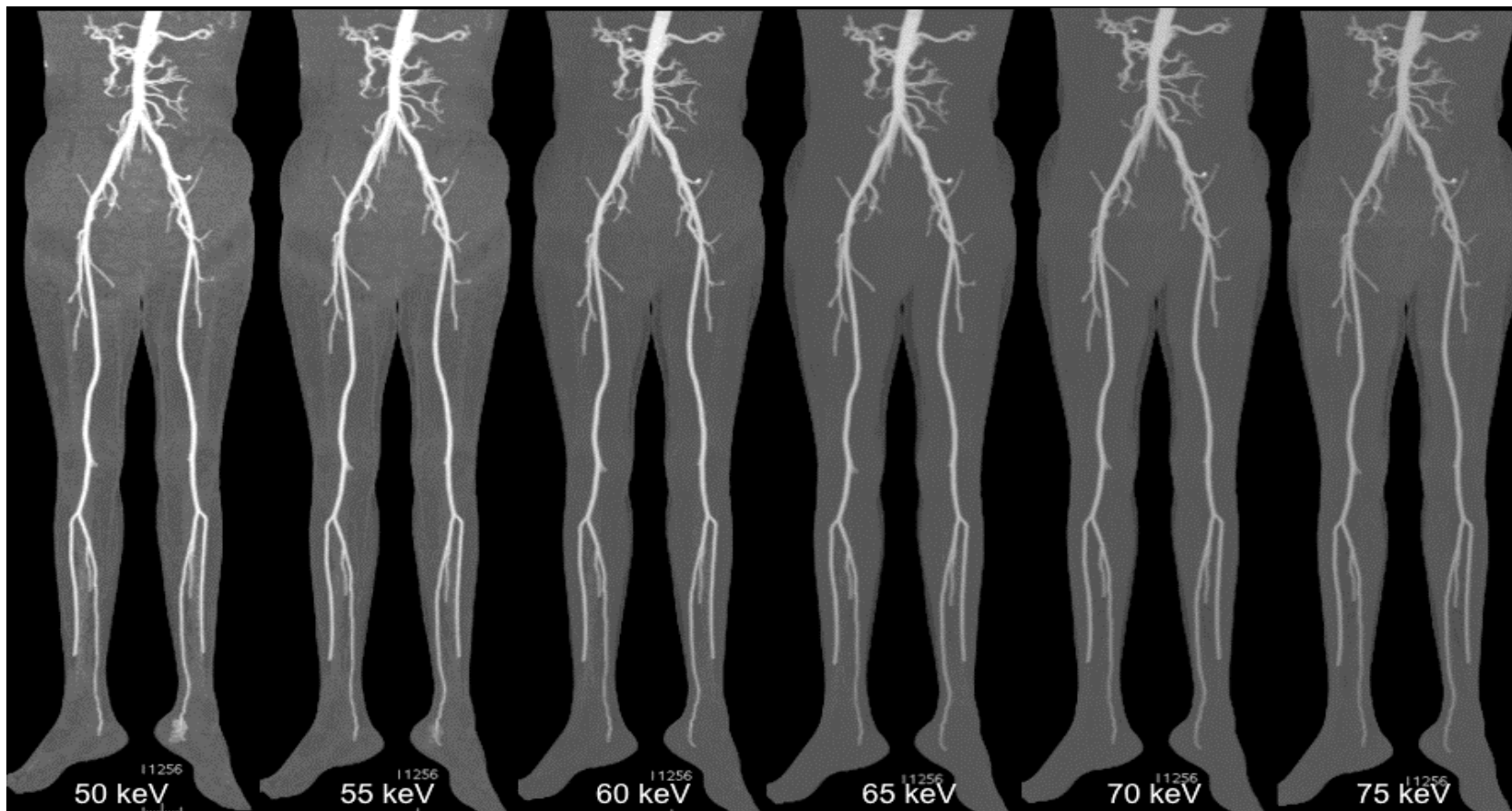


Figure 5.4. DECTA images acquired with different keV values using low contrast medium. A series of MIP images of DECTA were obtained in a 43-year-old male with body weight of 56 kg using 50 ml of contrast medium in the diagnostic assessment of peripheral arteries. Comparison among DECTA acquisitions in the different virtual monochromatic energies (50, 55, 60, 65, 70 and 75 keV) shows higher image noise at 50 and 55 keV which affects visualisation of the vascular lumen details. VMS images acquired at 65 keV were shown to have better image quality (higher SNR and CNR) compared to the other keVs.

Radiation dose did not show any marked difference between the experimental (lower dose) and control (routine dose) groups as a result of differences in DLP. The effective dose in this study was about 7.6 mSv for both groups, which is slightly higher than the 5.74 mSv reported by Dong et al. [21], but it is similar to the 7.0 mSv for DECT pulmonary angiography reported in a prospective randomised trial [4]. According to the effective dose range of various CT procedures [29], the radiation dose of DECTA in this study is within the acceptable limit, although a further reduction could be achieved with the advancement of new generation DECT. The effective dose in this study was calculated according to the latest methodology, and appears to be smaller than quantities used in previous studies because of the application of a new conversion coefficient for DECT of the lower extremities. Consequently, interpretation of results from this report needs to be carried out with care, particularly when making comparisons with results reported previously in the literature.

5.4.1 Limitations of the study

The present study is not without limitations:

- A single scanning centre was approached and a relatively small number of patients were incorporated into the study. The reason for this is the still emerging role of DECTA in PAD, which rendered recruitment of a larger number of patients difficult. This limitation could be overcome with multi-centre studies.
- No comparison has been made of DECTA with invasive angiography, which is regarded as the reference method for arterial imaging. As a result, no assurance of diagnostic accuracy is available in this study. The potential risk of radiation exposure, and the use of high volume contrast medium during invasive angiography, are responsible for its gradual replacement by less invasive and safer modalities such as CTA.
- Measurement of attenuation was performed at only three levels. This may be justified by noting that the inclusion of numerous variables led to the involvement of a combination of more than 600 subplots, making the results suitable for qualitative and quantitative analysis.
- DECT application is still at the developing stage in routine clinical practice and readers are still familiarising themselves with the assessment of image quality, which is probably the reason for the moderate degree of inter-observer agreement seen in this study.
- Inclusion of some patients whose body weight was ≥ 100 kg (which is associated with high image noise) made it difficult to apply the results of the present study.

5.5 Conclusion

Investigation of the performance of DECTA in imaging peripheral arteries was carried out by comparing the efficacy of low volume of contrast medium with a routine volume of contrast medium. The outcome of the investigative study was that the image quality of DECTA obtained from both groups was clinically acceptable. The quality of DECTA peripheral artery images received at 65 keV and 50% ASIR, with low contrast medium volume protocol, was comparable to images received using the routine contrast medium volume DECTA. It may therefore be concluded that lowering the contrast medium volume by 50% may lead to diagnostically satisfying images during DECTA of peripheral arteries, while reducing the risk of CIN in susceptible patients. Needless to say, more detailed and substantial research is necessary to reiterate the findings of the present investigation.

5.6 References

1. Rubin GD, Leipsic J, Joseph Schoepf U, Fleischmann D, Napel S. CT angiography after 20 years: a transformation in cardiovascular disease characterization continues to advance. *Radiology* 2014; 271(3):633–52. doi: 10.1148/radiol.14132232. PMID: 24848958.
2. Brown JR, Robb JF, Block CA, Schoolwerth AC, Kaplan AV, O'Connor GT et al. Does safe dosing of iodinated contrast prevent contrast-induced acute kidney injury? *Circ Cardiovasc Interv* 2010; 3(4):346–50. doi: 10.1161/circinterventions.109.910638. PMID: 20587788.
3. Owen AR, Roditi GH. Peripheral arterial disease: the evolving role of non-invasive imaging. *Postgradu Med J*. 2011; 87(1025):189–98. PMID: 854568800; 21273362.
4. Yuan R, Shuman WP, Earls JP, Hague CJ, Mumtaz HA, Scott-Moncrieff A et al. Reduced iodine load at CT pulmonary angiography with dual-energy monochromatic imaging: comparison with standard CT pulmonary angiography—a prospective randomized trial. *Radiology* 2012; 262(1):290–7. doi: 10.1148/radiol.11110648. PMID: 22084206.
5. Anzidei M, Menichini G, Catalano C. CT-Angiography. In: Catalano C, Anzidei M, Napoli A (eds) *Cardiovascular CT and MR Imaging*: Springer, Milan; 2013, pp. 1–20.
6. Oca Pernas R, Delgado Sanchez-Gracian C, Tardaguila de la Fuente G, Fernandez Del Valle A, Silva Priegue N, Gonzalez Vazquez M et al. Comparison of image quality and radiation dose in computed tomography angiography of the peripheral arteries using tube voltage of 80 kVp versus 100 kVp. *Radiologia* 2014; 56(6):541–7. doi: 10.1016/j.rx.2012.06.013. PMID: 23276715.
7. Utsunomiya D, Oda S, Funama Y, Awai K, Nakaura T, Yanaga Y et al. Comparison of standard- and low-tube voltage MDCT angiography in patients with peripheral arterial disease. *Eur Radiol* 2010; 20(11):2758–65. doi: 10.1007/s00330-010-1841-4. PMID: 20571804.
8. Karcaaltincaba M, Aktas A. Dual-energy CT revisited with multidetector CT: review of principles and clinical applications. *Diagn Interv Radiol* 2011; 17:181–194. doi: 10.4261/1305-3825.DIR.3860-10.0. PMID: 20945292.
9. Sudarski S, Apfaltrer P, W. Nance JJ, Schneider D, Meyer M, Schoenberg SO et al. Optimization of keV-settings in abdominal and lower extremity dual-source dual-energy CT angiography determined with virtual monoenergetic imaging. *Eur J Radiol* 2013; 82(10):e574–81. doi: 10.1016/j.ejrad.2013.04.040. PMID: 23763858.
10. Vlahos I, Chung R, Nair A, Morgan R. Dual-Energy CT: vascular applications. *AJR Am J Roentgenol* 2012; 199(5 Suppl):S87–S97. doi: 10.2214/AJR.12.9114. PMID: 23097172.
11. Yu L, Leng S, McCollough CH. Dual-energy CT-based monochromatic imaging. *Am J Roentgenol* 2012; 199(5 Suppl):S9–S15. doi: 10.2214/AJR.12.9121. PMID: 23097173.

12. Coursey CA, Nelson RC, Boll DT, Paulson EK, Ho LM, Neville AM et al. Dual-energy multidetector CT: how does it work, what can it tell us, and when can we use it in abdominopelvic imaging? *Radiographics* 2010; 30(4):1037–55. PMID: 733983184; 20631367.
13. Raju R, Thompson AG, Lee K, Precious B, Yang T-H, Berger A et al. Reduced iodine load with CT coronary angiography using dual-energy imaging: a prospective randomized trial compared with standard coronary CT angiography. *J Cardiovasc Comput Tomogr* 2014; 8(4):282–8. doi: <http://dx.doi.org/10.1016/j.jcct.2014.06.003>. PMID: 25151920.
14. Zheng M, Liu Y, Wei M, Wu Y, Zhao H, Li J. Low concentration contrast medium for dual-source computed tomography coronary angiography by a combination of iterative reconstruction and low-tube-voltage technique: feasibility study. *Eur J Radiol* 2014; 83(2):e92-e9. doi: <http://dx.doi.org/10.1016/j.ejrad.2013.11.006>. PMID: 24332352.
15. Seehofnerová A, Kok M, Muhl C, Douwes D, Sailer A, Nijssen E et al. Feasibility of low contrast media volume in CT angiography of the aorta. *Eur J Radiol* 2015; 2(0):58–65. doi: <http://dx.doi.org/10.1016/j.ejro.2015.03.001>.
16. Nijhof WH, van der Vos CS, Anninga B, Jager GJ, Rutten MJ. Reduction of contrast medium volume in abdominal aorta CTA: multiphasic injection technique versus a test bolus volume. *Eur J Radiol* 2013; 82(9):1373–8. doi: <http://dx.doi.org/10.1016/j.ejrad.2013.03.027>. PMID: 23726126.
17. Baxa J, Vendis T, Molacek J, Stepankova L, Flohr T, Schmidt B et al. Low contrast volume run-off CT angiography with optimized scan time based on double-level test bolus technique—feasibility study. *Eur J Radiol* 2014; 83(3):e147–55. *Epub* 2014/01/02. doi: 10.1016/j.ejrad.2013.12.004. PMID: 24380637.
18. Delesalle MA, Pontana F, Duhamel A, Faivre JB, Flohr T, Tacelli N et al. Spectral optimization of chest CT angiography with reduced iodine load: experience in 80 patients evaluated with dual-source, dual-energy CT. *Radiology* 2013; 267(1):256–66. doi: 10.1148/radiol.12120195. PMID: 23319663.
19. Shen Y, Sun Z, Xu L, Li Y, Zhang N, Yan Z et al. High-pitch, low-voltage and low-iodine-concentration CT angiography of aorta: assessment of image quality and radiation dose with iterative reconstruction. *Plos One* 2015; 10(2): e0117469. doi: 10.1371/journal.pone.0117469. PMID: 25643353.
20. Wang H, Xu L, Zhang N, Fan Z, Zhang Z, Sun Z. Coronary computed tomographic angiography in coronary artery bypass grafts: comparison between low-concentration Iodixanol 270 and Iohexol 350. *J Comput Assist Tomogr* 2015; 39(1):112–118. doi: 10.1097/RCT.0000000000000162. PMID: 25299799.
21. Dong J, Wang X, Jiang X, Gao L, Li F, Qiu J et al. Low-contrast agent dose dual-energy CT monochromatic imaging in pulmonary angiography versus routine CT. *J Comput Assist Tomogr* 2013; 37(4):618–25. doi: 10.1097/RCT.0b013e31828f5020. PMID: 23863541.
22. Saltybaeva N, Jafari ME, Hupfer M, Kalender WA. Estimates of effective dose for CT scans of the lower extremities. *Radiology* 2014; 273(1):153–9. doi: 10.1148/radiol.14132903. PMID: 24937693.

23. Almutairi A, Sun Z, Al Safran Z, Poovathumkadavi A, Albader S, Ifdailat H. Optimal scanning protocols for dual-energy CT angiography in peripheral arterial stents: an in vitro phantom study. *Int J Mol Sci* 2015; 16(5):11531–49. Epub 2015/05/27. doi: 10.3390/ijms160511531. PMID: 26006234.
24. Pinho DF, Kulkarni NM, Krishnaraj A, Kalva SP, Sahani DV. Initial experience with single-source dual-energy CT abdominal angiography and comparison with single-energy CT angiography: image quality, enhancement, diagnosis and radiation dose. *Eur Radiol* 2013; 23(2):351–9. doi: 10.1007/s00330-012-2624-x. PMID: 22918562.
25. Carrascosa P, Capunay C, Rodriguez-Granillo G, Deviggiano A, Vallejos J, Leipsic J. Substantial iodine volume load reduction in CT angiography with dual-energy imaging: insights from a pilot randomized study. *Int J Cardiovasc Imaging* 2014; 30(8):1613–20. doi: 10.1007/s10554-014-0501-1. PMID: 25053514.
26. Yagi M, Ueguchi T, Koizumi M, Ogata T, Yamada S, Takahashi Y et al. Gemstone spectral imaging: determination of CT to ED conversion curves for radiotherapy treatment planning. *J Appl Clin Med Phys* 2013; 14(5):173–86. PMID: WOS:000324165000016.
27. Maturen KE, Kaza RK, Liu PS, Quint LE, Khalatbari SH, Platt JF. ‘Sweet Spot’ for endoleak detection: optimizing contrast to noise using low keV reconstructions from fast-switch kVp dual-energy CT. *J Comput Assist Tomogr* 2012; 36(1):83–7. doi: 10.1097/RCT.0b013e31824258cb. PMID: 22261775.
28. Meyer BC, Werncke T, Hopfenmuller W, Raatschen HJ, Wolf KJ, Albrecht T. Dual energy CT of peripheral arteries: effect of automatic bone and plaque removal on image quality and grading of stenoses. *Eur J Radiol* 2008; 68(3):414–22. doi: 10.1016/j.ejrad.2008.09.016. PMID: 18963674.
29. Mettler Jr FA, Huda W, Yoshizumi TT, Mahesh M. Effective dose in radiology and diagnostic nuclear medicine: a catalog. *Radiology* 2008; 248:254–263. doi: 10.1148/radiol.2481071451. PMID: 18566177.

Every reasonable effort has been made to acknowledge the owners of copyright material. I would be pleased to hear from any copyright owner who has been omitted or incorrectly acknowledged.

Chapter 6 Dual energy CT angiography in imaging peripheral arterial stents: An investigation of optimal scanning protocols with regard to image quality and radiation dose⁴

Contrast medium optimisation for peripheral arterial disease was discussed in Chapter 5. This chapter focuses on the DECTA protocol optimisation for peripheral arterial stents, addressing the final objective of our study which is to apply the devised scanning protocol in experimental and clinical settings. It compares DECTA with conventional CTA in patients with peripheral arterial stents.

6.1 Introduction

Arterial stenosis and occlusions of the lower extremities are frequently treated with either balloon angioplasty or stents. In-stent restenosis after peripheral artery angioplasty is considered one of the major problems of this procedure. Patency rates for iliac arteries stenosis in the follow-up range from 78% in the first-year to 61% after five years [1]. Digital subtraction angiography (DSA) is the standard follow-up procedure for peripheral arterial disease (PAD), but there are some drawbacks to this technique, including invasiveness and limited assessment of the vessel structures. Less invasive imaging techniques, such as multi-detector computed tomography (MDCT), are increasingly used in clinical practice to serve as an alternative to DSA [2].

MDCT has the advantages of shorter procedural time, fewer motion artefacts, and the provision of 3D visualisations [2]. Despite these benefits it has its deficiencies, such as the potential risk of contrast medium-induced nephrotoxicity, the presence of blooming artefacts

⁴ This is a version of an article currently being considered by The International Journal of Cardiovascular Imaging: Almutairi A, Sun Z, Al Safran Z, AlZaabi S. Dual energy CT angiography in imaging peripheral arterial stents: An investigation of optimal scanning protocols with regard to image quality and radiation dose.

caused by stent struts, and high radiation dose. Further, MDCT has difficulty in differentiating different materials related to peripheral arterial stents. As assessment of in-stent restenosis is closely related to the stent materials, this may lead to an overestimation of lesion severity. Blooming and beam hardening artefacts which are commonly seen in conventional CT angiography (CTA) hamper the accurate assessment of in-stent restenosis [3], but these artefacts can be eliminated in dual-energy CT (DECT) applications. Huang et al. reported an improvement of hardbeam correction with DECT [4]. In a recent study by Mangold et al, reduction of blooming artefacts in imaging peripheral stents with improved image quality was achieved when 70 or 80 keV was used [5]. Stent lumen visibility for small stents was reported in a phantom study at high keV when a third generation of dual-source and DECT was used [6]. For large stent evaluation such as those in peripheral arteries, DECT may improve stent visualisation and decrease blooming artefacts better than for small stents.

DECT is a recently developed technique that offers a diversity of applications for improving image visualisation and material differentiation, based on CT attenuation obtained from two tube voltages [2, 7, 8]. The bone removal algorithm of DECT plays an important role in confirming the diagnosis and evaluation of the disease's progress [7, 9, 10]. Image quality in general is improved with DECT due to the utilisation of low energies. Creation of different kilo-electron volts (keV) as monochromatic images may allow optimisation of image quality. To the best of our knowledge, only a few studies have been published on the role of DECT angiography (DECTA) in peripheral arterial stents [5, 6, 11,12], and evidence of optimal scanning protocols of DECTA in peripheral arterial stents as compared to conventional CTA is lacking.

The aim of this study is to determine the optimal scanning protocols of DECTA in terms of radiation dose and image quality assessment at different keV levels in comparison to conventional CTA, in patients treated with peripheral arteries stents. We hypothesise that higher keV levels can be used to produce acceptable image quality at a lower radiation dose.

6.2 Material and methods

6.2.1 Patient population and stent characteristics

Twenty-nine patients (27 males and 2 females, mean age, 57.88 ± 9.7 years, ranging from 38 to 77 years and with a mean body mass index (BMI) of 27.76 ± 7.14) were prospectively enrolled in this study between September 2014 and December 2015. All patients had been diagnosed with PAD and were treated with peripheral arterial stents; 93.1% of the patients

were also diagnosed with diabetes mellitus (DM). For comparison with conventional CTA, we retrospectively reviewed 24 patients (23 males and 1 female, mean age 58.04 ± 10.53 years, between 38 and 77 years of age and with a mean BMI of 27.38 ± 6.86) from the same population as the prospective study, but who had undergone conventional CTA for lower extremities prior to our data collection. Exclusion criteria for subjects included renal dysfunction or renal failure and contraindication to intravenous administration of the iodine contrast medium. The study was approved by the Curtin Human Research Ethics (HR 167/2013) and King Fahad Specialist Hospital (KFSH-D) Committees (IRB-RAD029-FB). Informed consent was obtained from all participants.

Stent manufacturer and stent details were available for 86% (48/56) of the stents. The mean stent diameter was 6.9 ± 1.3 mm (ranging from 4.0 to 9.0 mm), and the mean length was 54.0 ± 29.6 mm (ranging from 9.0 to 150.0 mm). Five different stent types were used in this group of patients: ev3 Protégé Everflex self-expandable-*nitinol* (ev3 Endovascular Inc, Plymouth, MN) n=10; Abbott Omnilink (balloon mounted) *cobalt chromium* n=4; Cordis Genesis Balloon mounted *nitinol* (Cordis, Miami, FL) n=19; Cordis SMART self-expandable *stainless steel* (Cordis, Miami, FL) n=8, and Boston Scientific Wall Stent self-expandable *cobalt-based alloy* (Boston Scientific Corp., Natick, MA) n=7. Thirty-five (62.5%) stents were located in the common iliac artery (CIA), six (10.7%) in the external iliac artery (EIA), and 15 (26.8%) in the superficial femoral artery (SFA).

6.2.2 DECT scanning protocol

All CT procedures were performed in the DE mode with a fast kilovoltage-switching 64-slice CT scanner (Discovery CT HD 750; Gemstone Spectral Imaging, GE Healthcare, Milwaukee, WI) at KFSH-D. Details of the DECTA protocol have been described in Chapter 5, and were recently published [13]. Four sets of virtual monochromatic spectral images (VMS) at 65, 68, 70 and 72 keV were reconstructed with adaptive statistical iterative reconstruction (ASIR) at 50%.

Intravenous non-ionic iodinated contrast agent (1.5 ml/kg, 350 mgI/ml Xenetix, Guerbet, Sulzbach, Germany), was administered at flow rate of 4–5 ml/s followed by 40 ml of a saline chaser at the same flow of contrast, using a power injector (Envision CT injector, Medrad) through a minimum of 20G catheter in the cubital vein. A region of interest (ROI) was placed within the aorta close to the celiac trunk level with a threshold of 150 HU and CT acquisition was automatically initiated after five seconds.

6.2.3 Conventional CTA scanning protocol

CT examinations were accomplished on two type of scanner: a Discovery CT HD 750, GE Healthcare, Milwaukee, WI), and a 64-slice CT scanner (Brilliance 64, Philips Medical Systems, Cleveland, Ohio) KFSH-D, with the following protocols: section thickness: 1.0 mm, pitch values: 0.516 and 0.89; reconstruction interval: 50% overlap of the section thickness. Tube voltage was 120 kVp, with auto mAs and current modulation for all scans.

6.2.4 Image reconstruction and image quality assessment

The images were transferred to a 3D workstation (Gemstone Spectral Imaging Viewer, GE) for analysis. Post-processing reconstructions in multiple formats were obtained for all patients, including axial CT images, multiplanar reconstruction (MPR) and curved multiplanar reformation (CPR). Images were demonstrated with a window level and window width of 200/1200 HU to improve visualisation of the stent.

If the stent lumen appeared darker than the contrast-enhanced vessel lumen proximal to the stent, then the stent was considered to be occluded. Homogeneous enhancement inside the stent lumen or the absence of in-stent restenosis if it was similar to the reference vessel was considered to be normal stent patency.

According to the image quality in terms of stent lumen visibility, each stent was classified as patent or non-patent. The stent was considered patent when the lumen was noticeable and the contrast density of the lumen could be assessed without the effect of partial volume effects, metal artefacts caused by the stents and calcification in the arterial wall. Each peripheral artery was sub-divided into three zones based on the existing stent, including CIA, EIA and SFA locations, to allow appropriate analysis.

6.2.4.1 Qualitative assessment

Qualitative evaluations were performed independently by two experienced radiologists with 21 and 15 years in cardiovascular CT imaging, on a workstation with dedicated software (Gemstone Spectral Imaging Viewer, GE). Each reader evaluated the different VMS image groups of each individual patient randomly. Because different VMS values could easily be detected by visual inspection of the images, it was considered unnecessary to blind the readers.

The image quality of the different VMS series was evaluated in three parts; the assessments were subjective and based on a 3-point scale as follows: 1 non diagnostic; 2 moderate but sufficient for diagnosis; 3 excellent. Image noise within the stent was also evaluated on a 3-point scale: 1 – poor; 2 – adequate; 3 – good. Stent patency or lumen visualisation, was evaluated on a 4-point scale: 1 – stenosis or occlusion; 2 – $\geq 50\%$ or less lumen is opacified; 3 – 50–74% lumen is visualised or opacified; 4 – $\geq 75\%$ excellent opacification or visualisation. A score of 2 or above in all three assessments was considered clinically diagnostic.

6.2.4.2 Quantitative assessment

CT attenuation values were performed at a workstation by a reader with 15 years of experience in CT. A circular region of interest (ROI) was placed over the enhanced area of the stent on axial images. Measurement of image noise (the standard deviation of the CT number in Hounsfield units) was attained for each peripheral arterial stent by placing a defined ROI on all VMS series. The area of the ROI on all VMS series and conventional CTA based on the stent size was marked as large as possible in the vessel lumen. When calcification was noticed the ROI was placed in a different region to avoid the artefact. Additional CT attenuation values were measured at the level of the artery proximal to the stent, and other CT attenuation values for the background image noise were taken at the muscle closest to the stent.

Mean CT attenuation and image noise were computed for individual stents by averaging the values for each stent location resulting from both sides of the arteries. The signal-to-noise ratio (SNR) was calculated as a mean CT value of ROI divided by the mean image noise (SD), while the contrast-to-noise ratio (CNR) was calculated as a mean CT value of stent minus the CT value of background muscle divided by the mean image noise (SD) of a stent, which is:

$$\text{CNR} = (\text{Mean CT value}_{\text{stent}} - \text{Mean CT value}_{\text{muscle}}) / \text{SD}_{\text{stent}}. \quad (5)$$

6.2.5 Radiation dose estimation

The volume CT dose index (CTD_{vol}) and dose length product (DLP) were recorded from the CT console for each subject. The multiplication product of DLP and a conversion factor (k) where $\{k = 0.0056 \text{ mSv} / (\text{mGy} \times \text{cm})\}$ is the conversion coefficient which used for both DECTA and conventional CTA lower extremities examinations, to estimate the effective dose [14], and the effective doses were compared between the two protocols.

6.2.6 Statistical analysis

A commercial software SPSS version 22.0 (SPSS Inc., Chicago, IL) was used in this study.

A P value of <0.05 was considered to indicate a statistically significant difference.

Quantitative variables were considered as mean \pm standard deviation. Categorical variables were presented as counts and percentages.

Statistical analyses were undertaken at two levels, as follows:

- (1) Patients were regarded as ‘blocks’ in a randomised block analysis of variance, with five imaging processes (four DECT, one conventional CT) as ‘treatments’. Duncan’s Multiple Range Test was employed to aid interpretation in those analyses exhibiting statistically significant treatment effects.
- (2) The effects of observed patient attributes (e.g., sex, BMI, stent type) on expressions of image quality were assessed via analysis of variance/covariance (the General Linear Model procedure in SPSS). Image quality for a given measure was taken as the arithmetic average of the corresponding four values within each patient from the DECT processes. Conventional CT values were excluded. Because of severe skewness in the observed frequencies of categorical attributes (e.g., 27 males, 2 females; 25 hypertensives, 4 non-hypertensives) a forward stepping search procedure was adopted, starting with each variable (whether factor or covariate) fitted alone. The variable yielding the most significant single contribution to the model was then fitted. Each of the remaining variables in the candidate pool were then also fitted, one at a time, to that model, then removed, and the variable yielding the most significant single contribution from among those was then fitted, along with the first variable so identified. This process continued, provided each term fitted made a significant improvement to the current model. As and when any two factors were fitted, then a term representing the interaction effects between them became eligible, and was added to the pool of candidate terms. The same protocol was employed as and when any factor and any covariate were fitted.

A repeated measures analysis of variance, combining patient attributes (between-subjects level) and VMS profiles (within-subjects level) into a single analysis was considered, but frequency imbalances and variance/covariance heterogeneity issues rendered this inappropriate.

Interobserver variability was assessed with Cohen’s Kappa Statistic to measure the degree of ‘more-than-chance’ agreement between the two readers for various parameters, and interpreted as follows: ($k= 0.01–0.20$, slight; $0.21–0.40$, fair; $0.41–0.60$, moderate; $0.61–0.80$, good; $0.81–1.0$, excellent agreement).

6.3 Results

All procedures were successfully completed in all subjects without the incidence of any complications, and all examinations were of diagnostic image quality at good to excellent stent visibility. A total of 56 stents (one to three stents per patient) were evaluated. Patient characteristics are shown in Table 6.1.

Table 6.1. Patient characteristics of the study groups

Patient characteristics	Dual-energy CTA (n = 29)	
	Conventional CTA (n = 24)	
Male: Female	27:2	23:1
Age (yrs)	57.88 ± 9.71	58.04 ± 10.53
Height (cm)	166.45 ± 8.06	166.46 ± 7.68
Weight (kg)	75.33 ± 16.59	74.23 ± 16.38
BMI (kg/m ²)	27.76 ± 7.14	27.38 ± 6.86
Radiation dose		
DLP) (mGy·cm)	1246.93 ± 44.12	1318.45 ± 450.31
Effective dose (mSv)	6.98 ± 0.24	7.63 ± 2.48

*Conversion factor for peripheral DECTA conventional CTA = 0.0056 mSv/mGy*cm

CTA = Computed tomography angiography, BMI = body mass index; DLP = dose length product

For quantitative analysis between subjects based on personal attributes associated with variations in DECT image quality, we found the average CNR varied significantly with BMI ($P=0.027$): a unit increase in BMI was associated with a decrease of 0.843 units of CNR, while average SNR appeared not to vary significantly with any of the available factors or covariates. The average CT value varied significantly with BMI ($P=0.043$): a unit increase in

BMI was associated with a decrease of 5.747 HUs. Average image noise varied significantly with type of stent ($P=0.025$). CT attenuation of all VMS was found to vary significantly with DM ($P = 0.037$) and with BMI ($P = 0.010$). On average, diabetic patients exhibited 190.056 HU more than non-diabetic patients, once controlled for BMI. Controlling for DM, each additional unit of BMI was associated with a reduction of 7.158 HU. The model accounted for 41% of total variation. Image noise was found to vary significantly with DM ($P = 0.018$). On average, patients with diabetes exhibited 18.66 noise units fewer than non-diabetic patients. The model accounted for 29% of the total variation. The small number of observations for DECT and conventional CTA at CIA (19, 14), EIA (3, 2) and SFA (7, 6) combined with considerable clustering of cases in the binary categories of factors (gender, BMI, and DM) rendered almost all factor interaction effects untestable, as shown in Table 6.2.

6.3.1 Image quality assessment

Image quality was assessed by taking the overall mean CT value and mean image noise for all stent zones. The image quality of 22 (39.3%) stents was good of a further 27 (48.2%) stents was moderate; the stent lumen was occluded in the remaining 7 (12%) stents. The reason for the interpretability of the images of these seven was the stent occlusion.

Regarding quantitative image quality, DECTA images had less noise than CTA images, for CIA stents with high significance ($P<0.001$) and EIA stents with significance ($P = 0.044$). There were no significant differences for image noise of SFA stents between DECTA and CTA, but DECTA had greater CNR than the CTA images for both CIA and EIA stents, and very highly significant differences from the VMS images ($P<0.001$,) and ($P = 0.005$) respectively. Post hoc analyses using Duncan's Multiple Range Test indicated that the mean CNR for the four VMS and conventional CTA was significantly different from the other four CNR means; although the test did not detect significant differences between the CNR means of the all VMS sets, it was very close ($P = 0.053$). For SNR there was no evidence of difference between the VMS and conventional CTA for CIA and SFA stents, but SNR was found highly significant ($F(2, 7) = 46.81, P=0.006$) for EIA stents. The main effect of CT attenuation on CIA stents was found to be a very highly significant difference between VMS on both CIA and SFA stents ($F(18, 67) = 16.22, P<0.001$), and ($F(4, 23) = 4.80, P=0.006$) respectively. Details of ANOVA results for quantitative image quality are shown in Table 6.3, Fig. 6.1(A-D) and Fig. 6.2 (A-F), with an image example in Fig. 6.3 (A-D).

Reduction in CT values at all stent zones was associated with an increase in keV, with a reduction of 18 to 21% between 65 keV and 72 keV for all stent zones. Image noise was found to be highest at 65 keV and a very minimal change between 70 and 72 keV, as shown in Table 6.3.

Table 6.2. Quantitative assessment of image quality based on stents location

Stent location	DECTA protocols	CT attenuation	Image noise	SNR	CNR	
1 CIA	DECTA (19)	65	462.20 ± 101.62	42.10 ± 17.72	12.88 ± 8.53	20.44 ± 16.80
		68	420.50 ± 90.43	38.45 ± 16.17	12.93 ± 9.11	19.37 ± 13.40
		70	397.50 ± 87.52	38.51 ± 15.47	11.65 ± 7.62	17.65 ± 10.67
		72	374.50 ± 82.84	38.59 ± 15.54	10.93 ± 7.35	15.72 ± 8.81
	Conventional CTA (14)		428.70 ± 92.17	48.46 ± 23.70	11.11 ± 5.60	9.62 ± 4.92
2 EIA	DECTA (3)	65	562.70 ± 36.50	32.78 ± 13.20	18.40 ± 8.49	20.20 ± 2.14
		68	508.80 ± 33.10	31.52 ± 13.27	17.42 ± 8.28	19.61 ± 3.33
		70	476.40 ± 31.20	31.34 ± 13.59	16.47 ± 8.01	18.38 ± 4.03
		72	446.20 ± 29.42	31.53 ± 14.04	15.33 ± 7.49	16.82 ± 4.55
	Conventional CTA (2)		637.00 ± 447.72	61.52 ± 39.67	10.12 ± 0.75	8.93 ± 1.43
3 SFA	DECTA (7)	65	320.80 ± 199.60	48.19 ± 23.42	8.83 ± 9.65	18.87 ± 19.06
		68	288.90 ± 181.78	45.25 ± 21.04	8.46 ± 9.44	17.63 ± 17.81
		70	269.70 ± 171.10	43.95 ± 19.55	8.04 ± 9.05	16.14 ± 16.23
		72	251.70 ± 161.14	42.97 ± 18.26	8.90 ± 8.88	14.57 ± 14.88
	Conventional CTA (6)		427.10 ± 147.84	63.69 ± 17.84	7.52 ± 3.78	6.42 ± 3.58

CT = number in Hounsfield units, SNR = Signal-to-noise ratio in the stented area, CNR = Contrast-to-noise ratio, Image process = comparison between 4 keVs and conventional CTA. CIA- = common iliac artery, EIA- = external iliac artery, SFA = superficial femoral artery.

Table 6.3.Results of ANOVA

Source	CT value			Image noise		SNR		CNR	
	df	F	p-value	F	p-value	F	p-value	F	p-value
CIA (19)	(18,67)	9.963	0.001	19.22	0.001	12.25	0.001	11.928	0.001
Image process (5)	(4,67)	6.966	0.001	6.066	0.001	1.274	0.289	7.445	0.001
EIA (3)	(2,7)	0.984	0.420	8.467	0.014	46.81	0.001	7.089	0.021
Image process (5)	(4,7)	0.486	0.747	4.341	0.044	9.707	0.006	9.900	0.005
SFA(7)	(6,23)	11.93	0.001	9.383	0.001	37.52	0.001	66.00	0.001
Image process (5)	(4,23)	4.804	0.006	1.804	0.162	0.795	0.541	2.556	0.066

Df = degrees of freedom, CT value = CT number in Hounsfield units, SNR = Signal-to-noise ratio in the stented area, CNR = Contrast-to-noise ratio, F = value of test statistic of F-test for corresponding effect; P = corresponding p-value, Image process = comparison between 4 keVs and conventional CT, CIA = common iliac artery, EIA = external iliac artery, SFA = superficial femoral artery.

With regard to image quality based on stent type, CNR was obviously higher for all VMS than conventional CTA for all stents, while image noise was found to be low for all VMS compared with conventional CTA. The Omnilink stents achieved the highest CNR and the Wallstent stents recorded the lowest image noise. Cordis SMART stents received the lowest CT attenuation for all VMS while conventional CTA achieved high CT attenuation, as presented in Table 6.4.

A total of 116 keV images of the stents were evaluated with 564 measurements in our study. The mean scores of protocol assessment for all VMS stes were 2.69 ± 0.46 , 2.69 ± 0.46 , 2.45 ± 0.46 , 2.46 ± 0.49 , respectively, and for stent patency assessment the scores of all VMS stes were 1.96 ± 0.49 , 2.22 ± 0.56 , 2.63 ± 0.48 and 2.81 ± 0.40 respectively. The scores of stent lumen assessment were, 3.00 ± 0.76 , 3.17 ± 0.77 , 3.36 ± 0.81 and 3.50 ± 0.78 , respectively. Both readers ranked the 72 keV results as excellent. Inter-reader agreement was good on protocol assessment ($k = 0.71$), good on stent patency assessment ($k = 0.78$), and excellent on stent lumen assessment ($k = 0.82$). Overall, the qualitative assessments of image quality showed that all images were satisfactory for clinical use.

Table 6.4. Quantitative assessment of image quality based on stent type

Stent type	keV	CNR	SNR	CT attenuation	Image Noise
Missing stent details (8)	65	12.13 ± 9.12	6.26 ± 6.50	272.42 ± 212.08	33.33 ± 25.85
	68	11.37 ± 8.43	6.37 ± 6.94	248.58 ± 195.50	30.90 ± 24.48
	70	10.44 ± 7.59	6.15 ± 6.78	232.70 ± 183.85	29.90 ± 23.71
	72	9.39 ± 6.74	5.79 ± 6.38	217.84 ± 172.95	29.27 ± 23.08
Conventional CTA (6)		10.38 ± 2.70	12.00 ± 3.15	472.76 ± 29.69	42.96 ± 15.41
ev3 Protégé Everflex (self-expandable) (10)	65	14.06 ± 7.01	8.68 ± 8.22	395.17 ± 168.70	44.92 ± 23.87
	68	14.14 ± 6.63	8.22 ± 4.65	359.52 ± 154.19	43.33 ± 23.46
	70	13.21 ± 6.10	7.69 ± 4.30	337.98 ± 145.46	43.01 ± 23.35
	72	12.13 ± 5.53	7.09 ± 3.88	317.87 ± 137.36	43.29 ± 43.64
Conventional CTA (5)		7.54 ± 5.34	9.31 ± 6.05	383.13 ± 68.87	52.13 ± 18.19
Abbott Omnilink (balloon Mounted) (4)	65	21.12 ± 4.67	18.72 ± 7.38	527.08 ± 80.65	33.32 ± 11.17
	68	21.04 ± 4.09	16.87 ± 7.13	481.79 ± 65.63	32.34 ± 10.94
	70	20.21 ± 3.78	15.57 ± 6.78	454.42 ± 56.66	31.53 ± 10.73
	72	18.95 ± 3.71	14.25 ± 6.24	428.84 ± 48.29	30.75 ± 10.21
Conventional CTA(3)		7.17 ± 1.10	8.56 ± 1.50	377.60 ± 84.49	47.42 ± 20.62
Cordis Genesis (Balloon mounted) (19)	65	20.25 ± 17.91	14.13 ± 9.53	463.74 ± 150.95	33.61 ± 14.66
	68	19.87 ± 14.39	13.70 ± 7.92	421.43 ± 136.53	32.32 ± 13.17
	70	17.83 ± 11.91	12.79 ± 7.07	396.12 ± 128.06	31.95 ± 12.70

Stent type	keV	CNR	SNR	CT attenuation	Image Noise
	72	15.78 ± 10.21	12.90 ± 9.64	373.43 ± 120.84	31.70 ± 13.28
Conventional CTA (17)		10.73 ± 4.12	12.23 ± 4.62	481.51 ± 133.57	46.52 ± 23.68
Cordis SMART (self-expandable) (8)	65	9.99 ± 13.78	6.29 ± 9.91	244.65 ± 226.47	42.32 ± 36.80
	68	8.64 ± 10.32	6.85 ± 10.90	222.82 ± 207.30	37.65 ± 33.98
	70	8.21 ± 9.99	6.55 ± 10.32	208.93 ± 194.51	36.50 ± 33.04
	72	7.39 ± 9.15	6.10 ± 9.57	195.94 ± 182.66	35.80 ± 32.14
Conventional CTA (4)		7.35 ± 3.70	8.38 ± 3.91	418.14 ± 154.87	57.91 ± 20.41
Boston Scientific Wallstent (self-expandable) (7)	65	19.68 ± 19.31	12.87 ± 12.92	409.63 ± 267.01	34.12 ± 21.86
	68	18.70 ± 17.91	13.20 ± 12.98	375.90 ± 246.53	30.76 ± 19.54
	70	17.15 ± 16.19	12.92 ± 12.96	355.52 ± 234.33	30.58 ± 19.73
	72	15.50 ± 14.75	12.59 ± 12.74	336.57 ± 223.10	30.56 ± 20.23
Conventional CTA (4)		4.60 ± 1.79	5.45 ± 1.95	336.94 ± 107.18	50.02 ± 21.70

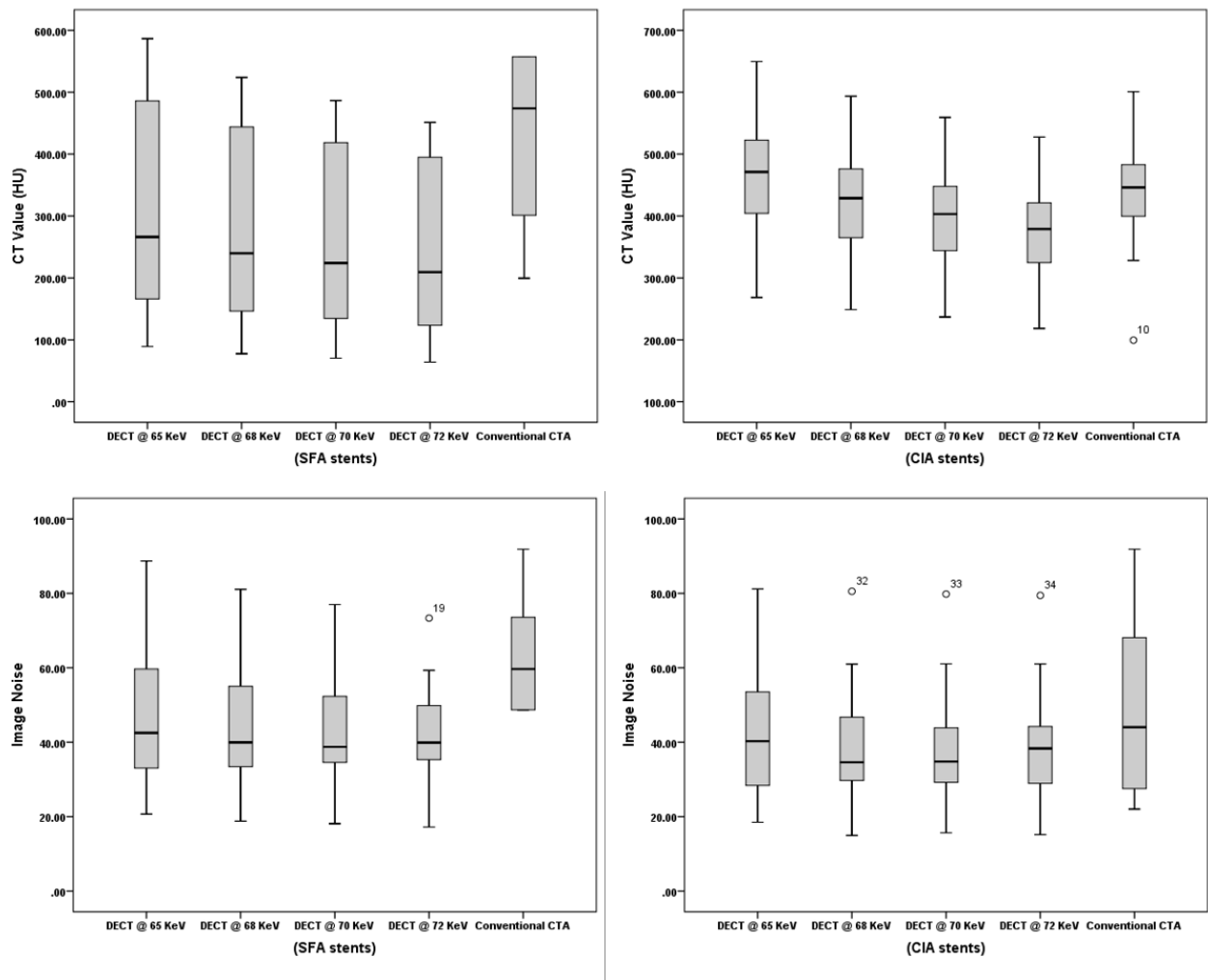


Figure 6.1. Box-and-whisker plots of image quality.

A-D: Comparison between the 4 VMS and conventional CTA of CT attenuation value (HU) and image noise in measured in CIA and SFA stents. Box-and-whisker plots (O, outliers) show difference of image quality in different stent locations.

VMS- virtual monochromatic spectral, CTA-CT angiography, CIA-common iliac artery, SFA-superficial femoral artery

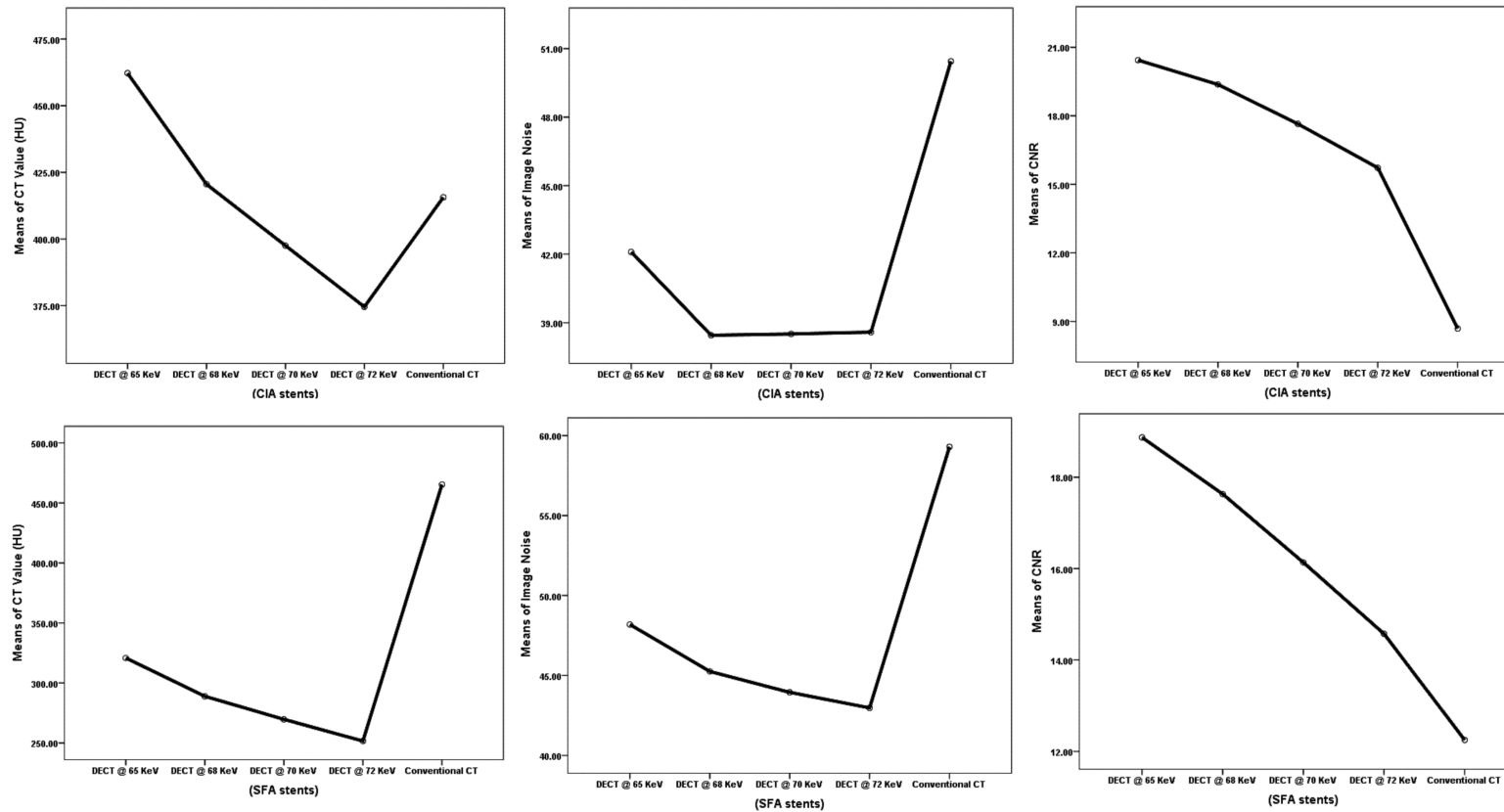


Figure 6.2.A line graph of comparison between the 4 VMS and conventional CTA for stents at CIA and SFA. A and D: CT attenuation (HU) shows the highest CT value at the lower keV; B and E: image noise demonstrates that the lowest image noise was found at 72 keV protocol and the highest image noise at the conventional CTA, followed by 65 keV protocol, and C and F contrast-to-noise ratio (CNR) of CIA shows that CNR decreased with increase in VMS; all the VMS were found to be better than conventional CTA.

VMS = virtual monochromatic spectral, CTA =CT angiography, CIA =common iliac artery.

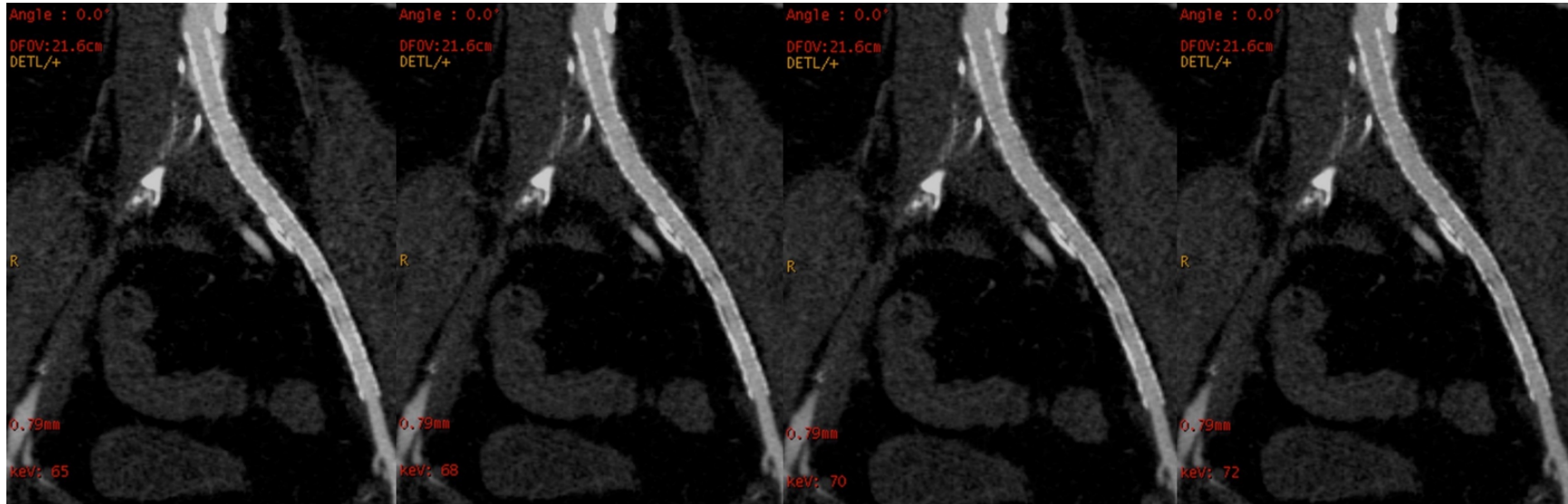


Figure 6.3.Example of mage quality of multiplanar reformatted images at different VMS of CIA stents at (a) 65 keV (b) 68 keV (c) 70 keV and (d) 72keV. The protocol of 72 keV shows the optimal image quality.

VMS = virtual monoenergetic spectral; CIA = common iliac artery.

6.3.2 Radiation dose

On the basis of our protocols, DLP and effective radiation dose for lower extremities CTA acquisition in DECT (1246.93 ± 64.33 mGy*cm, and 6.98 ± 0.36 mSv, respectively) with fixed CTDI_{vol} of 9.05 mGy, were significantly lower compared than those in conventional CTA the CTDI_{vol}, DLP and the effective radiation dose (1318.45 ± 450.31 mGy*cm and 7.36 ± 2.48 mSv) ($P < 0.0001$), although this has slightly significant difference ($P= 0.047$).

6.4 Discussion

In this stud, 56 peripheral arterial stents were evaluated using 64-section single source DECT, and 49 (88%) of these images were interpretable. Image quality of peripheral arterial stents using DECT can be useful with optimised keV. This implies that a perfect visualisation of the stent lumen may not always be seen in a single keV level only, and might vary depending on the stent characteristics.

For technically adequate angiographic imaging, a CT attenuation of 250HU was generally used for vascular assessment. The results of this study demonstrate that a DECTA protocol of 70–72 keV with 50% ASIR and a minimum average CT attenuation of 251.70 HU results in diagnosable images that can distinguish between stent material and contrast, with optimal CT attenuation and low image noise in comparison with other VMS levels, and with high CNR compared to conventional CTA.

The outcome of this study is consistent with findings in a phantom study Chapter 4, which demonstrated the acquisition of optimal image quality of VMS was achieved between 65 and 70 keV [11]. Throughout the VMS, an increase in keV was associated with a decrease in mean all-stent attenuations. Higher in-stent attenuation probably results from beam-hardening artefacts affected by the reconstruction algorithm [15]. With DECT, blooming artefacts in stents depend on the keV level, as higher keV is associated with lower blooming; however, the higher keV level leads to a significant reduction of CT attenuation, which may affect the diagnosis of in-stent stenosis evaluation. In the present study, the use of 70–72 keV in the differentiation between stent materials, contrast medium and neointimal hyperplasia in a run-off DECTA gave better results than the other two keV evaluated.

Only a few studies have used DECT and monochromatic imaging in the evaluation of peripheral arterial stents, and most of these evaluate the imaging of coronary stents [16–18]. Their results studies vary in the identification of the optimal keV, ranging from as low as 55 keV to >80 keV. However, a recent study found 70 and 80 keV achieved optimal image

quality with use of DECTA in 31 patients with 45 stents. Increasing keV to over 80 (90–150 keV) did not show any improvement in either image quality or diagnostic confidence [5]. Studies that have evaluated lower extremities with DECT have found that optimal image quality falls between 55 to 70 keV [13, 19, 20].

In this study, the DECTA protocol of 72 keV was considered optimal for evaluating peripheral arterial stents as it returned the lowest image noise as well as good differentiation between the contrast medium within the stents and the neointima within the stents. In addition, the subjective judgement of image quality by both readers indicates that the 72 keV was the protocol achieving the best image quality. For the objective evaluation in CIA, EIA and SFA stents lower image noise was found with 70 keV, but the type of stent was a significant factor: the Boston Scientific Wallstent, Cordis Genesis and Abbott Omnilink had the lowest image noise and highest SNR and CNR in comparison with conventional CTA and other VMS values. This study's findings therefore support the use of higher keV in DECTA of peripheral arterial stents.

Radiation dose was significantly lower with DECT, with a mean DLP of 1276.53 mGy*cm compared with 1318.45 mGy*cm for conventional CTA. The conversion coefficient used for calculation of the most effective dose for CTA of lower extremities followed most recent approaches, and seemed to result in smaller quantities than are used in literature. As stated, this new conversion coefficient is provided for lower extremities allowing for estimation of effective dose for clinical CTA was lower than reported in the literature as it was used high conversion coefficient factor.

Our study has several potential limitations. The main limitation is the small number of participated subjects; this was unavoidable as our primary aim was to exploit a homogenous group in terms of implanted stent type and size. Moreover, as subjects could only be recruited from a single centre, a limited number were available for the study. There is also extreme imbalance, in the personal attributes of the subject factors; for example, of the 19 subjects with first stents in the CIA zone only one was female and 18 were males; and 2 non diabetics and 17 diabetics in the DM factor. Further, a very limited number of stent types was evaluated in this study. A further concern is that we were not able to assess the treatment outcome, because we did not perform any DSA procedures, and no direct comparison could be drawn between DECTA and DSA.

6.5 Conclusion

This prospective clinical study of DECTA in imaging peripheral arterial stents was carried out by comparing VMS with conventional CTA. The outcomes demonstrate that the image quality of VMS achieved with DECTA is clinically acceptable. Results of this study indicate that the image quality of DECTA in peripheral arterial stents is achieved at 70 keV and 50% ASIR, is higher compared with other VMS and conventional CTA. This protocol is considered optimal to achieve lower image noise with adequate clinically diagnostic images. Further studies based on a large population group are warranted.

6.7 References

1. Kalmar PI, Portugaller RH, Schedlbauer P, Bohlsen D, Deutschmann HA. Placement of hemoparin-coated stents in the iliac arteries: early experience and midterm results in 28 patients. *Eur J Radiol* 2014; 83(7):1205–1208. doi:10.1016/j.ejrad.2014.04.006
2. Brockmann C, Jochum S, Sadick M, Huck K, Ziegler P, Fink C et al. Dual-energy CT angiography in peripheral arterial occlusive disease. *Cardiovasc Intervent Radiol* 2009; 32(4):630–637. doi:10.1007/s00270-008-9491-5
3. Maintz D, Burg MC, Seifarth H, Bunck AC, Ozgun M, Fischbach R, Jurgens KU, Heindel W. Update on multidetector coronary CT angiography of coronary stents: in vitro evaluation of 29 different stent types with dual-source CT. *Eur Radiol* 2009; 19(1):42–49. doi:10.1007/s00330-008-1132-5
4. Huang SY, Nelson RC, Miller MJ, Kim CY, Lawson JH, Husarik DB, Boll DT. Assessment of vascular contrast and depiction of stenoses in abdominopelvic and lower extremity vasculature: comparison of dual-energy MDCT with digital subtraction angiography. *Acad Radiol* 2012; 19(9):1149–1157. doi:10.1016/j.acra.2012.04.014
5. Mangold S, De Cecco CN, Schoepf UJ, Yamada RT, Varga-Szemes A, Stubenrauch AC, Caruso D, Fuller SR, Vogl TJ, Nikolaou K, Todoran TM, Wichmann JL. A noise-optimized virtual monochromatic reconstruction algorithm improves stent visualization and diagnostic accuracy for detection of in-stent re-stenosis in lower extremity run-off CT angiography. *Eur Radiol* 2016; doi:10.1007/s00330-016-4304-8
6. Mangold S, Cannaó PM, Schoepf UJ, Wichmann JL, Canstein C, Fuller SR, Muscogiuri G, Varga-Szemes A, Nikolaou K, De Cecco CN. Impact of an advanced image-based monoenergetic reconstruction algorithm on coronary stent visualization using third generation dual-source dual-energy CT: a phantom study. *Eur Radiol* (Epub ahead of print) 2015 doi:10.1007/s00330-015-3997-4
7. Kau T, Eicher W, Reiterer C, Niedermayer M, Rabitsch E, Senft B, Hausegger KA. Dual-energy CT angiography in peripheral arterial occlusive disease-accuracy of maximum intensity projections in clinical routine and subgroup analysis. *Eur Radiol* 2011; 21(8):1677–1686. doi:10.1007/s00330-011-2099-1
8. Ho LM, Yoshizumi TT, Hurwitz LM, Nelson RC, Marin D, Toncheva G, Schindera ST. Dual energy versus single energy MDCT: measurement of radiation dose using adult abdominal imaging protocols. *Acad Radiol* 2009; 16(11):1400–1407. doi:10.1016/j.acra.2009.05.002
9. Yamamoto S, McWilliams J, Arellano C, Marfori W, Cheng W, McNamara T, Quinones-Baldrich WJ, Ruehm SG. Dual-energy CT angiography of pelvic and lower extremity arteries: dual-energy bone subtraction versus manual bone subtraction. *Clin Radiol* 2009; 64(11):1088–1096. doi:10.1016/j.crad.2009.07.009
10. Meyer BC, Werncke T, Hopfenmuller W, Raatschen HJ, Wolf KJ, Albrecht T. Dual energy CT of peripheral arteries: effect of automatic bone and plaque removal on

- image quality and grading of stenoses. *Eur J Radiol* 2008; 68(3):414–422. doi:10.1016/j.ejrad.2008.09.016
11. Almutairi A, Sun Z, Al Safran Z, Poovathumkadavi A, Albader S, Ifdailat H. Optimal scanning protocols for dual-energy ct angiography in peripheral arterial stents: an in vitro phantom study. *Int J Mol Sci* 2015; 16(5):11531-11549. doi:10.3390/ijms160511531
 12. Kohler M, Burg MC, Bunck AC, Heindel W, Seifarth H, Maintz D. Dual-Source CT Angiography of peripheral arterial stents: in vitro evaluation of 22 different stent types. *Radiol Res Pract* 2011:103873. doi:10.1155/2011/103873
 13. Almutairi A, Sun Z, Poovathumkadavi A, Assar T. Dual Energy CT Angiography of peripheral arterial disease: feasibility of using lower contrast medium volume. *PLoS One* 2015; 10(9):e0139275. doi:10.1371/journal.pone.0139275
 14. Saltybaeva N, Jafari ME, Hupfer M, Kalender WA. Estimates of effective dose for CT scans of the lower extremities. *Radiology* 2014; 273(1):153–159. doi:10.1148/radiol.14132903
 15. Lenhart M, Volk M, Manke C, Nitz WR, Strotzer M, Feuerbach S, Link J. Stent appearance at contrast-enhanced MR Angiography: in vitro examination with 14 stents. *Radiology* 2000; 217(1):173–178
 16. Ebersberger U, Tricarico F, Schoepf UJ, Blanke P, Spears JR, Rowe GW, Halligan WT, Henzler T, Bamberg F, Leber AW, Hoffmann E, Apfaltrer P. CT evaluation of coronary artery stents with iterative image reconstruction: improvements in image quality and potential for radiation dose reduction. *Eur Radiol* 2013; 23(1):125–132. doi:10.1007/s00330-012-2580-5
 17. Stehli J, Fuchs TA, Singer A, Bull S, Clerc OF, Possner M, Gaemperli O, Buechel RR, Kaufmann PA. First experience with single-source, dual-energy CCTA for monochromatic stent imaging. *Eur Heart J Cardiovasc Imaging* 2015; 16(5):507–512. doi:10.1093/ehjci/jeu282
 18. Fuchs TA, Stehli J, Fiechter M, Dougoud S, Gebhard C, Ghadri JR, Husmann L, Gaemperli O, Kaufmann PA. First experience with monochromatic coronary computed tomography angiography from a 64-slice CT scanner with Gemstone Spectral Imaging (GSI). *J Cardiovasc Comput Tomogr* 2013; 7(1):25–31. doi:10.1016/j.jcct.2013.01.004
 19. Pinho DF, Kulkarni NM, Krishnaraj A, Kalva SP, Sahani DV. Initial experience with single-source dual-energy CT abdominal angiography and comparison with single-energy CT angiography: image quality, enhancement, diagnosis and radiation dose. *Eur Radiol* 2013; 23(2):351–359. doi:10.1007/s00330-012-2624-x
 20. Sudarski S, Apfaltrer P, Nance JW, Jr., Schneider D, Meyer M, Schoenberg SO, Fink C, Henzler T. Optimization of keV-settings in abdominal and lower extremity dual-source dual-energy CT angiography determined with virtual monoenergetic imaging. *Eur J Radiol* 2013; 82(10):e574–581. doi:10.1016/j.ejrad.2013.04.040

Every reasonable effort has been made to acknowledge the owners of copyright material. I would be pleased to hear from any copyright owner who has been omitted or incorrectly acknowledged.

Chapter 7 Conclusion and future directions

7.1 Conclusion

This chapter summarises the key outcomes in relation to the main aim and objectives of this study (as outlined in Chapter 1). Since the thesis is relevant to DECTA protocol optimisation for peripheral arterial stents, it is important to highlight the main aim of this study, which is to optimise the scanning protocol for DECTA in peripheral artery stenting to improve the image quality and to reduce the radiation dose level. Four specific objectives were proposed to address this aim: first, to pinpoint factors (machine related) that influence the image quality (including visualisation of stent lumen) and the radiation dose; second, to improve the scanning protocol in accordance with the identified factors; third, to inspect the quality of images that are generated using the advised imaging protocol; and fourth, to implement the new scanning protocol in experimental and clinical settings.

Previous studies on peripheral arterial stents were reviewed in Chapters 1–3, with the importance of protocol optimisation demonstrated in the evaluation of peripheral arterial stents using CT scanning. Advances in CT technology have opened opportunities to improve image quality as well as to reduce the radiation dose administered to patients who undergo CTA examination of the lower extremities. Most previous studies have found that DECT improves the image quality compared with conventional CT, but very few have evaluated peripheral arterial stents using DECT. To help fill this gap Chapters 4–6 concentrated on DECTA protocol optimisation of peripheral arterial CTA, with an anthropomorphic phantom developed in Chapter 4 to assess peripheral arterial stents with different DECTA protocols. The conclusion of this chapter is in agreement with Chapters 2 and 3, all suggesting the use of a faster rotation time with pitch value of 0.984 combined with a reconstructed VMS between 65 and 70 keV with 50% of ASIR. The optimal protocol defined in these early chapters was implemented in the clinical studies reported in Chapters 5 and 6. These chapters also evaluated the recommended protocol and found that a low contrast medium achieved an optimal diagnostic image quality at 65 keV, while stent evaluation was best visualised at 72 keV.

The major findings of this research are summarised as follows:

- Using DECTA in peripheral arterial disease and stent evaluation can be achieved with a low radiation dose when a higher pitch value is used combined with appropriate IR

without compromising diagnostic image quality. Although this has been established in the literature in different DECT protocols, this study further validates the use of VMS in peripheral arterial stent evaluation compared with conventional CTA.

- Although using iterative reconstruction techniques with DECT in peripheral arterial stents was found to improve the overall performance by decreasing both noise and radiation dose, ASIR values > 40% were found to further improve image quality.
- Using a low contrast medium with DECTA attained a satisfactory image quality when lower extremities were investigated. With use of a low contrast medium, this modality may eventually lead to better evaluation of stent patency in the peripheral arteries.
- For peripheral arterial stent evaluation, VMS images outperform conventional CTA with better image quality as well as requiring a lower radiation dose. Image quality was found to depend on the stent location in the peripheral artery tree and on the type of stent used.

7.2 Future directions

Given the rapid progress of advanced CT technologies, methods for obtaining optimal protocols will soon become readily available and accessible. There are numerous issues for future research in the field of dual-energy CTA in peripheral arterial stenting. According to research reported in the literature, some issues can be further addressed:

- Studies need to be conducted on DECT applications at different VMS to evaluate stent types based on their materials.
- Research focusing on the diagnostic accuracy of DECT in peripheral arterial stents is required, in particular with a focus on the long-term outcomes of peripheral arterial stenting.
- More research into the differences between different DECT scanner applications for peripheral arterial stent evaluation should be undertaken.
- Multi-energy CT represents a new diagnostic direction which may offer more material differentiation, and thus may be useful for assessing the in-stent restenosis within the peripheral arterial stents.
- A multicentre study is recommended to validate these findings.

Appendix A

A.1 Permission to reproduce published figures

A.2 Permission to reproduce published

November 3, 2015

Abdulrahman Almutairi
27 Vancouver Dr.
Canning Vale WA 6155
Australia

Dear Abdulrahman Almutairi:

The Radiological Society of North America (RSNA®) is pleased to grant you permission to reproduce the following figures in electronic format for educational, non-profit use only in your thesis/dissertation, provided you give full credit to the authors of the original publication.

Figures 3, 4, 9

McCollough C H, Leng S, Yu L, et al. Dual-and multi-energy CT: Principles, technical approaches, and clinical applications. *Radiology* 2015;276:637-653.

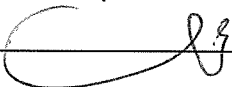
This permission is a one-time, non-exclusive grant for English-language use and is exclusively limited to the usage stated and underlined above. The requestor guarantees to reproduce the material as originally published. Permission is granted under the condition that a full credit line is prominently placed (i.e. author name(s), journal name, copyright year, volume #, inclusive pages and copyright holder).

This permission becomes effective upon receipt of this signed contract. Please sign a copy of this agreement, return a signed copy to me and retain a copy for your files. Thank you for your interest in our publication.

[Print Name]:

Abdulrahman Almutairi

SIGNATURE:

 Date: 18/4/2016

Sincerely,



Ashley E. Daly
Senior Manager, Journal Rights & Communications
Publications

Phone: 630-590-7771

Fax: 630-590-7724

E-mail: permissions@rsna.org

A.2 Permission to reproduce published

BENTHAM SCIENCE PUBLISHERS LICENSE TERMS AND CONDITIONS

Jul 14, 2016

This Agreement between Abdulrahman Almutairi ("You") and Bentham Science Publishers ("Bentham Science Publishers") consists of your license details and the terms and conditions provided by Bentham Science Publishers and Copyright Clearance Center.

License Number	3907440666582
License date	Jul 13, 2016
Licensed Content Publisher	Bentham Science Publishers
Licensed Content Publication	Current Medical Imaging Reviews
Licensed Content Title	Dual Energy Computed Tomography Angiography in the Peripheral Arterial Imaging: A Systematic Review of Image Quality, Radiation Dose and Diagnostic Value
Licensed Content Author	Abdulrahman Almutairi and Zhonghua Sun
Licensed Content Date	Dec 31, 1969
Type of Use	Thesis/Dissertation
Requestor type	Academic institution
Format	Electronic
Portion	chapter/article
Rights for	Main product
Duration of use	Life of current edition
Creation of copies for the disabled	no
With minor editing privileges	no
In the following language(s)	Original language of publication
With incidental promotional use	no
The lifetime unit quantity of new product	0 to 499
The requesting person/organization is:	Curtin University
Title of your thesis / dissertation	Scanning protocol optimisation for dual-energy computed tomography angiography in peripheral artery stenting
Expected completion date	Jul 2016
Expected size (number of pages)	150
Billing Type	Invoice
Billing Address	Abdulrahman Almutairi 27 Vancouver Dr Canning vale, Australia 6155 Attn: Abdulrahman Almutairi
Requestor Location	Abdulrahman Almutairi 27 Vancouver Dr Canning vale, WA 6155 Australia

Attn: Abdulrahman Almutairi

Billing Type

Invoice

Billing AddressAbdulrahman Almutairi
27 Vancouver DrCanning vale, Australia 6155
Attn: Abdulrahman Almutairi**Total**

0.00 AUD

Terms and Conditions**STANDARD TERMS AND CONDITIONS FOR REPRODUCTION OF MATERIAL
Introduction**

The publisher for this copyrighted material is Bentham Science Publishers Ltd. By clicking "accept" in connection with completing this licensing transaction, you agree that the following terms and conditions apply (along with the Billing and Payment terms and conditions established by Copyright Clearance Center, Inc. ("CCC"), at the time that you opened your CCC account and that are available at any time at <http://myaccount.copyright.com>).

Limited License

Publisher hereby grants to you a non-exclusive license to use this material. Licenses are for one-time use only with a maximum distribution equal to the number that you identified in the licensing process; any form of republication must be completed within 180 days from the date hereof (although copies prepared before then may be distributed thereafter); and any electronic posting is limited to a period of 180 days.

Geographic Rights: Scope

Licenses may be exercised anywhere in the world.

Altering/Modifying Material: Not Permitted

You may not alter or modify the material in any manner, nor may you translate the material into another language without permission from the Publisher.

Reservation of Rights

Publisher reserves all rights not specifically granted in the combination of (i) the license details provided by you and accepted in the course of this licensing transaction, (ii) these terms and conditions and (iii) CCC's Billing and Payment terms and conditions.

License Contingent on Payment

While you may exercise the rights licensed immediately upon issuance of the license at the end of the licensing process for the transaction, provided that you have disclosed complete and accurate details of your proposed use, no license is finally effective unless and until full payment is received from you (either by publisher or by CCC) as provided in CCC's Billing and Payment terms and conditions. If full payment is not received on a timely basis, then any license preliminarily granted shall be deemed automatically revoked and shall be void as if never granted. Further, in the event that you breach any of these terms and conditions or any of CCC's Billing and Payment terms and conditions, the license is automatically revoked and shall be void as if never granted. Use of materials as described in a revoked license, as well as any use of the materials beyond the scope of an unrevoked license, may constitute copyright infringement and publisher reserves the right to take any and all action to protect its copyright in the materials.

Copyright Notice: Disclaimer

It is a condition of this license that on all copies you republish, display or distribute you (i) provide full bibliographical information for the licensed material, including but not limited to author name, title and publication date of the work, volume and number if applicable, publisher name (Eureka Science Ltd.), page reference, (ii) include the statement, "Reprinted by permission of Eureka Science Ltd."; and (iii) include the copyright notice that appears in the work as published by Eureka Science Ltd..

Warranties: None

Publisher makes no representations or warranties with respect to the licensed material.

Indemnity

You hereby indemnify and agree to hold harmless publisher and CCC, and their respective

officers, directors, employees and agents, from and against any and all claims arising out of your use of the licensed material other than as specifically authorized pursuant to this license.

No Transfer of License

This license is personal to you and may not be sublicensed, assigned, or transferred by you to any other person without publisher's written permission.

No Amendment Except in Writing

This license may not be amended except in a writing signed by both parties (or, in the case of publisher, by CCC on publisher's behalf).

Objection to Contrary Terms

Publisher hereby objects to any terms contained in any purchase order, acknowledgment, check endorsement or other writing prepared by you, which terms are inconsistent with these terms and conditions or CCC's Billing and Payment terms and conditions. These terms and conditions, together with CCC's Billing and Payment terms and conditions (which are incorporated herein), comprise the entire agreement between you and publisher (and CCC) concerning this licensing transaction. In the event of any conflict between your obligations established by these terms and conditions and those established by CCC's Billing and Payment terms and conditions, these terms and conditions shall control.

Jurisdiction: Not Required*

This license transaction shall be governed by and construed in accordance with the laws of the United Arab Emirates. You hereby agree to submit to the jurisdiction of the federal and state courts located in Dubai for purposes of resolving any disputes that may arise in connection with this licensing transaction.

Other Terms and Conditions:

v1.0

Questions? customercare@copyright.com or +1-855-239-3415 (toll free in the US) or +1-978-646-2777.
